2010-01-01

Granulometry And Geochemistry Of Dust Emission From Owens (dry) Lake, California

Analila Rojo
University of Texas at El Paso, rojolucero@elp.rr.com

GRANULOMETRY AND GEOCHEMISTRY OF DUST EMISSION FROM OWENS (DRY) LAKE, CALIFORNIA

ANALILA ROJO

Environmental Science and Engineering

APPROVED:

Thomas E. Gill, Ph.D., Chair

Richard P. Langford, Ph.D.

Melanie A. Barnes, Ph.D.

Peter Golding, Ph.D.

Russell R. Chianelli, Ph.D.

Dale A. Gillette, Ph.D.

Patricia D. Witherspoon, Ph.D.
Dean of the Graduate School

GRANULOMETRY AND GEOCHEMISTRY OF DUST EMISSION FROM OWENS (DRY) LAKE, CALIFORNIA

by

Analila Rojo, MS

DISSERTATION

Presented to the Faculty of the Graduate School of

The University of Texas at El Paso

in Partial Fulfillment

of the Requirements

for the Degree of

DOCTOR OF PHILOSOPHY

Environmental Science and Engineering

THE UNIVERSITY OF TEXAS AT EL PASO

August 2010

ACKNOWLEDGEMENTS

I extend my gratitude to my committee members for their support and eternal patience. To Dr. Gill, thank you for your trust and keeping the faith in me after such a long journey. This journey would have not been possible without the financial support from the "Pathways to Geosciences Fellowship" program at the University of Texas at El Paso. A very special thank to Dr. Kate Miller and Tina Carrick, and to Dr. Richard Langford for his recommendation. I thank my family and friends for their care and support.

Initial collection of the samples analyzed and studied in this dissertation was supported by contracts with the California Air Resources Board and California State Lands Commission. I thank the many participants in LODE, especially Dr. Gillette, Dr. Gill, and Dr. Thomas Cahill, for designing the LODE studies and collecting and archiving the samples. Subsequent sample analyses and data interpretations were funded by Grant 003644-0327-1999 to Dr. Gill from the Texas Higher Education Coordinating Board- Advanced Research Program, and the U.S. Department of Energy HBCU/MI Environmental Technology Consortium to Dr. Gill through DOE Cooperative Agreement #DE-FC02-02EW15254. Additional support was provided to Dr. Gill for this work by the University of Texas - El Paso College of Science.

ABSTRACT

Owens (dry) Lake, the terminus of Owens River, is located in the Basin and Range physiographic province in east-central California. The transformation of Owens Lake into a desiccated desert playa (approximately 280 km^2) via diversion of the river into the Los Angeles Aqueduct (in 1913) led to extensive wind erosion, making the playa one of the most intense sources of airborne dust in the Western Hemisphere. The processes that direct the chemical and mineralogical composition of surface sediments at Owens (dry) Lake and the physical mechanisms of wind erosion, saltation and dust emission at Owens (dry) Lake are well-understood. However, prior research has not investigated the effects of spatial and temporal variations of individual aeolian dust events on the particle size distribution and elemental composition of dust aerosols as they are emitted. This study investigates the variations of particle size (measured by laser diffraction) and elemental composition of individual aeolian sediment samples collected from four sequential wind events (approximately one week apart) at six different heights above the land surface at seven different locations along an 1.2 km upwind-downwind sampling transect on the Owens playa. Laser diffraction's ability to measure grains in their dry state as collected from a dust trap, as was done here, allows us to measure the actual size of the often-agglomerated, salt-bearing particles moving in the wind, as opposed to other techniques which require the disaggregation of particles and/or dissolution of salts in liquid. The samples also presented the opportunity to inter-compare two elemental analysis techniques (Particle-Induced X-Ray Emission Spectrometry [PIXE] and Inductively-Coupled Plasma Atomic Emission Spectroscopy [ICP-AES]) as complementary methods for analysis of airborne dusts and sediments.

Results show that dust from Owens (dry) Lake contains several potentially toxic elements including As, Cd, Co, Cr, Pb, Mo and Zn with possible detrimental health effects and environmental impacts. Spatial and temporal variations within and between individual dust storms were reflected in the volumetric particle size distributions and elemental compositions of the dust. For example, dust grain size was strongly correlated at a significance level of $\alpha = 0.01$

to the height at which the particles were captured above the playa surface and showed a significant difference ($p < 0.05$) between individual wind storms (becoming coarser with each sequential dust event), but did not present a significant correlation with location along the linear transect where samples were collected. The overall mean percent volume of finer particles (<20 μm) was greater than the overall mean percent volume of coarser particles (>250 μm). The analysis of the mean percent volume of dust particles in eleven size classes with respect to height allowed the determination of the height of transition between particles moving in saltation and suspension, an essential parameter in equations developed to investigate vertical and horizontal flux of particles from eroding surfaces. Elemental concentrations of the dust varied with height above the land surface, distance downwind of the dust source, and between individual dust storms, as well as with dust particle size. For example, Na and S concentrations (indicative of a layer of efflorescent salts atop the playa) covaried with the concentrations of submicron to silt-sized particles during each event, increased with height above the ground, and decreased with distance downwind of the dust source and with each sequential dust storm, suggesting quick and efficient removal of fine salts from the playa. Al, Ti, Mn, K, Fe, and Rb concentrations covaried with the percentages of fine/medium sand particles in the first two events and coarse sand in the third event, suggesting these elements were borne on saltating particles of clastic sediments. The combination of techniques reveals particle size/chemical fractionation and spatial variability of sediment properties during dust emission at aeolian "hotspots," with implications to dust emission modeling, geochemical cycling, and aerosol source/receptor relationships.

Statistically significant differences ($p < 0.05$) were shown between PIXE and ICP-AES analytical results for splits of the same dust samples. Variability between PIXE and ICP data is explained by inherent differences between the analytical techniques, sample preparation methods, and/or variability in sample matrices. For example, PIXE determined higher concentrations of Al, As, Cu, Fe, K, Mn, Ni, Sr, Ti, and Zn in all samples. Combined with low ICP-AES percent recoveries of Al, Fe, K, Mn, and Ti for NIST SRM 2710, these results indicated incomplete dissolution during digestion (EPA Method 3050B) of elements bound in

silicate structures. These findings point out the care which must be taken in selection of elemental analysis methods for environmental samples and in evaluation of elemental concentrations obtained by different techniques.

TABLE OF CONTENTS

LIST OF TABLES

LIST OF FIGURES

CHAPTER 1. INTRODUCTION

Owens (dry) Lake is located in the Basin and Range physiographic province of the Western United States in east-central California. It is surrounded by the Sierra Nevada to the west, the Inyo Mountains to the east, and the Coso Mountains to the southeast. Owens Lake is the terminus of the Owens River, which drains a watershed over 160 km long on the east side of the Sierra Nevada (Schultz, 2001). The geological composition of the surroundings mostly consisting of limestone, dolomite, shale, conglomerate, quartzite (Inyo Mountains), granitic and volcanic rocks (Coso Mountains) and granodioritic plutons (Sierra Nevada) (Bischoff and Cummins, 2001) has contributed to the past and current composition of the now- dry lake bed as well as mining activities of silver and lead at Cerro Gordo in the Inyo Mountains, which led to the dumping of mining waste into the lake in the late 1800's (Reheis et al., 2002).

Owens Lake was transformed into a desiccated desert playa (approximately 280 km^2) as a consequence of water diversion of the Owens River into the Los Angeles Aqueduct in 1913 (Gill and Cahill, 1992). The lake became essentially dry between 1921 and 1926 leaving a large playa with a central brine pool. Salts from the lake, saline groundwater residing just below the playa surface, and minerals from the surrounding mountains and mining activities dissolved in the lake's water and crystallized depositing abundant amounts of sulfate and carbonate rich salts (Levy et al., 1999) which form an alkali salt crust that covers most of the lakebed today (Gillette et al., 2004). These salts are generated at the lakebed surface via evaporation of upflowing ground water due to the closeness of the capillary fringe to the surface of the lakebed (Ryu et al., 2002). The surface of the playa (dry lake) has been susceptible to extensive wind erosion making the playa one of the most significant sources of PM10 in the Western Hemisphere (Cahill et al., 1996; Gill, 1996; Gill et al., 2002). The dust from Owens (dry) Lake not only affects visibility in neighboring towns, national parks (Sequoia, Kings Canyon, and Death Valley), national forests and wilderness areas (Gill, 1996), but also causes environmental and

health problems posing threats due to inhalation of dust that contains potentially hazardous concentrations of SO4, As (Levy et al., 1999), Ni, Cr, and Pb (Gill et al., 2002).

Owens (dry) Lake has been the site of a considerable number of geoscientific studies on aeolian processes, including two international collaborations (the Lake Owens Dust Experiments, LODE) to determine the physical mechanisms of wind erosion and transport processes. Dust storms emanating on the south sand sheet of Owens (dry) Lake, site of the LODE experiments, have been investigated to determine sources and magnitude of coarse saltating particles, understand meteorological and atmospheric conditions related to dust emissions, and study how the motion of saltating particles across different types of playa surfaces results in the generation of PM10 and aeolian sediment (e.g., Cahill et al., 1996; Gillette et al., 1996, 1997, 2001; Niemeyer et al., 1999). Other research projects at Owens (dry) Lake have been implemented to test potential mechanisms for dust mitigation (e.g., Dahlgren et al., 1997; Lancaster et al., 1998; Kim et al., 2000; Gill et al., 2003; Roney and White, 2006).

The geochemical processes that direct the chemical and mineralogical composition of saline groundwater and surface salts at Owens (dry) Lake (e.g., Tyler et al., 1997; Levy et al., 1999; Ryu et al., 2002; Güler and Thyne, 2004) and the physical mechanisms of wind erosion, dust emission, and saltation processes at Owens (dry) Lake (e.g., Cahill et al., 1996; MacKinnon et al., 1996; Gillette et al., 1996, 1997, 2001; Niemeyer et al., 1999; Ono, 2006) are now well-understood. However, previous research at Owens Lake has not focused on the effects of spatial and temporal variations on particle size distribution (PSD) and elemental composition of aeolian dust and sand particles at their time of emission. Until recently, minimal data of dust chemistry derived from Owens (dry) Lake has been documented. Some studies have shown that dusts and their parent sediments contain high concentrations of several potentially toxic elements such as arsenic, barium, bromine, chromium, copper, lead, molybdenum, nickel, rubidium, strontium, thorium, uranium, zinc, and zirconium (Gill et al., 2002; Reheis et al., 2002; Ryu et al., 2002).

Aerosols sampled from Owens (dry) Lake dust storms frequently contain significant amounts of arsenic concentrated in the <10μm fraction (Ryu et al., 2002). Given these potentially high concentrations a concern exists about potential health effects and environmental impacts of metals that may be present in the dust (Gill et al., 2002). With this motivation, the research undertaken for this dissertation documents the particle size of the sediments moving just above the playa surface during their emission from Owens (dry) Lake, the elemental chemistry of these materials, and how they are interrelated with each other and with height above the playa surface, position on the playa surface, and temporal sequence of wind events.

Inductively coupled plasma atomic emission spectroscopy (ICP-AES) and particle induced X-ray emission spectrometry (PIXE) are two analytical methods that are widely used to determine the elemental composition and concentrations for soils, sediments, aerosols, and other environmental samples. The current research also led to the opportunity to inter-compare these two elemental analysis techniques as complementary techniques and to verify measured concentrations obtained for the same elements in splits of the aeolian dust samples. The inter-comparison of ICP-AES and PIXE allows the evaluation of factors such as detection limits, methodology of the analytical techniques, and design of sample collection and preparation which may result in variability of sample matrices and particle size.

References

Bischoff, J.L., Cummins, K. 2001. Wisconsin Glaciation of the Sierra Nevada 79,000–15,000 yr B.P. as Recorded by Rock Flour in Sediments of Owens Lake, California. *Quaternary Research 55 (1): 14-24.*

Cahill, Thomas A., Gearhart, Elizabeth A., Gill, Thomas E., Gillette *et al*., Dale A., and Reid, Jeffrey S. 1996. Saltating Particles, Playa Crusts and Dust Aerosols at Owens dry Lake, California. *Earth Surface Processes and Landforms 21: 621-637.*

Dae Seong Kim, Greg H. Cho and Bruce R. White 2000. A Wind-tunnel Study of Atmospheric Boundary-Layer Flow over Vegetated Surfaces to Suppress PM10 Emission on Owens (dry) Lake. *Boundary-Layer Meteorology 97 2 309-329.*

Dahlgren,R. A., Boettinger, J. L., Huntington, G. L,. Amundson, R. G. 1997. Soil development along an elevational transect in the western Sierra Nevada, California. *Geoderma* 78 3-4 207-236.

Gill, T.E., Cahill, T.A. 1992. Playa-generated dust storms from Owens Lake. In: Hall, C.A. Jr., Doyle-Jones, V., Widawski, B. (Eds.), The History of Water: Eastern Sierra Nevada, Owens Valley, White-Inyo Mountains. *University of California Press, Los Angele 63–73.*

Gill, T.E. 1996. Eolian sediments generated by anthropogenic disturbance of playas, human impacts on the geomorphic system and geomorphic impacts on the human system. *Geomorphology, 17, 207- 228.*

Gill, T.E., Gillette D.A., Niemeyer T. and Winn R.T., 2002. Elemental geochemistry of wind-erodible playa sediments, Owens Lake, California. *Nuclear Instruments and Methods in Physics Research Section B- Beam Interactions with Materials and Atoms*, 189, 209–213.

Gill, T.E., Cahill, T.A., Copeland, S.A., and White, B.R., 2003. Sand fences for control of wind erosion and dust emission at Owens Lake, CA: Full-scale testing, field deployment, and evaluation of effectiveness. *Proceedings of the 11th International Conference on Wind Engineering, Lubbock, TX, June 2003, vol. 2, pp. 2773- 2780.*

Gillette DA, Herbert G, Stockton PH, Owen PR. 1996. Cause of the fetch effect in wind erosion. *Earth Surf. Proc. Landforms* **21:** 641- 660.

Gillette, D. A., Fryrear, D. W., Gill, T. E., Ley, T., Cahill, T. A., Gearhart, E. A. 1997. Relation of Vertical Flux of Particles Smaller than 10 um to Total Aeolian Horizontal Mass Flux at Owens Lake. *Journal of Geophysical Research 102:D22 26,009-26,015.*

Gillette, D.A., Niemeyer, T.C. Helm, P.J. 2001. Supply-limited horizontal sand drift at an ephemerally crusted, unvegetated saline playa. *Journal of Geophysical Research 106:D16 18085-18098.*

Gillette, D.A., Ono, D., Richmond, K. 2004. A combined modeling and measurement technique for estimating windblown dust emissions at Owens dry Lake, California. *Journal of Geophysical Researc 109(F1): F01003.*

Güler, Cüneyt and Thyne, Geoffrey D. 2004. Hydrologic and geologic factors controlling surface and groundwater chemistry in Indian Wells-Owens Valley area, southeastern California, USA. *Journal of Hydrology 285:1-4 177-198.*

Lancaster, Nicholas and Baas, Andy 1998. Influence of vegetation cover on sand transport by wind: field studies at Owens Lake, California. Earth Surface Processes and Landforms 23 1 69 – 82.

Levy, D.B., Schramke, J.A., Esposito, K.J., Erickson, T.A., Moore, J.C. 1999. The shallow ground water chemistry of arsenic, fluorine, and major elements: Eastern Owens Lake, California *Applied Geochemistry 14(1): 53-65.*

MacKinnon, David J., Chavez, Pat S. jr., Fraser, Robert S., Niemeyer, Tezz C., Dale A., Gillette 1996. Calibration of GOES-VISSR, visible-band satellite data and its application to the analysis of a dust storm at Owens Lake, California. *Geomorphology 17:1-3 229-248.*

Niemeyer, Tezz C., Gillette, Dale A., Deluisi, John J., Kim, Young J., Niemeyer, William F., Ley, Trevor, Gill, Thomas E. and Ono, Duane 1999. Optical depth, size distribution and flux of dust from Owens Lake, California. *Earth Surf. Process. Landforms* 24 463-479.

Ono, D. 2006. Application of the Gillette model for windblown dust at Owens Lake, CA. *Atmospheric Environment, 40:17 3011-3021.*

Reheis, M.C., Budahn J.R. and Lamothe P.J. 2002. Geochemical evidence for diversity of dust sources in the southwestern United States. Geochimica et Cosmochimica Acta, 66, 1569-1587.

Roney A., White R. 2006. Estimating fugitive dust emission rates using an environmental boundary layer wind tunnel. *Atmospheric Environment 40:40 7668-7685.*

Ryu, J. I. H., Gao, S., Dahlgren, R.A., Zierenberg, R.A. 2002. Arsenic distribution, speciation and solubility in shallow groundwater of Owens Dry Lake, California. *Geochimica et Cosmochimica Acta 66(17): 2981-2994.*

Schultz, B.W. 2001. Extent of vegetated wetlands at Owens Dry Lake, California, U.S.A, between 1977 and 1992. *Journal of Arid Environments 48: 69–87.*

Tyler, S.W., Kranz, S., Parlange, M.B., Albertson, J., Katul, G.G., Cochran, G.F., Lyles, B.A., Holder, G. 1997. Estimation of groundwater evaporation and salt flux from Owens Lake, California, USA. *Journal of Hydrology 200:1-4 110-135*.

CHAPTER 2. PARTICLE SIZE DISTRIBUTION OF NEAR-SURFACE AEOLIAN DUST EMISSIONS FROM OWENS (DRY) LAKE, CALIFORNIA

Abstract

Aeolian dust particles, collected at the time of their emission at Owens (dry) Lake, California during a sequence of dust events in March 1993 were analyzed (in bulk) via laser diffraction to quantify their particle size distributions (PSD) along a 1.2 km linear upwind-downwind transect. The samples were collected at different heights and distances downwind of the source. The dust particle size distributions were divided into eleven size intervals to evaluate the influence of the natural characteristics of temporal (dust events) and spatial (height above the playa surface and location along the playa) variation on the mean percent volume of particles at each size interval. The overall particle size distribution was multimodal with dominant peaks for coarse silt (20-50 μm) and very fine sand (50-100 μm). The mean percent volume of dust particles at each size interval showed a significant ($p < 0.05$) variation from dust event to dust event with the exception of medium sand ($p = 0.30$) at a significance level of $\alpha = 0.05$. The mean percent volume at each size interval was strongly correlated (at a significance level of $\alpha = 0.01$) with height (at 10, 20, 30, 50, 60 and 100 cm) for the combined dust events and the individual dust events with the exception of the mean percent volume of very fine sand (50-100 μm). Very fine sand divided the suspended (<50 μm) particle size intervals from the saltating (>50μm) particle size intervals. The mean percent volume of suspended particles varied inversely to the mean percent volume of saltating particles with respect to height. The correlation of the mean percent volume of dust particles between locations was significant at $\alpha = 0.01$ for the combined dust events and separate dust events. In general, the particle size distribution (in percent volume) along the 1.2 km line transect (study area) showed that the S1, S2, and S3 (south sampling locations) accounted for higher mean percent volumes of saltating particles (> 50 um) for the 17 March dust event and fine sand (100-250) for the 23 March dust event.

Introduction

Mineral aerosol production by wind erosion in arid areas makes up nearly half the global aerosol yearly production (Alfaro and Gomes 2001) and such aerosols can be transported long distances downwind of the source regions (Alfaro *et al*. 2000; Borge 2007; Pongkiatkul 2007). Because mineral aerosol makes up close to 50% of the global aerosol, it can be regionally and locally important in volume and potential chemical effects (Reynolds *et al*. 2007). Dust emissions from arid and semi-arid soils are possibly the primary source of dust globally. These zones occupy approximately 1/3 of the global land area. Playa lakes, areas of alluvial outwash, and floodplains are some of the major dust source areas (Lawrence and Neff 2009). Owens (dry) Lake, California (Figure 2.1) is a dry playa lake and has the highest long-term dust flux of any area in the United States with transport distances of up to 400 km (Pelletier 2006). Owens (dry) Lake dust events were reported to have among the highest aerosol concentrations recorded for North America (Gill 1996; Niemeyer *et al*. 1999) with estimated dust production estimates of up to 8 million Mg per year (Gill 1996) and PM_{10} (airborne particulate matter smaller than 10 μm aerodynamic diameter) concentrations measured over a two hour period greater than 40,000 $\mu g/m^3$ (Gill 1996). According to previous studies, Owens (dry) Lake may be one of the largest single sources of anthropogenic dust released into the atmosphere per unit area in the United States (Gill and Gillette 1991; Cahill *et al.* 1996; Roney and White 2006). The transport and deposition of these fine particles has the potential to greatly affect visibility, public health, and the downwind ecological and geological environments (Cahill *et al.* 1996; Reheis *et al*. 2002).

The Owens (dry) Lake surface behaves as a dynamic "wet playa" with regards to aeolian processes as described by Reynolds *et al*. (2007). Evaporation of surface water, lack of wet conditions, saline groundwater just below the surface and presence of an erodible surface allow dust to be generated when surface wind speeds exceed approximately 7 m s^{-1} (Cahill *et al*. 1996). The ephemeral layer of loose, powdery efflorescent salts that cover the playa at the end of winter is extremely vulnerable to wind erosion (Cahill *et al*. 1996; Ryu *et al.* 2002;) and is quickly deflated. The salt-silt-clay crust underneath is in turn eroded by subsequent dust events (Cahill

et al. 1996). The nature of the surface layer controls the particle entrainment by wind from the playa. Broken pieces of the surface crust itself ("auto-abrasion" as defined by Warren *et al.* 2007) as well as sand from dunes that surround parts of the playa (Cahill *et al*. 1996; Roney and White 2006) supply sufficient saltating particles to abrade the crust and generate abundant dust. It has been observed that the majority of the dust produced from the playa of Owens (dry) Lake is derived from abrasion of the weakly-cemented salt-silt-clay crusts by saltating particles (Cahill *et al*. 1996), including its auto-abrasion.

Temporal and spatial variability may also influence dust concentrations and its particle size distribution. Studies have shown the variability of the average PM_{10} concentrations during dust events at different sites (Lee *et al.* 2006). The spatial distribution and temporal variability of dust particles can also be influenced by its location, elevation, and distance from the source (Anuforom 2007). In order to assess the influence of spatial variability (height), dust samplers can be placed at different heights at the sampling sites (Gillette *et al.* 1997; Gillette *et al.* 2001; Zobeck *et al.* 2003; Breuning-Madsen and Awadzi 2005). Particle size characteristics, specifically particle size distributions, can then be used as proxies for dust sources (Crouvi *et al*. 2008) or to investigate wind intensity related to dust events (Parker and Bloemendal 2005). The size distributions of the saltating particles from Owens (dry) Lake and other dust producing areas are essential data in the investigation of vertical and horizontal dust flux from eroding surfaces and in defining the transition layer from saltation to suspension (Gillette *et al*. 1997; Goossens and Offer 2000; Ni *et al.* 2002; Offer and Goossens 2004; Li *et al*. 2008; Lawrence and Neff 2009; Dong *et al*. 2010). Finer-grained particle sizes in aeolian dust are in general, transported by surface winds and move from one position to the next, in suspension events. Larger particles categorized as saltating particles follow different trajectories where their characteristics are dependent on elevation above the surface (Li *et al.* 2008). Various factors may influence the measured particle size distribution of aeolian dust, such as pedogenesis, composition of the

parent material, transport medium, atmospheric conditions, redistribution and sorting of particles, sampling method, sample preparation, and instrumentation (Parker and Bloemendal 2005).

The purpose of the present study was to use laser diffraction to determine the particle size distribution of aeolian dust samples collected during four sequential dust events at a single, intensely wind-eroding region of Owens (dry) Lake, California in March 1993 and evaluate the particle size distributions. This study also investigated how the temporal sequence of the dust events, the height of sample collection above the playa surface, and the location of sample collection along the playa interacted to control the particle size distribution of the aeolian dust particles emitted from the playa surface. The distribution of suspended and saltating particles was assessed with respect to height to identify a possible transition layer from saltation mode to suspension mode. It is hypothesized, based on field reconnaissance by Cahill *et al.* (1996), that the sequence of storms, height above the dry playa, and location along the dry playa may influence the variation of the dust particle size.

Study Site Setting

Owens Lake, the remnant of Pleistocene pluvial Lake Owens, is located in the Basin and Range physiographic province of the Western United States (Figure 2.1) (Tyler *et al*. 1997) at the southern end of the Owens Valley, a narrow but deep north-south trending basin surrounded by the Sierra Nevada to the west, the Inyo Mountains to the east and Coso Mountains to the southeast (Levy *et al.* 1999; Ryu *et al.* 2002). The Owens River valley in southeast central California drains a watershed over 160 km long, dominated by streams flowing from the Sierra Nevada (Schultz 2001) where bedrock is dominated by granodioritic plutons (Bischoff and Cummins 2001). Limestone, dolomite and smaller amounts of shale, conglomerate, and quartzite dominate the sedimentary rocks of the Inyo Mountains (Levy *et al.* 1999). The Coso Mountains at the southern end of the valley consist of granitic and volcanic rocks (Güler and Thyne 2004). During Pleistocene wet periods, pluvial Lake Owens filled the basin, accumulating

sediments shed from these surrounding highlands. In historic times, Owens Lake was a shallow, perennial saline lake covering approximately 280 km^2. It is estimated that the historic shoreline of Owens Lake was at an elevation of 1094 m above sea level (a.s.l.) while the lowest point in the dry playa is 1083 m (a.s.l.) (Tyler *et al*. 1997). Anthropogenic water diversions beginning in 1913 with the construction of the Los Angeles Aqueduct led to the desiccation of Owens Lake by the late 1930's (MacKinnon et al. 1996; Tyler *et al*. 1997; Ono 2006) leaving a large, dust-emitting playa, approximately 285 km^2 with a brine pool at the lowest part of the basin (Gillette *et al.* 2004). The dissolved minerals and salts in the Owens Lake water crystallized during desiccation and left behind copious surface deposits of sulfate and carbonate rich salts (Levy *et al.* 1999; Ryu *et al*., 2002) and a puffy, alkaline salt-silt-clay crust that covers much of the lakebed surface (Cahill *et al*. 1996; Gillette *et al*. 2004). The surface of Owens (dry) Lake is essentially formed and re-formed in an annual cycle through the dissolution and re-crystallization of salts, admixed with lacustrine sediments, as the moisture of the playa surface and subsurface is evaporated (Gill 1996; Cahill *et al*. 1996). Salt efflorescence is generated at the lakebed during dry periods via evaporation of discharging saline ground water due to the closeness of the capillary fringe to the surface of the lakebed (Cahill *et al.* 1996; Ryu *et al*. 2002).

The climate of the Owens (dry) Lake basin is typical of high desert conditions where mean annual precipitation varies from 100 to 140 mm (Ryu *et al.* 2002) falling predominantly in winter (Cahill *et al.* 1996). Temperatures average 27ºC in the summer and 3ºC in winter time (Ryu *et al.* 2002). Mean daily evaporation (by microlysimeter) is 0.29 mm (Tyler *et al.* 1997). Owens Valley has a bidirectional regime of prevailing winds near the surface matching and enhanced by the generally North to South topographic alignment of the deep basin. The highest wind speeds typically occur in early to late spring (March–May), with sustained winds that may exceed 25 m s^{-1} (Cahill *et al.* 1996).

Experimental Details

Field sample collection

Bulk dust samples were collected from the playa of Owens (dry) Lake during the LODE (Lake Owens Dust Experiment) (Gillette *et al*. 1996; Cahill *et al*. 1996), an international field campaign in March 1993. The sampling site was located on the "South Sand Sheet" on the southern portion of Owens (dry) Lake and had been identified as a locus of regular dust event initiation. The sampling site and the locations for sample collection were selected by Cahill *et al*. (1996) based on earlier fieldwork on the Owens (dry) Lake bed and two years of field reconnaissance (Cahill *et al*. 1996; Gillette *et al.* 1996, 1997) prior to the dust monitoring study in March 1993. A sequence of individual dust events occurred on 11, 17, 23, and 24 March, 1993. Close observation of playa surface conditions by Cahill *et al.* (1996) during and after the Mar (1993) dust events provided a basic understanding of the geomorphic state of Owens (dry) Lake playa which set the premise for this study.

BSNEs (Big Spring Number Eight dust traps) (Fryrear 1986) were used to capture aeolian sediment during the dust events (further described in Gillette *et al*. 1996) at different heights and at different locations along a line transect extending 1.2 km nearly north-south across the playa. The BSNE (Figure 2.2) is made of 28- gauge galvanized metal, galvanized 18- mesh screen, and stainless steel 60-mesh screen. Aeolian sediment passes through the vertical 20mm x 50mm opening. As air speed is reduced inside the sampler, the particles settle in a collection pan and the air is released through the top of the sampler consisting of a 60 mesh screen. The 18 mesh screen decreases the movement of the deposited material and prevents breakdown of the collected sediment and potential loss of fine particles through the top of the screen (Goossens and Offer 2000). The BSNE is described as a passive dust collector that has the capability to maintain 90% collection efficiency for particles >50 μm for all winds as opposed to particles <50 μm where the BSNE collection efficiency decreases for silt sized grains (Gillette *et al*. 1997).

The BSNEs were placed at seven locations (H1, H2, H3, H4, S1, S2, and S3) along the 1.2 km long linear transect (Figure 2.2) at the presumed zero dust emission initiation point (H1 location at point A in Figure 2.2) and at 50, 100, 150, 520, 874, and 1057 meters south based on several years of advance field reconnaissance (Cahill *et al.* 1996; Gillette *et al*. 1996, 1997). The BSNE line was oriented from roughly the north to south along the direction of the prevailing wind from the initial zero point (site H1) at the boundary where presumably the crust was the hardest and most resistant to erosion (Cahill *et al*.; 1996, Gillette *et al.* 1996; Gill *et al.* 2002). At each location, individual BSNE collectors were placed with inlets at elevations of 10, 20, 30, 50, 60, and 100 cm (Figure 2.2) above the initial playa surface, resulting in a total of 42 possible aeolian dust samples per dust event.

These elevations were based on the concept that most soil material raised by aeolian transport in desert environments is dominated by saltating sand grains in the top ~20 to 30 cm and dominated by silt and clay (dust) sized particles after being suspended for 1 to 1.5 meters above the surface (Fryrear and Saleh 1998). Particles with equivalent diameter > 20μm and sedimentation velocities > 5 to 10 cm s^{-1} are assumed to generally be removed from the dust plume by gravitational forces after a few minutes to several hours (Littmann 1997) whereas particles finer than 20 μm can be transported over long distances of up to hundreds or thousands of kilometers (Alfaro et al. 2004). After each event, LODE field participants emptied each BSNE into a clean, dry, plastic bag. Each bag was labeled according to location, height, and date event (Cahill *et al*. 1996; Gillette *et al.* 1996, 1997). The samples were stored in dry conditions for subsequent analysis.

Meteorological conditions

The passage of a cold front started the 11 March event (postfrontal passage dust event) which resulted in moderate to high northerly winds for about 6 to 12 hours. This dust event was the first dust event of the spring season and quickly deflated the playa's loose efflorescent salt

covering. In less than 3 hours the salt-silt-clay layer just below the efflorescent crust became exposed and was progressively degraded through subsequent dust events. Moderate dust production was observed during this first dust event (Cahill *et al*. 1996). The next dust event took place on 17 March. This storm was initiated by strong morning southerly winds that transported dust northward, but by mid-morning the wind direction shifted and backwashed the dust to the south. By mid-afternoon, winds from west-northwest generated additional dust production along the line transect. The 17 March dust event began to degrade the salt-silt-clay surface through saltation abrasion. The total amounts of dust produced during the event of 17 March were the least of the four dust events. The last two dust events considered for this study took place on 23 and 24 March. Both were characterized by winds blowing from south to north, moving saltating sands across the line transect and degrading the salt-silt-clay surface generating significant amounts of dust. Throughout the four storms, it was observed how the changes in playa surface conditions influenced the availability of particles for aeolian erosion.

Particle size analysis

Particle size distributions of the sediment samples collected from the BSNEs were measured on the Malvern Mastersizer 2000 laser diffraction instrument (Malvern Instruments Ltd.) equipped with the Scirocco 2000 for dry analysis. The particle size analysis was carried out at the University of Texas at El Paso, Geological Sciences Department. The Scirocco 2000 for dry measurements was used to determine the actual particle size of suspended dust in its dry (potentially agglomerated, containing compound grains) form as collected immediately after emission from the playa surface. The Mastersizer's wide angular range (0.01° to beyond 130°) allows continuous detections as well as measurements of particle size distributions in up to 100 size intervals (or size bands) between 0.01- 2000 μm as the minimum and maximum limits, respectively. The particle size distributions generated by the Malvern software are expressed as the measured sample volume spaced logarithmically between 0.01 and 2000 μm). Figure 2.3 is an example graph for three dust samples where the x-axis (log scale) represents the particle size

diameter in (μm) and the y-axis denotes the volume of sample at a given size interval expressed as a percentage. The size intervals are fully controlled by the end-user and the spacing between size bands can be set as either logarithmic or linear. Changing the number of size intervals does not alter the distribution. It allows the user to investigate the volumetric particle size distribution at very narrow or wide size intervals. For the purpose of this study, the particle size distributions were set up to 11 size intervals between 0.01- 2000 μm. The size intervals were set to correspond to the same particle size intervals used in previous work by Gillette *et al.* (1997) on vertical flux of aeolian dust particles from Owens (dry) Lake. Table 2.1 provides the numerical value of each size interval in microns and its corresponding particle size description.

Part of the calibration of the Mastersizer was performed using four grades of Arizona Test Dust manufactured by Powder Technology, Inc., Burnsville, Minnesota. The four grades are defined as: ISO 12103-1 A1 (ultrafine, nominal 0-10 μm size), ISO 12103-1 A2 (fine, nominal 0-80 μm size), ISO 12103-1 A3 (Medium, nominal 0-80 μm size with a lower 0-5 μm content than ISO 12103-1), A2 Fine Test Dust), and ISO 12103-1 A4 (coarse, nominal 0-180 μm size). A dust sample of sufficiently large quantity from the current investigation was also used as a primary source for calibration through regular reanalysis. This allowed us to continuously check the integrity of the measurements.

Data were collected with Malvern's Mastersizer 2000 software version 5.22. The Mastersizer 2000 takes 1000 readings (snaps) per second. Each dust sample measurement was set to run for 12 seconds (thus providing 12,000 readings) and three measurement cycles. The average of the three successive runs for each sample was then used for particle size distribution analyses. The volume of sample required for particle size analysis, for this particular study, varied between 1g to 6g depending on the composition of the sample which regulated the rate of sediment flow through the instrument. Sandy samples required greater amounts than fine or very fine material.

Data analysis

SPSS software package version 14.0 for Windows was used to perform basic statistical analyses of the particle size data. Since the data generated by the Malvern software was expressed in percent volume of dust particles (y-axis) in each respective size interval (x-axis), all data analysis was based on the evaluation of the "percent volume of dust particles" at eleven size intervals with respect to dust event date, height above the playa surface, and location along the 1.2 km transect. Therefore the non-parametric Kruskal–Wallis test, Spearman's rho, and Pearson correlation were used to test for statistical significance between the mean percent volume of dust particles with respect to dust events, heights above the playa surface and location along the playa surface. For the hypothesis test in this analysis, rejection of the null hypothesis required that the attained significance level (ρ) be less than 0.05 (95% confidence level).

Results

The particle size distributions for the 133 aeolian dust samples collected from Owens (dry) Lake during four sequential dust events presented a multimodal distribution (Figure 2.4). The mean percent volume at each size interval (Table 2.1) for the combined dust events also reflected the high peaks for coarse silt and very fine sand (Figure 2.5), but the distribution of the mean percent volumes varied with respect to dust event at each size interval (Figure 2.6).

Evaluation of the percent volumes of the dust particle distribution with respect to height for the combined dust events and for the separate dust events revealed different distributions of dust particles (in percent volume) as illustrated by the variation of percent volume given in Table 2.2. The analysis throughout the study was based on the variation of the "mean percent volume of dust particles" (also referred to as "mean percent volume") for the combined and separate dust events. This breakdown was done for two reasons: First, to assess the difference in the distribution of the percent volume for the combined dust events and the separate dust events since the mean may conceal slight variations in the particle size distribution as a whole (Parker

and Bloemendal 2005). Secondly, to assess the potential influence of temporal and spatial variation on the mean percent volumes at each size interval. Temporal variations were known (Cahill *et al.* 1996) to influence the variability of particle sizes due to the natural characteristics of each dust event, specifically atmospheric conditions and playa composition. It was expected that the percent volume of dust particles at the respective size intervals would vary as the playa's surface changed from dust event to dust event (Cahill *et al*. 1996) and at different heights above the playa surface.

In general, the mean percent volume of suspended particles (<50 μm) varied inversely with saltating particles (>50 μm) with respect to height (Figure 2.7) The mean percent volume in the 50- 100 μm size intervals (very fine sand) did not consistently vary with respect to height (Figure 2.8) as did the mean percent volume at the other size intervals. The 50- 100 μm particle size interval falls in the range of the boundary between saltating particles defined in this study as particles > 50 μm and suspended particles <50 μm.

The variation of the mean percent volume distribution of dust particles at each location/size interval was not obvious as to height (Figure 2.9). Coarse silt (20- 50 μm) and very fine sand (50- 100 μm) were the highest with percent volumes ranging from ~20% to less than 25%, respectively. Particles at the ends of the size interval distribution, very fine suspended particles and very coarse saltating particles, respectively, had the lowest mean percent volumes (Figure 2.9). The percent volume at each size interval did not present a considerable variation from dust event to dust event with respect to location (Figure 2.10) The most apparent variation was for the percent volume of very fine sand (50-100 μm) which varied from less than 20% for the 11 March and 17 March dust events to over 20% for the 23 March and 24 March dust events.

Discussion

Influence of temporal variation on particle size distribution

The overall raw particle size distribution (Figure 2.4) of the dust samples along the line transect was multimodal with dominant size fraction peaks in percent volume for coarse silt (20-50 μm) and very fine sand (50-100 μm) indicative of weakly suspended materials (Gillette *et al*. 1997). A third major peak was observed for fine sand (100- 250 μm) indicative of saltating particles and a fourth, less dominant but significant, peak constituted silt and clay particles (1-20μm). This size range, which can be transported over long distances, was known to have high elevated concentrations of several potentially toxic elements (As, Cu, Cr, Pb, etc.) (Ryu *et al.* 2002). The concentration of K, Al, Ti, Mn, Fe, and Rb were known to vary inversely proportional to the mean percent volume of particles in the 0.01–1 μm and 20–100 μm size range during the three dust events (Rojo *et al*. 2008). A less defined peak consisted of coarse sand particles (500 μm - 1000 μm) representing large saltating particles.

The total mean percent volume of dust particles for the combined dust events (Figure 2.5) followed a similar distribution at each respective size interval. Coarse silt particles (20- 50 μm) were the dominant particle size fraction (~22%) followed by very fine sand particles (50-100 μm), ~20%. The left-tail of the distribution exhibited a dominance of fine particles < 20 μm over the right-tail of coarser particles > 250 μm, 37% and 8%, respectively. This dominance is expected for aeolian transport of sediments (Pye 1984; Sun *et al*. 2002). Caution must be taken, however, when using the mean or any other single parameter to assess the distribution of aeolian dust samples since the mean may conceal the effect of temporal and spatial variation on the particle size distribution (Parker and Bloemendal, 2005) and may obscure the extreme values at each size interval. For instance, the maximum and minimum percent volume for coarse silt for the combined dust events was ~34% and ~9%, respectively (Table 2.3), compared to the total mean percent volume of ~22% presented in Figure 2.5. The dust sample containing ~34% in volume of coarse silt was collected during the first dust event on 11 March at a height of 60 cm above the playa surface and the dust sample containing the lowest percent volume of coarse silt

(~9%) was collected during the 23 March dust event at a height of 10 cm above the playa surface. This demonstrates the effect of temporal and spatial variations on the distribution of dust particles and their percent volume at each respective size intervals. Table 2.3 provides the basic statistical parameters for the 133 dust samples analyzed with respect to size interval for the combined dust events and the individual dust events. The negative skewness (tail to the left) indicated that there were more dust samples with percent volumes higher than the mean (to the right of the mean) whereas the positive skewness (tail to the right) indicated that there were more dust samples with percent volumes lower than the mean percent volume at each respective size interval and dust event.

The influence of temporal variation (the sequence of dust events) on the mean percent volume of dust particles at each size interval was evident when each dust event was analyzed separately. Figure 2.6 showed some variation of mean percentages at each size interval. Coarse silt and very fine sand (20-50 μm and 50-100 μm, respectively) continued to be the dominating size fractions, but the percent volume of dust particles at these size intervals varied slightly across the four dust events. The most evident variation in percent volume was for the coarsest saltating particles, coarse sand (500- 1000 μm) and very coarse sand (1000- 2000 μm) where the percent volume of these size intervals increased from dust event to dust event. This is in agreement with the expected changes in the playa's surface composition with dust events and the increasing domination of saltation across the playa. The salt-silt-clay crust gradually eroded on a storm by storm basis (Cahill *et al.* 1996). The first dust event, 11 March, generated minimal amounts of coarse sand and very coarse sand, but produced the second highest mean percent volume of dust particles smaller than 10 μm (PM_{10}) and the second highest mean percent volume of dust particles smaller than 20 μm (PM_{20}), reflecting primarily the deflation of the first layer consisting of efflorescent evaporites. The second dust event, on 17 March, also resulted in high proportional emissions of dust-sized particles, actually generating a slightly higher mean percent volume of dust particles of PM_{10} and PM_{20} than the 11 March dust event. However, there is a

possibility that the high percent volumes of PM_{10} and PM_{20} in the samples collected during 17 March dust event reflect the "blowback" and re-deposition (fallout) of dust back into the array with the reversal of wind direction during this dust event (Cahill *et al.* 1996). Coarser particles were more prominent in the 3rd and 4th dust events (23 March and 24 March, respectively) after the removal of the loose, fine evaporites by the first events (Rojo *et al*. 2008) and the movement of saltating particles, including sand from the Dirty Socks Dunes and Olancha Dunes, north across the transect by southerly winds (Cahill *et al*. 1996). Dust production in the last two events thus had shifted from a suspension-deflation process to a saltation- abrasion process.

The Kruskal–Wallis statistical test (Table 2.4) indicated that the mean percent volume of dust particles at respective size intervals were statistically significantly different at a significance level of $\alpha = 0.05$ for at least two dust events with the exception of medium sand size particles (250-500 μm), $p = 0.30$. Such medium sand particles would be moving in saltation, jumping with the wind just above the surface and playing a role in disintegrating the puffy crusts and releasing finer, dust-sized particles as they impact the surface (Cahill *et al.* 1996; Alfaro *et al*. 1997; Grini *et al*. 2002; Reynolds *et al*. 2007). The saltating medium sands in this case may be comprised of broken pieces of the crust itself (autoabrasion), which has been observed in other intensely-dust- generating playas such as the Bodele Depression of the Sahara (Warren *et al*. 2007), and/or dune sands from the unstabilized Dirty Socks Dunes and Olancha Dunes which were located immediately south of the transect. The movement of saltating particles is directly dependent on wind threshold velocity for which saltating particles can be set in motion. Previous studies show that movement of saltating particles at Owens (dry) Lake may begin at wind speeds of the order of 7 m s^{-1} (Cahill *et al*. 1996).

Influence of spatial variation on particle size distribution

Particle size distribution with respect to height

The Spearman's rho correlation analysis was used to assess the strength and relationship between the mean percent volume of dust particles (in the 11 respective size classes) and height (10, 20, 30, 50, 60 and 100 cm above the playa surface) for the combined and individual dust events (Table 2.5). The mean percent volume at each size interval was strongly correlated with height at a significance level of 0.01 (or 0.05 for some correlations) for the combined dust events and the individual dust events with the exception of the mean percent volume of very fine sand (50-100 μm) with a correlation coefficient of $\rho = 0.12$ (combined dust events) and $\rho = 0.13$ (11 March) (Table 2.5). Very fine sand was significant at $\alpha = 0.05$ for the 17, 23, and 24 March dust events. For the 17 March dust event however, it presented a negative correlation ($\rho = -.40$) indicating a possible decrease in percent volume with increasing height. As previously noted, this dust event was initiated by strong morning southerly winds emitting and transporting dust to the north. Rapid shifts in wind direction backwashed the transported, now-settling dust, north to south back into the sampling array (Cahill *et al*. 1996). This shift in wind direction and backwash and fallout of dust particles may explain the negative correlation on 17 March.

Table 2.2 and Figure 2.8 illustrate that the mean percent volume of very fine sand (50-100 μm) steadily increased from 10 cm to 50 cm for the 11 March dust event and to 30 cm for 17 March through 24 March, but then decreased with increasing height. Unlike the distribution of the mean percent volume of very fine sand, the mean percent volume of clay and silt particles (suspended particles <50 μm) increased with height above the playa, and the mean percent volume of medium to very coarse sand (saltating particles) generally decreased as the heights increased for the four separate dust events (Table 2.2) Particles smaller than 50 μm (silt and clay, "dust") are generally considered suspensive material based on the upper limit of suspension $Vg/u^* = 0.7$ where Vg is the gravitational settling velocity of particles and u^* is the friction velocity defined by $u^* = \sqrt{(\tau/\rho)}$, where τ is the shear stress and ρ is the air density (Qin 2005). Very fine sand size particles on the other hand and also can be weakly suspended (based on

gravitational settling) and not be completely confined to the saltation layer (Gillette *et al*. 1997) but can also be transported by saltation (Menéndez *et al.* 2007). Very fine sand clearly divided the suspended (smaller than 50 μm) particle size intervals from the saltating (greater than 50μm) particle size intervals (Table 2.2). Consequently, dust particles <50 μm were expected to be preferably collected in the upper BSNE collectors (30, 50, 60, and 100 cm) (Figure 2.2) above the transition from saltation to suspension (Fryrear and Saleh 1998) at each height. Saltating particles >50 μm were expected to be captured in the lower BSNE collectors (10 and 20 cm) more than at the BSNE collectors above 20 cm. It is important to note, however, that particles >50 μm may also be uplifted, transported, and deposited in the BSNEs upper collectors. Deposition of particles at a given height depends on a number of factors including wind energy, surface condition, and dust concentrations in the atmosphere (Goossens 2000; Lawrence and Neff 2009).

Figure 2.7 shows that the mean percent volume of suspended particles varied inversely to the mean percent volume of saltating particles with respect to height. From Figure 2.7, it can also be seen that the transition boundary (height in cm) from saltation to suspension mode of the dust particles (Fryrear and Saleh 1998) for the 11 March and 17 March dust events was near 20 cm above the playa's surface where the mean percent volume of saltating and suspended particles were almost equal. For the 23 March and the 24 March data, the transition data boundary (height) from saltation mode to suspension mode of the dust particles was higher, approximately at 30 cm above the playa surface.

The mean percent volume of particles ranging from 100 μm to 2000 μm presented a negative correlation with respect to height (Table 2.5) indicating that the mean percent volume for these particle sizes (fine sand through very coarse sand) consistently decreased as the height above the playa surface increased. The mean percent volume for very coarse sand (1000- 2000 μm) was not correlated to height for the 17 March and 24 March dust events. The inconsistency

of the mean percent volume with respect to height is reflected by the values in Table 2.2. It was not expected to find very coarse particles in the BSNE collectors at height of 50 to 100 cm above the playa surface and that expectation was confirmed in the particle size measurements by laser diffraction for some of the dust samples. It is very possible that coarse sand and very coarse sand particles were not necessarily present in some of the BSNE collectors placed at 50 to 100 cm above the playa; possibly the reported data was erroneous due to measurement error or agglomeration of particles during their storage before analysis. Some of the dust samples analyzed were of limited quantities, and if insufficient sample material is placed in the feeder of the laser diffraction particle sizer, it is possible that the material will run out before the measurement runs are completed. Under these conditions, the lack of material may be reported as spurious presence particles ranging anywhere from ~650 μm to ~2000 μm (based on the author's observations done during cleanout of the equipment after each sample measurement). It is also possible that some particles within this size range were readily available on the playa's surface and were momentarily uplifted and transported by heavy winds. The 11 March dust event generated extremely low percent volumes of coarse and very coarse sand size particles at the different heights above the playa as compared to the other three dust events (Table 2.2). The influence of the reversal of wind direction and re-deposition (fallout) of dust back into the array could also have been reflected in the slightly higher mean percent volume for these coarser dust particles with respect to height for the 17 March dust event. During the 23 and 24 March dust events, winds were blowing from south to north and degrading the salt-silt-clay surface by moving saltating sands, likely including very coarse particles, from the Dirty Socks and Olancha dunes streaming northwards in saltation down across the line transect (Cahill *et al*. 1996).

Particle size distribution with respect to location

The mean percent volume of dust particles for the combined dust events remained fairly constant at each size interval with respect to location (Table 2.6 and Figure 2.9), particularly for the clay, silt, coarse sand and very coarse sand particles. The mean percent volume of fine sand

(100-250 μm) varied the most along the 1.2 km transect increasing approximately by 4% from the H3 location to H4 (Figure 9, Table 2.6). The mean percent volume of particles ranging from very fine to medium silt (2-20 μm), varied proportionally to one another and were almost unchanged from location to location. The percent volume of coarse silt and very fine sand continue to be the predominant percent volumes of the size distribution. Medium sand (250-500 μm) had a slight spike between locations H3 and H4. Coarse sand and very coarse sand were present at all locations at percent volumes <2.5% and 1.5%, respectively.

The variability of the percent volume of the particle size distribution along the transect is important to consider in the sense that the surface of the playa was not homogenous (Gillette *et al.* 2001), and that particle size of grains moving under aeolian action may affect wind erosion of the surface beneath (especially if crushed), sandblasting, saltation, and vertical profiles of aeolian mass flux. The size distribution of the particles in the saltation layer at any wind friction velocity dictates the sandblasting efficiency over this size distribution (Grini *et al*. 2002).

Figure 10 shows the mean percent volume of dust particles with respect to location and dust event. Location S3 for 23 March and S1, S2, and S3 for 24 March are not shown since sample material was unavailable for these location due to adverse conditions which prevented sample collection. In general, the particle size distribution at individual collection points represented a unimodal distribution of particles ranging in size from submicron to very coarse sand. The variation in mean percent volume of dust particles from one location to the other was not obvious with the exception of the (anomalous) 17 March storm, and a slight variation in some of the size interval from dust event to dust event. The correlation of the mean percent volume of dust particles between locations was significant at the 0.01 level for the combined dust events and separate dust events (Pearson correlation test, Table 2.7) indicating that the percent volumes of dust particles were not statistically significantly different between locations. The strength of the correlation of the mean percent volume of dust particles between locations either

became stronger or weaker with respect to dust events (Table 2.7). The most obvious decrease in the Pearson correlation coefficient from the combined dust events to the individual dust events was for the (already shown to be anomalous) 17 March dust event as presented in Table 2.7. Most of the Pearson coefficients were lower between locations as compared to the combined events' correlations. For the 11 March dust event some of the correlations between locations increased and others decreased. For the 23 March dust event, the mean percent volume of dust particles was highly correlated from one location to the other (although the southernmost, farthest-apart S sites could not be sampled). This dust event produced a significant amount of dust generated by southerly winds, and the mean dust concentrations rose from 11 March dust event to the 23 March storm (Cahill *et al*. 1996). The strong correlations, (i.e. $\rho > .90$) may be either confounding or may be explained by the number of factors affecting the nature and rate of dust production, transport, physical change during transport, and deposition.

Conclusions

Particle size distributions of aeolian dust samples collected from Owens (dry) Lake, California during four sequential dust events in March 1993 were measured by laser diffraction (Malvern Mastersizer 2000) to evaluate the influence of temporal and spatial variations of the particle size distributions. Each sample was collected at a unique collection point defined by dust event (four possible dust events), height (10, 20, 30, 50, 60, or 100 cm) above the playa surface and location (seven possible locations) along the 1.2 km line transect. The overall particle size distribution presented its highest peaks at 20- 50 μm, 50- 100 μm and 100- 250 μm (coarse silt to fine sand) with mean percent volumes of ~22% , ~20%, and ~13%, respectively, although particles in the 10- 20 μm range followed by ~12%. The total mean percent volume of finer particles (< 20 μm) was greater than the total mean percent volume of coarser particles (> 250 μm). Statistical tests showed that there was a difference between the mean percent volumes of dust particles at each size interval for at least two dust events with the exception of medium sand (250- 500 μm). Table 2.8 shows that 17 March, when dust was backwashed across the

sampling array after generation, generated the highest percent volume of fine particles between .01 μm and 50 μm. The saltation-dominated 23 March dust event generated the highest mean percent volume of dust particles between 50 μm and 250 μm and the saltation-dominated 24 March generated the highest mean percent volume of dust particles ranging from 250 μm to 2000 μm.

The particle size distribution (in percent volume) along the 1.2 km line transect (study area) revealed that the south sampling locations (S1, S2, S3), in general, experienced higher mean percent volumes of saltating particles (> 50 um) for the 17 March dust event and fine sand (100-250) for the 23 March dust event. The presence of coarse-grained material was most likely moving saltating sand size particles from the Dirty Socks and Olancha dunes streaming northwards in saltation down across the line transect (Cahill *et al.* 1996). Percent volumes of finer dust particles in the north locations (H1, H2, H3, H4) were not notably higher nor lower than the south locations despite being closer to the presumed source area.

Data analysis by dust event provided an overview of the influence of temporal and spatial variation during each dust event. The mean percent volume of dust particles for the overall samples, in most instances, concealed the low and high percent volumes of the distributions. This was best seen in the evaluation of the mean percent volume of dust particles with respect to height. 11 March and 17 March dust events generated an insignificant amount of coarser particles compared to the 23 March and 24 March dust events, otherwise concealed by the overall mean percent volume (Table 2.2). The analysis of the mean percent volume of dust particles with respect to height led to the opportunity to identify a possible transition layer from saltating mode to suspension mode (Figure 2.7) for the aeolian dust events of March 1993 at Owens (dry) Lake, California. This transition boundary (height) is essential data in several equations developed to investigate vertical and horizontal flux of particles from eroding surfaces, in suspension mode, or saltating mode (Goossens and Offer 2000; Ni *et al*. 2002; Offer and

Goossens 2004; Gillette 2007; Li *et al*. 2008; Lawrence and Neff 2009; Dong *et al*. 2010). Very fine sand was identified as the particle size dividing the salting particles from suspension particles. The distribution of the mean percent volume of salting particles (with respect to height) is comparable to the distribution of the total percent mass of saltating particles (with respect to height) calculated from total mass values reported by Cahill *et al*. (1996) as shown in Figure 2.11 and Figure 2.12. These two distributions were highly correlated (best fit power function) with an $R^2 = 0.97$ and $R^2 = 0.95$, respectively. This high correlation not only shows the effect of height on particle size distribution, but also indicates that the results obtained through laser diffraction are reliable. Laser diffraction analysis is a convenient approach to particle size analysis especially when time and sample availability is limited. The ability to measure particles in their dry state, as collected from a dust trap, as was done here, allows us to measure the actual size of the often-agglomerated, salt-bearing particles moving in the wind, as opposed to other techniques which require the disaggregation of particles and dissolution of salts in liquid. Caution must be taken however, in assuring that the correct parameters are used and that sufficient sample is available for accurate and reliable results (Bale 1996; Buurman *et al.* 1997; Sperazza *et al.* 2004; Zobeck 2004).

References

Alfaro, S. C., Gaudichet, A., Gomes, L., Maille, M. 1997. Modeling the size distribution of a soil aerosol produced by sandblasting. *Journal of Geophysical Research 102 (D10): 11239-11249.*

Alfaro, S. C., Rajot, J. L., Gaudichet, A. 2000. Modeling mineral aerosol production by wind erosion: Part 1. Physical bases. *Journal of Aerosol Science 31 (1): 426-427*.

Alfaro, S.C., Gomes, L. 2001. Modeling mineral aerosol production by wind erosion: Emission intensities and aerosol size distribution in source areas. *Journal of Geophysical Research 106 (D16): 18075-18084.*

Alfaro, S. C., Rajot, J. L., Nickling, W. 2004. Estimation of PM20 emissions by wind erosion: main sources of uncertainties. *Geomorphology 59 (1-4): 63-74.*

Anuforom, A.C. 2007. Spatial distribution and temporal variability of Harmattan dust haze in sub-Sahel West Africa. *Atmospheric Environment 41(39): 9079-9090.*

Bale, A.J. 1996. In situ laser optical particle sizing. *Journal of Sea Research 36 (1-2): 31-36*.

Bischoff, J.L., Cummins, K. 2001. Wisconsin Glaciation of the Sierra Nevada 79,000–15,000 yr B.P. as Recorded by Rock Flour in Sediments of Owens Lake, California. *Quaternary Research 55 (1): 14-24.*

Borge, R., Lumbreras, J., Vardoulakis, S., Kassomenos, P., Rodríguez E. 2007. Analysis of long-range transport influences on urban PM10 using two-stage atmospheric trajectory clusters. *Atmospheric Environment 41 (21): 4434-4450.*

Breuning-Madsen, H., Awadzi, T. W. 2005. Harmattan dust deposition and particle size in Ghana. *Catena 63(1): 23-38*.

Buurman, P., de Boer K., Pape, Th. 1997. Laser diffraction grain-size characteristics of Andisols in perhumid Costa Rica: the aggregate size of allophane. *Geoderma 78(1-2): 71-91*.

Cahill, T.A., Gill, T.E., Reid, J.S., Gearhart, E.A., Gillette, D.A. 1996. Saltating Particles, Playa Crusts and Dust Aerosols at Owens dry Lake, California. *Earth Surface Processes and Landforms 21 (7): 621-639.*

Crouvi, O., Amit, R., Enzel, Y., Porat, N., Sandler, A. 2008. Sand dunes as a major proximal dust source for late Pleistocene loess in the Negev Desert, Israel. *Quaternary Research 70(2): 275-282.*

Dong, Z., Man, D., Luo, W., Qian, G., Wang, J., Zhao, M., Liu, S., Zhu, G., Zhu, S. 2010. Horizontal aeolian sediment flux in the Minqin area, a major source of Chinese dust storms. *Geomorphology 116 (1-2): 58-66.*

Fryrear, D. W. 1986. A field dust sampler. *Journal of Soil and Water Consservation. 41(2): 117-120.*

Fryrear, D.W., Saleh, A. 1993. Field wind erosion: vertical distribution. *Soil Science 155:4 294-300.*

Gill, T. E., Gillette, D.A. 1991. Owens Lake: A natural laboratory for aridification, playa desiccation and desert dust. *Geological Society of America Abstracts with Programs 23(5): 462.*

Gill, T.E. 1996. Eolian sediments generated by anthropogenic disturbance of playas: human impacts on the geomorphic system and geomorphic impacts on the human system. *Geomorphology 17 (1-3):207-228.*

Gill, T.E., Gillette, D.A., Niemeyer, T., Winn, R.T. 2002. Elemental geochemistry of wind-erodible playa sediments, Owens Lake, California. *Nuclear Instruments and Methods in Physics Research B189: 209- 213.*

Gillette, D.A., Herbert, G., Stockton, P.H., Owen, P.R. 1996. Causes of the fetch effect in wind erosion. *Earth Surface Processes and Landforms 21: 621- 639.*

Gillette, D. A., Fryrear, D. W., Gill, T. E., Ley, T., Cahill, T. A., Gearhart, E. A. 1997. Relation of Vertical Flux of Particles Smaller than 10 um to Total Aeolian Horizontal Mass Flux at Owens Lake. *Journal of Geophysical Research 102(D22): 26009- 26015.*

Gillette, D.A., Niemeyer, T.C. Helm, P.J. 2001. Supply-limited horizontal sand drift at an ephemerally crusted, unvegetated saline playa. *Journal of Geophysical Research 106 (D16): 18085-18098.*

Gillette, D.A., Ono, D., Richmond, K. 2004. A combined modeling and measurement technique for estimating windblown dust emissions at Owens dry Lake, California. *Journal of Geophysical Researc 109(F1): F01003.*

Goossens, D., Offer, Z.Y. 2000. Wind tunnel and field calibration of six aeolian dust samplers. *Atmospheric Environment 34(7): 1043-1057.*

Grini, A., Zender, C.S., Colarco, P.R. 2002. Saltation Sandblasting behavior during mineral dust aerosol production. *Geophysical Research Letters 29(18): 1868.*

Güler, C., Thyne, G.D. 2004. Hydrologic and geologic factors controlling surface and groundwater chemistry in Indian Wells-Owens Valley area, southeastern California, USA. *Journal of Hydrology 285(1-4): 177-198.*

Harrison, R. M., Deacon, A. R., Jones, M. R., Appleby R. S. 1997. Sources and processes affecting concentrations of PM10 and PM2.5 particulate matter in Birmingham U.K.. *Atmospheric Environment 31(24): 4103-4117.*

Lawrence, C.R., Neff, J.C. 2009. The contemporary physical and chemical flux of aeolian dust: A synthesis of direct measurements of dust deposition. *Chemical Geology 267(1-2): 46-63.*

Lee, B.K., Lee, H.K., Jun, N.Y. 2006. Analysis of regional and temporal characteristics of PM10 during an Asian dust episode in Korea. *Chemosphere 63(7): 1106-1115.*

Levy, D.B., Schramke, J.A., Esposito, K.J., Erickson, T.A., Moore, J.C. 1999. The shallow ground water chemistry of arsenic, fluorine, and major elements: Eastern Owens Lake, California *Applied Geochemistry 14(1): 53-65.*

Li, Z.S., Feng, D.J., Wu, S.L., Borthwick, A.G.L., Ni J.R. 2008. Grain size and transport characteristics of non-uniform sand in aeolian saltation *Geomorphology 100(3-4): 484-493.*

Littmann, T. 1997. Atmospheric input of dust and nitrogen in the Nizzana sand dune ecosystem, north-western Negev, Israel. *Journal of Arid Environments 36: 433-457.*

MacKinnon, D.J., Chavez, P.S. Jr., Fraser, R.S., Niemeyer, T.C., Gillette, D.A. 1996. Calibration of GOES-VISSR, visible-band satellite data and its application to the analysis of a dust storm at Owens Lake, California. *Geomorphology 17(1-3): 229-248.*

Menéndez, I., Díaz-Hernández, J.L., Mangas, J., Alonso, I., Sánchez-Soto, P.J. 2007. Airborne dust accumulation and soil development in the North-East sector of Gran Canaria, Canary Islands, Spain. *Journal of Aird Environments 71(1): 57-81.*

Ni, J. R., Li, Z. S., Mendoza, C. 2002. Vertical profiles of aeolian sand mass flux. *Geomorphology 49(3-4): 205-218.*

Offer, Z., Goossens, D. 2004. Thirteen years of aeolian dust dynamics in a desert region, Negev desert, Israel: analysis of horizontal and vertical dust flux, vertical dust distribution and dust grain size. *Journal of Arid Environments 57(1): 117-140*.

Ono, D. 2006. Application of the Gillette model for windblown dust at Owens Lake, CA. *Atmospheric Environment, 40(17): 3011-3021.*

Parker, E.J., Bloemendal, J. 2005. Aeolian process and pedogenesis under the influence of the East Asian monsoon: A statistical approach to particle-size distribution variability. *Sedimentary Geology 181(3-4): 195-206.*

Pelletier, J.D. 2006. Sensitivity of playa windblown-dust emissions to climatic and anthropogenic change. *Journal of Arid Environments 66(1): 62-75.*

Pongkiatkul, P., Oanh, N. T. K. 2007. Assessment of potential long-range transport of particulate air pollution using trajectory modeling and monitoring data. *Atmospheric Research 85(1): 3-17.*

Pye, K. 1984. Loess. *Progress in Physical Geography 8: 176 - 217.*

Qin, Xiaoguang, Cai, Binggui, Liu, Tungsheng 2005. Loess record of the aerodynamic environment in the east Asia monsoon area since 60,000 years before present. *Journal of Geophysical Research 100D: B01204.*

Reynolds, R.L., Yount, J.C., Reheis, M., Goldstein, H., Chavez Jr., P., Fulton, R., Whitney, J., Fuller, C., Forester, R.M. 2007. Dust emission from wet and dry playas in the Mojave Desert, USA. *Earth Surface Processes and Landforms 32: 1811–1827*.

Rojo, L., Gill, T.E., Gillette, D.A. 2008. Particle size/composition relationships of wind-eroding sediments, Owens dry Lake, California, USA. *X-Ray Spectrometry 37: 111- 115.*

Roney A., White B. R. 2006. Estimating fugitive dust emission rates using an environmental boundary layer wind tunnel. *Atmospheric Environment 40(40): 7668-7685.*

Ryu, J. I. H., Gao, S., Dahlgren, R.A., Zierenberg, R.A. 2002. Arsenic distribution, speciation and solubility in shallow groundwater of Owens Dry Lake, California. *Geochimica et Cosmochimica Acta 66(17): 2981-2994.*

Schultz, B.W. 2001. Extent of vegetated wetlands at Owens Dry Lake, California, U.S.A, between 1977 and 1992. *Journal of Arid Environments 48: 69–87.*

Sperazza, M., Moore, J.N., Hendrix, M.S. 2004. High-Resolution Particle Size Analysis of Naturally Occurring Very Fine-Grained Sediment Through Laser Diffractometry. *Journal of Sedimentary Research 74(5): 736-743.*

Sun, D., Bloemendal, J., Rea, D.K., Vandenberghe, J., Jiang, F., An, Z., Su, R. 2002. Grain-size distribution function of polymodal sediments in hydraulic and aeolian environments, and numerical partitioning of the sedimentary components. *Sedimentary Geology 152: 263-277.*

Tyler, S.W., Kranz, S., Parlange, M.B., Albertson, J., Katul, G.G., Cochran, G.F., Lyles, B.A., Holder, G. 1997. Estimation of groundwater evaporation and salt flux from Owens Lake, California, USA. *Journal of Hydrology 200(1-4): 110-135.*

Warren, A., Chappell, A., Todd, M.C., Bristow, C., Drake, N., Engelstaedter, S., Martins, V., M'bainayel, S., Washington, R. 2007. Dust-raising in the dustiest place on Earth. *Geomorphology 92(1): 25- 37.*

Zobeck,T. M., Sterk, G., Funk, R., Rajot, J.L., Stout, J.E., Van Pelt, R.S. 2003. Measurement and data analysis methods for field-scale wind erosion studies and model validation. *Earth Surface Processes and Landforms 28(11): 1163- 1188.*

Zobeck, T.M. 2004. Rapid particle size analyses using laser diffraction. *Applied Engineering in Agriculture 20(5): 633-639.*

Tables

Table 2.1 Size intervals for assessment of aeolian dust particle size (μm)

very fine clay	clay	very fine silt	Fine silt	medium silt	coarse silt	very fine sand	fine sand	medium sand	coarse sand	very coarse sand
vfc	c	vfs	Fs	Ms	cs	vfsd	fsd	msd	csd	vcsd
.01-1	1-2	2-5	5-10	10-20	20-50	50-100	100-250	250-500	500-1000	1000-2000

Table 2.2 Percent volume of dust particles with respect to location and dust event

Dust Event	VFC (.01-1)	C (1-2)	VFS (2-5)	FS (5-10)	MS (10-20)	CS (20-50)	VFSD (50-100)	FSD (100-250)	MSD (250-500)	CSD (500-1000)	VCSD (1000-2000)
Mar 1993 – combined dust events											
10 cm	.48	2.70	5.82	6.38	7.06	12.62	17.90	30.23	13.57	2.12	1.13
20	.89	2.92	6.70	7.79	8.66	16.20	20.10	22.94	10.28	2.22	1.30
30	2.10	3.42	9.16	11.26	12.24	23.28	22.05	10.42	3.62	1.54	.91
50	2.63	3.39	10.14	12.66	13.77	25.94	21.64	6.18	1.10	1.53	1.01
60	2.82	3.50	10.59	13.12	14.42	27.60	21.03	4.95	.57	.88	.52
100	2.91	3.59	10.94	13.62	15.37	27.53	18.97	4.57	1.44	.96	.09
11 Mar											
10 cm	.56	2.89	6.51	7.57	8.20	13.18	16.96	30.01	12.81	.88	.43
20	1.14	2.96	7.48	9.39	10.17	17.25	19.36	22.14	8.63	.78	.69
30	2.34	3.20	9.66	12.39	13.05	24.11	20.49	10.46	4.05	.24	.00
50	2.83	3.28	10.59	13.67	14.19	27.39	21.73	5.12	.72	.47	.00
60	2.91	3.41	10.97	13.65	14.07	28.77	21.15	3.92	.89	.26	.00
100	3.26	3.66	12.77	16.29	16.91	27.52	16.64	2.82	.12	.00	.00
17 Mar											
10 cm	.55	2.60	5.94	6.55	7.07	12.26	17.31	33.55	12.95	.99	.25
20	1.45	2.97	7.80	9.24	10.04	18.23	19.23	21.08	6.86	1.29	1.80
30	2.97	3.63	10.98	13.62	14.74	25.68	19.36	6.35	1.63	.69	.36
50	3.23	3.77	11.88	15.07	16.56	27.22	17.10	3.36	1.34	.47	.00
60	3.23	3.77	11.85	15.10	16.97	28.10	16.06	2.50	.26	1.18	.99
100	3.32	3.79	12.03	15.24	17.74	29.66	15.04	1.66	1.25	.28	.00
23 Mar											
10 cm	.35	2.42	4.94	5.21	6.14	12.57	19.70	29.49	13.01	3.64	2.52
20	.50	2.79	5.58	6.22	7.38	15.76	22.42	24.53	11.31	2.41	1.08
30	1.31	3.31	7.27	8.76	10.09	21.87	25.87	12.91	3.76	3.05	1.81
50	2.04	3.21	8.40	10.21	11.78	25.45	26.33	9.43	.87	1.29	.97
60	2.40	3.30	9.18	11.12	12.80	26.94	24.58	7.11	.73	1.22	.62
100	2.40	3.32	9.10	10.96	12.87	26.32	22.43	7.20	2.76	2.33	.31
24 Mar											
10 cm	.42	2.89	5.80	5.82	6.46	12.15	17.58	27.57	16.53	3.43	1.34
20	.54	3.00	6.11	6.26	6.93	13.24	18.58	23.60	14.64	5.05	2.05
30	1.40	3.53	8.02	9.17	9.90	19.98	23.38	13.75	6.26	2.74	1.88
50	2.13	3.18	8.92	10.33	11.15	21.91	22.40	8.08	1.67	5.60	4.63
60	2.58	3.49	9.82	11.73	13.01	25.70	24.24	7.80	.29	.88	.46
100	2.74	3.62	10.25	12.50	14.02	26.16	22.01	6.76	1.09	.85	.00

Table 2.3 Basic statistical parameters: mean percent volume of dust particles

Statistical Parameter	very fine clay	clay	very fine silt	fine silt	medium silt	coarse silt	very fine sand	fine sand	medium sand	coarse sand	very coarse sand
	.01-1	1-2	2-5	5-10	10-20	20-50	50-100	100-250	250-500	500-1000	1000-2000
March 93 -combined dust events											
Mean	2.0	3.3	8.9	10.9	12.0	22.4	20.4	12.9	4.9	1.5	0.8
Median	2.3	3.3	9.1	10.7	12.3	24.9	20.4	8.3	2.0	0.3	0.0
Kurtosis	-1.4	0.5	-0.8	-1.0	-1.1	-0.9	-0.7	-0.1	0.2	6.4	10.0
Skewness	-0.3	-0.7	0.0	0.0	-0.1	-0.6	0.1	1.0	1.2	2.3	2.8
Minimum	0.1	1.4	3.5	3.6	4.5	9.1	12.3	1.0	0.0	0.0	0.0
Maximum	3.7	4.3	15.1	18.4	19.5	34.3	30.3	43.6	22.6	14.0	10.5
11-Mar-93											
Mean	2.1	3.2	9.5	11.9	12.5	22.8	19.6	13.0	4.8	0.5	0.2
Median	2.6	3.2	9.7	12.9	13.4	25.1	19.8	6.3	1.8	0.0	0.0
Kurtosis	-1.3	0.4	-0.6	-1.1	-1.2	-0.8	0.4	-1.1	0.8	4.3	15.1
Skewness	-0.6	-0.3	0.0	-0.2	-0.4	-0.4	0.3	0.8	1.3	2.2	3.7
Minimum	0.3	2.1	5.1	5.8	6.1	9.4	12.3	2.0	0.0	0.0	0.0
Maximum	3.7	4.2	15.1	18.4	17.8	34.3	28.8	34.3	22.6	3.1	3.0
17-Mar-93											
Mean	2.6	3.5	10.4	13.0	14.4	24.4	17.3	9.7	3.4	0.8	0.5
Median	3.1	3.7	11.1	13.9	16.0	26.5	17.0	4.2	1.3	0.0	0.0
Kurtosis	0.1	-0.1	-0.4	-0.1	-0.1	0.7	-0.6	1.9	3.6	13.7	13.8
Skewness	-1.2	-0.9	-0.9	-1.0	-1.0	-1.4	0.4	1.8	2.0	3.4	3.5
Minimum	0.2	1.8	4.1	4.3	5.1	9.7	12.6	1.0	0.0	0.0	0.0
Maximum	3.6	4.3	13.5	17.0	19.5	32.7	24.2	43.6	20.8	8.3	6.9
23-Mar-93											
Mean	1.5	3.1	7.4	8.7	10.2	21.5	23.6	15.1	5.4	2.3	1.2
Median	1.4	3.3	7.4	9.1	10.5	22.7	23.8	11.6	2.0	1.5	0.4
Kurtosis	-1.6	1.1	-1.1	-1.2	-1.1	-1.1	-0.5	0.4	-1.2	6.4	-0.3
Skewness	0.1	-1.2	-0.3	-0.3	-0.3	-0.5	0.0	1.1	0.7	2.2	1.0
Minimum	0.1	1.4	3.5	3.6	4.4	9.0	17.2	4.5	0.0	0.0	0.0
Maximum	3.1	3.9	10.7	12.6	14.8	29.2	30.3	42.0	16.6	14.0	5.1
24-Mar-93											
Mean	1.6	3.3	8.2	9.3	10.2	19.9	21.4	14.6	6.7	3.1	1.7
Median	1.9	3.4	8.2	9.5	10.3	20.7	21.9	9.8	4.3	3.1	0.4
Kurtosis	-1.6	-0.7	-1.2	-1.2	-1.4	-1.4	-0.8	-0.7	-0.8	-0.5	4.8
Skewness	-0.1	-0.7	-0.2	-0.2	-0.1	-0.4	-0.4	0.8	0.8	0.6	2.1
Minimum	0.4	2.6	5.1	5.0	5.9	10.7	14.6	4.8	0.0	0.0	0.0
Maximum	3.0	3.8	11.0	13.4	14.9	26.7	26.5	33.1	20.7	10.1	10.5

Table 2.4 Kruskal-Wallis Test: difference in percent volume between dust events

	VFC (.01-1)	C (1-2)	VFS (2-5)	FS (5-10)	MS (10-20)	CS (20-50)	VFSD (50-100)	FSD 100-250	MSD (250-500)	CSD (500-1000)	VCSD (1000-2000)
Chi-Square	24.89	12.09	27.42	31.12	28.75	11.31	48.40	20.40	3.69	19.59	22.37
Df	3	3	3	3	3	3	3	3	3	3	3
Asymp. Sig.	.000	.007	.000	.000	.000	.010	.000	.000	.297	.000	.000

Grouping Variable: Dust Event

Table 2.5 Spearman's rho correlation: between mean percent volume and height

Correlation of mean percent volume of dust particles and height (10,20,30,50,60,100cm)

Dust events	VFC (.01-1)	C (1-2)	VFS (2-5)	FS (5-10)	MS (10-20)	CS (20-50)	VFSD (50-100)	FSD (100-250)	MSD (250-500)	CSD (500-1000)	VCSD (1000-2000)
Combined dust events at each size interval											
Mar-93	0.73	0.53	0.69	0.69	0.73	0.83	0.12(nc)	-0.83	-0.78	-0.46	-0.35
Individual dust events at each size interval											
11-Mar	0.82	0.52	0.77	0.75	0.75	0.82	0.13(nc)	-0.93	-0.79	-0.54	-0.46
17-Mar	0.72	0.55	0.65	0.70	0.81	0.88	-.40(*)	-0.94	-0.67	-.39(*)	-0.30(nc)
23-Mar	0.80	0.57	0.81	0.82	0.83	0.85	.34(*)	-0.91	-0.76	-0.51	-0.49
24-Mar	0.93	0.67	0.90	0.93	0.95	0.92	.52(*)	-0.90	-0.87	-.43(*)	-0.28(nc)

correlation was significant at the 0.01 level unless noted otherwise (2- tailed)

(*) correlation is significant at the 0.05 level (2- tailed)

(nc) no correlation

Table 2.6 Percent volume of dust particles with respect to location and dust events

Loc.	VFC (.01-1)	C (1-2)	VFS (2-5)	FS (5-10)	MS (10-20)	CS (20-50)	VFSD (50-100)	FSD (100-250)	MSD (250-500)	CSD (500-1000)	VCSD (1000-2000)
H1	2.22	3.48	9.44	11.66	12.79	23.76	20.75	10.45	3.97	1.02	.46
H2	2.09	3.40	9.06	10.92	12.10	22.96	20.47	11.97	4.54	1.52	.97
H3	2.19	3.47	9.39	11.24	12.30	23.23	19.94	10.66	4.99	1.81	.76
H4	1.78	3.29	8.49	10.03	11.13	20.93	19.25	14.31	7.69	2.16	.95
S1	1.96	3.27	9.26	11.08	11.81	20.74	19.75	15.74	4.51	.92	.97
S2	1.86	2.90	8.43	10.60	11.96	22.33	21.62	13.75	4.10	1.70	.74
S3	1.76	2.71	8.11	10.32	11.61	22.22	21.07	15.28	4.21	1.56	1.16

Table 2.7 Pearson correlation between locations (percent volume)

Dust events		H1	H2	H3	H4	S1	S2	S3
Combined dust events	H1		0.74	0.76	0.76	0.83	0.85	0.75
	H2	0.74		0.89	0.87	0.76	0.71	0.61
	H3	0.76	0.89		0.88	0.75	0.72	0.62
	H4	0.76	0.87	0.88		0.84	0.78	0.74
	S1	0.83	0.76	0.75	0.84		0.93	0.96
	S2	0.85	0.71	0.72	0.78	0.93		0.93
	S3	0.75	0.61	0.62	0.74	0.96	0.93	
11-Mar	H1		0.63	0.67	0.63	0.92	0.97	0.90
	H2	0.63		0.65	0.76	0.64	0.65	0.66
	H3	0.67	0.65		0.77	0.68	0.69	0.68
	H4	0.63	0.76	0.77		0.74	0.68	0.74
	S1	0.92	0.64	0.68	0.74		0.97	0.97
	S2	0.97	0.65	0.69	0.68	0.97		0.95
	S3	0.90	0.66	0.68	0.74	0.97	0.95	
17-Mar	H1		0.48	0.48	0.58	0.69	0.75	0.60
	H2	0.48		1.00	0.84	0.66	0.67	0.57
	H3	0.48	1.00		0.84	0.66	0.67	0.56
	H4	0.58	0.84	0.84		0.82	0.82	0.74
	S1	0.69	0.66	0.66	0.82		0.94	0.96
	S2	0.75	0.67	0.67	0.82	0.94		0.91
	S3	0.60	0.57	0.56	0.74	0.96	0.91	
23-Mar	H1		0.94	0.97	0.95	0.90	0.84	na
	H2	0.94		0.97	0.98	0.98	0.85	na
	H3	0.97	0.97		0.98	0.94	0.84	na
	H4	0.95	0.98	0.98		0.96	0.86	na
	S1	0.90	0.98	0.94	0.96		0.88	na
	S2	0.84	0.85	0.84	0.86	0.88		na
	S3	na	na	na	na	na	na	na
24-Mar	H1		0.91	0.96	0.89	na	na	na
	H2	0.91		0.97	0.93	na	na	na
	H3	0.96	0.97		0.96	na	na	na
	H4	0.89	0.93	0.96		na	na	na
	S1	na	na	na	na	na	na	na
	S2	na	na	na	na	na	na	na
	S3	na	na	na	na	na	na	na

All correlations were significant at the 0.01 level (2-tailed)
na - no sample available

Table 2.8 Mean percent volume of dust particles: per size interval and dust events

Dust Event	.01-1	1-2	2-5	5-10	10-20	20-50	50-100	100-250	250-500	500-1000	1000-2000
11-Mar	2.1	3.2	9.5	11.9	12.5	22.8	19.6	13.0	4.8	0.5	0.2
17-Mar	2.6	3.5	10.4	13.0	14.4	24.4	17.3	9.7	3.4	0.8	0.5
23-Mar	1.5	3.1	7.4	8.7	10.2	21.5	23.6	15.1	5.4	2.3	1.2
24-Mar	1.6	3.3	8.2	9.3	10.2	19.9	21.4	14.6	6.7	3.1	1.7

Figure 2.1 Owens (dry) Lake, California (www.nasa.gov/centers/johnson)

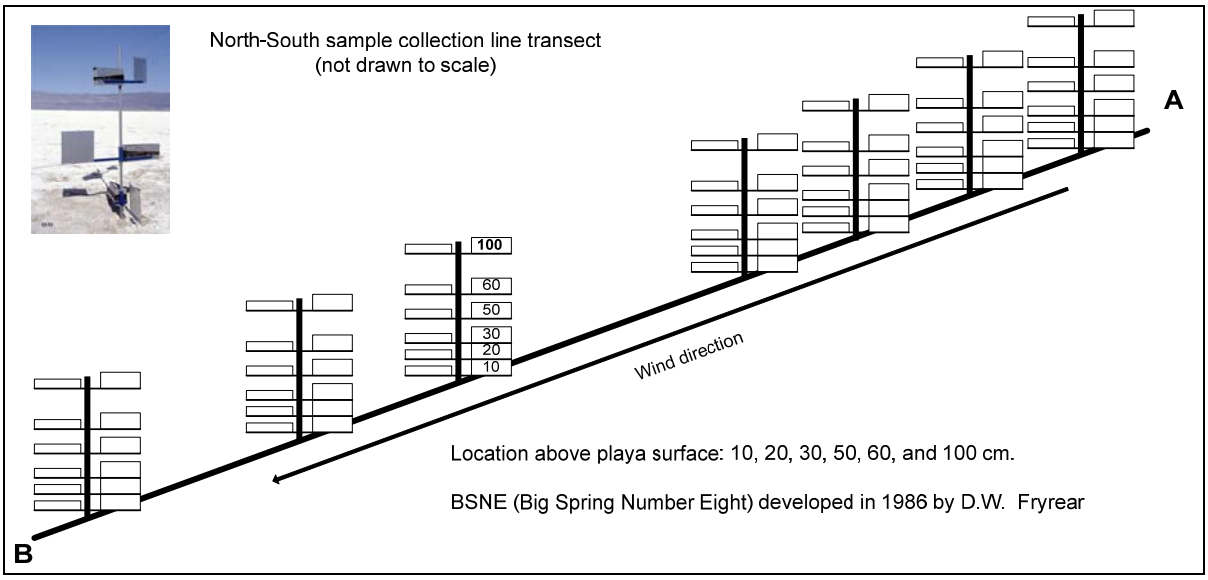

Figure 2.2 BSNE and 1.2 km line transect

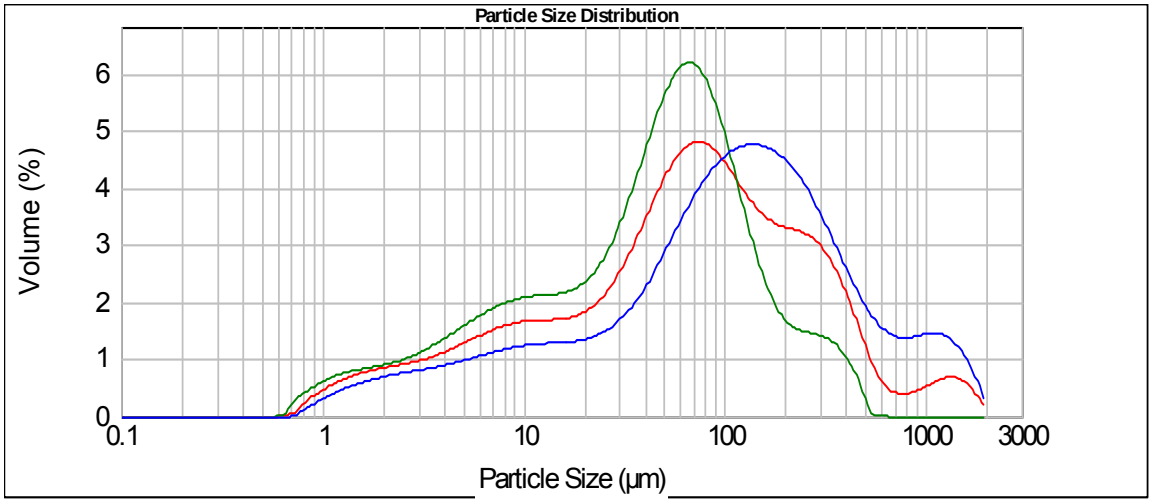

Figure 2.3 Sample particle size distribution for three samples measured by laser diffraction

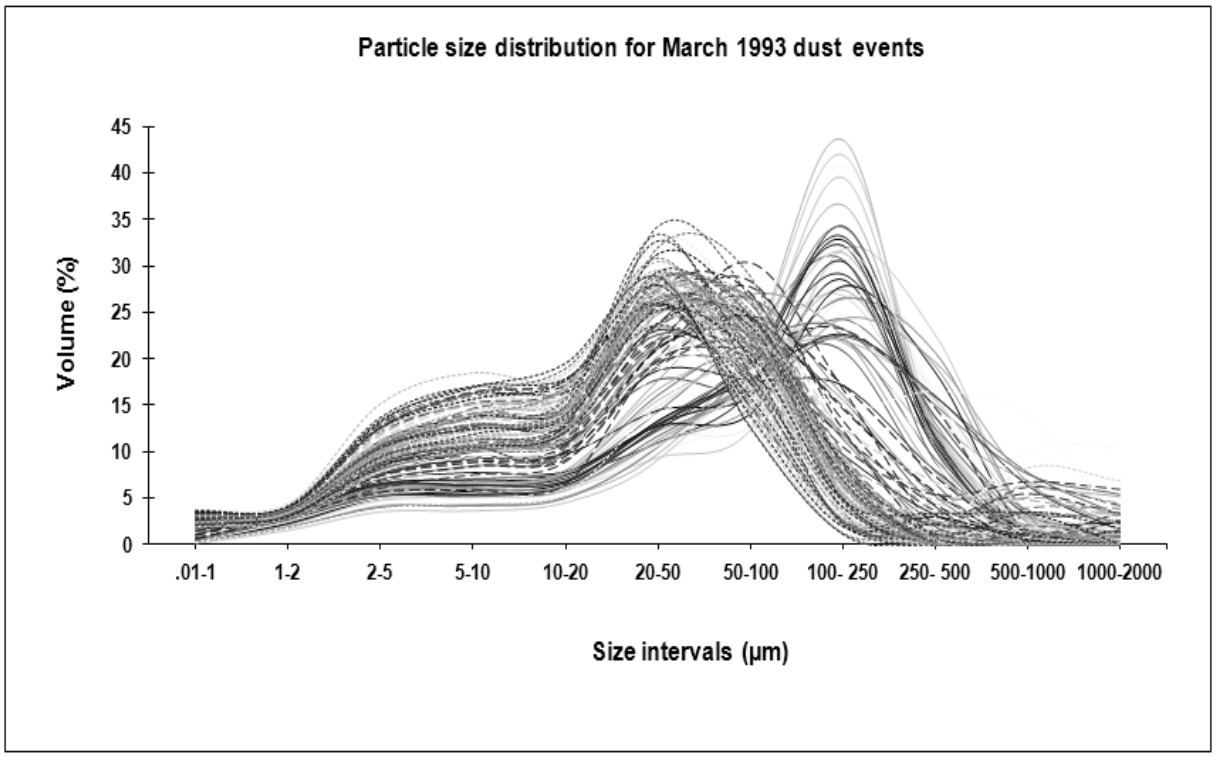

Figure 2.4 Particle size distribution for the combined March 1993 dust events

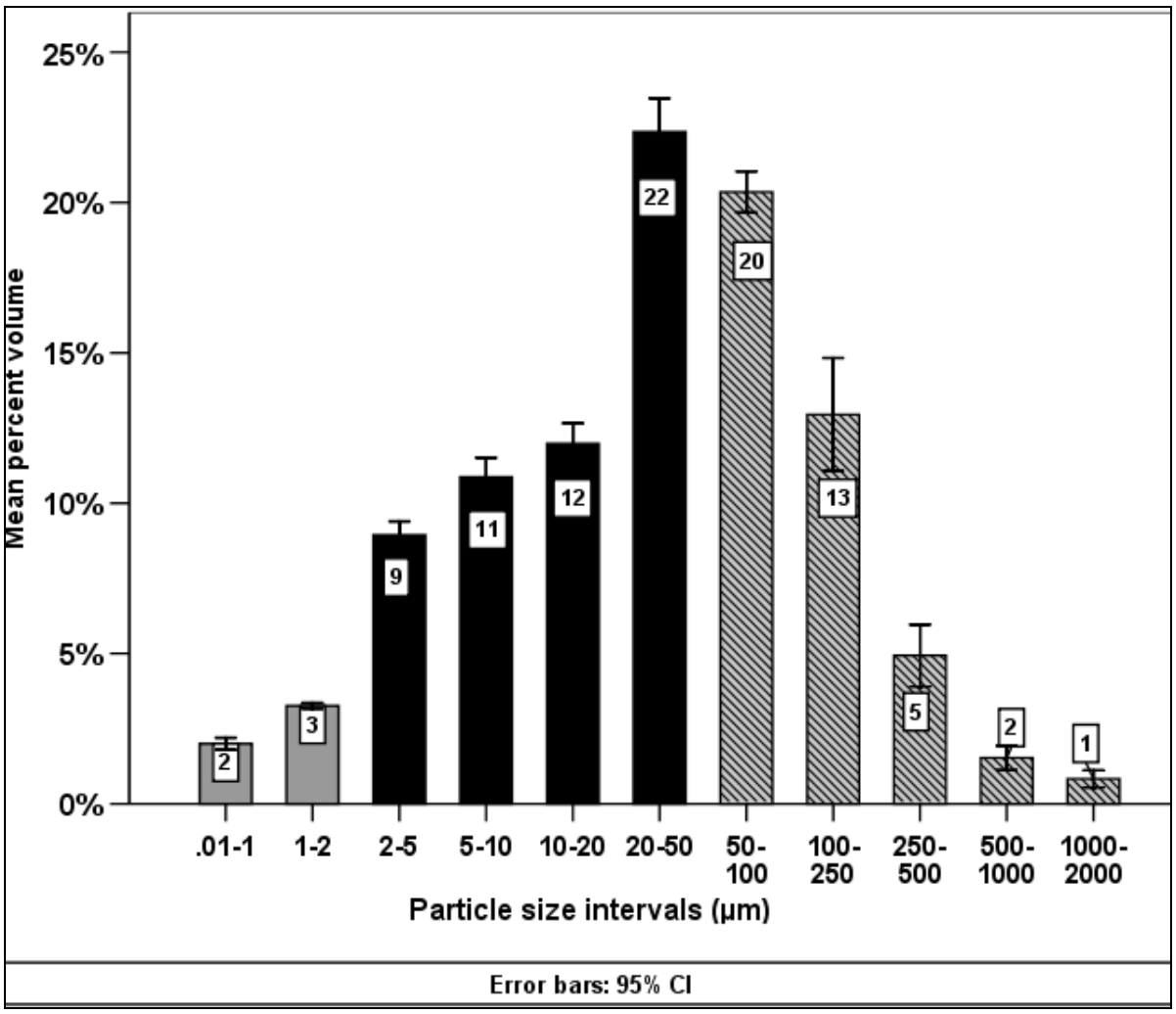

Figure 2.5 Mean percent volumes: clay (solid gray), silt (black) and sand (lined) March 1993

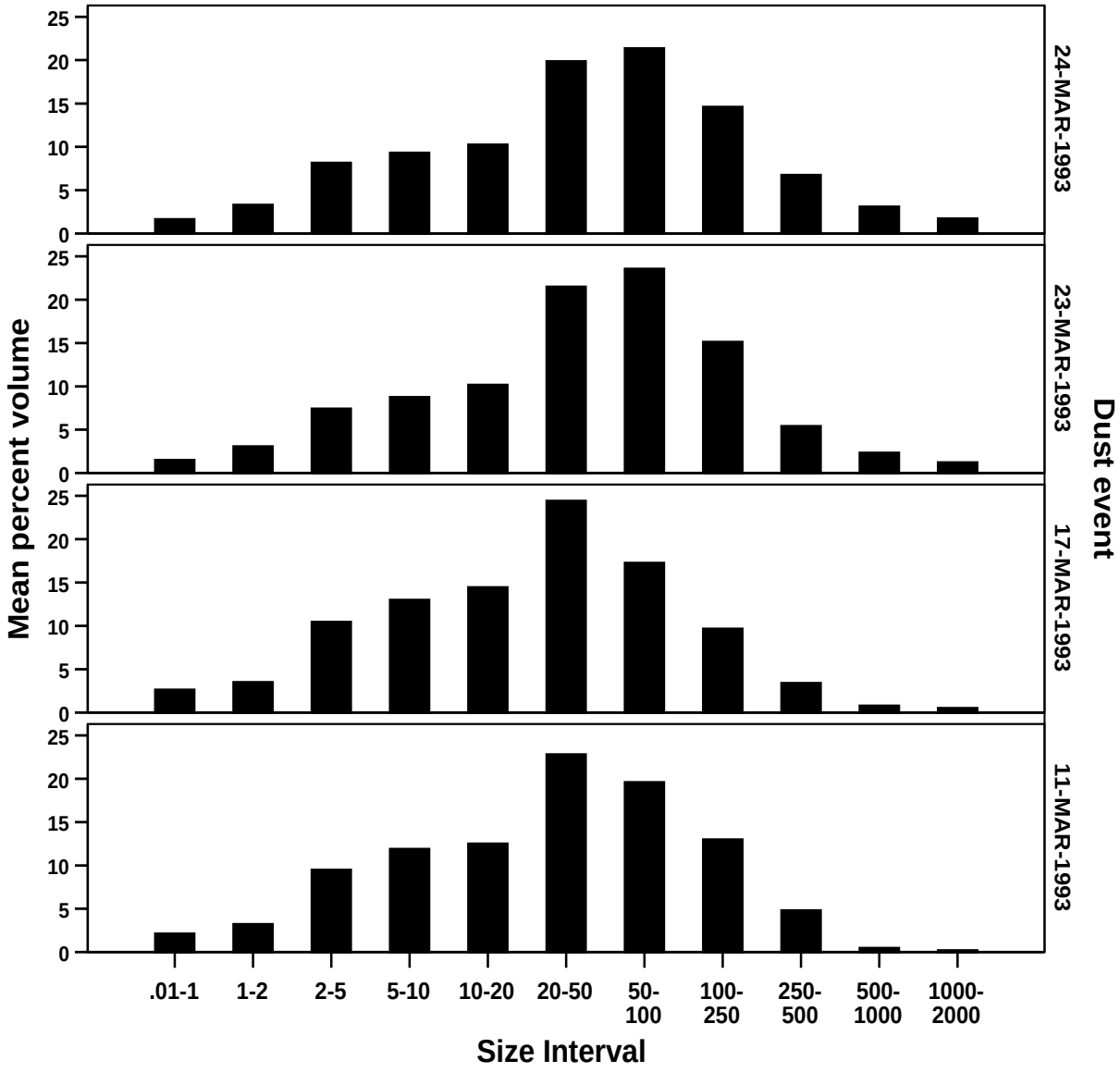

Figure 2.6 Mean percent volume of dust particles: Four dust events

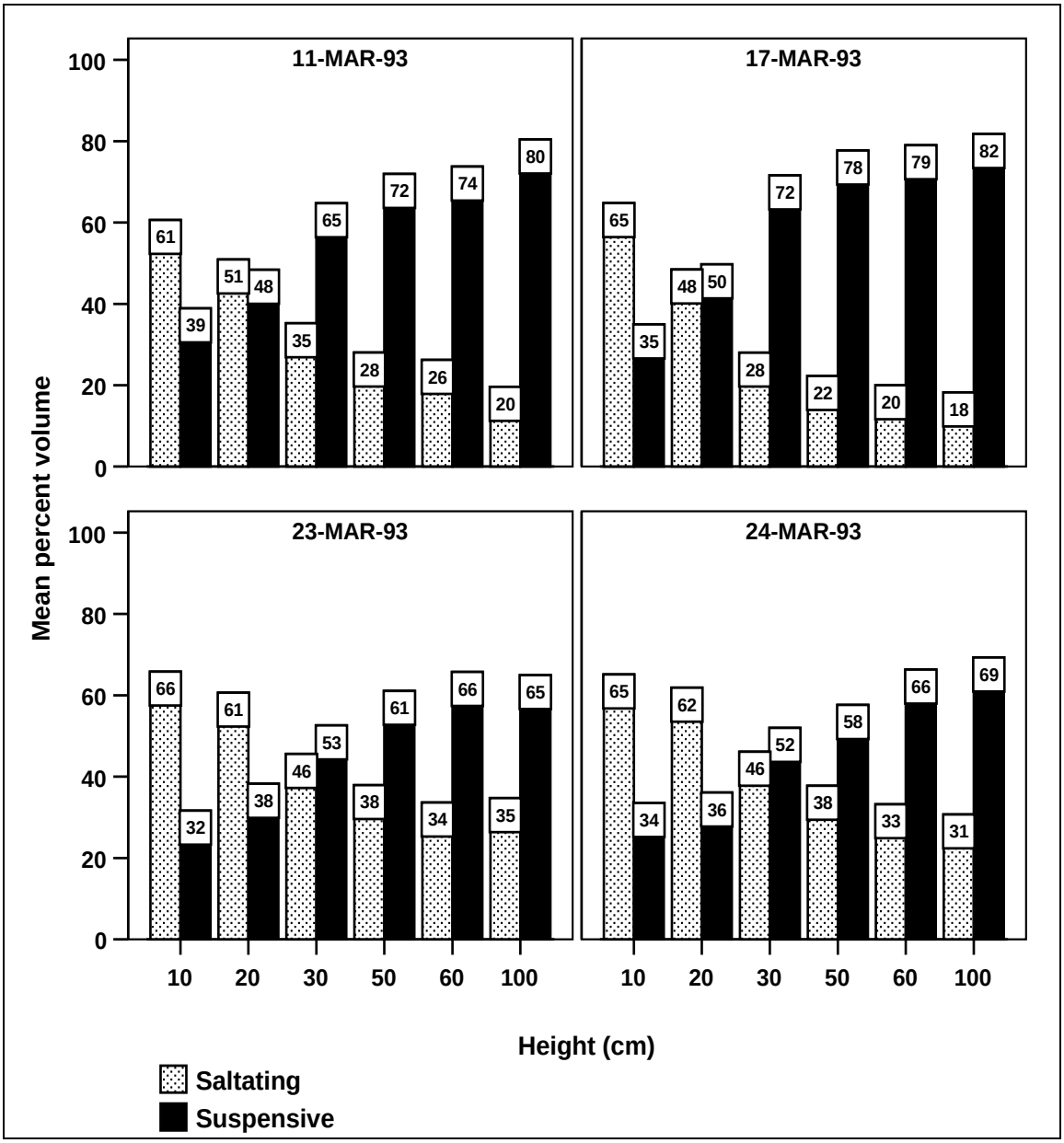

Figure 2.7 Mean percent volume of saltating/suspended particles: height and dust event

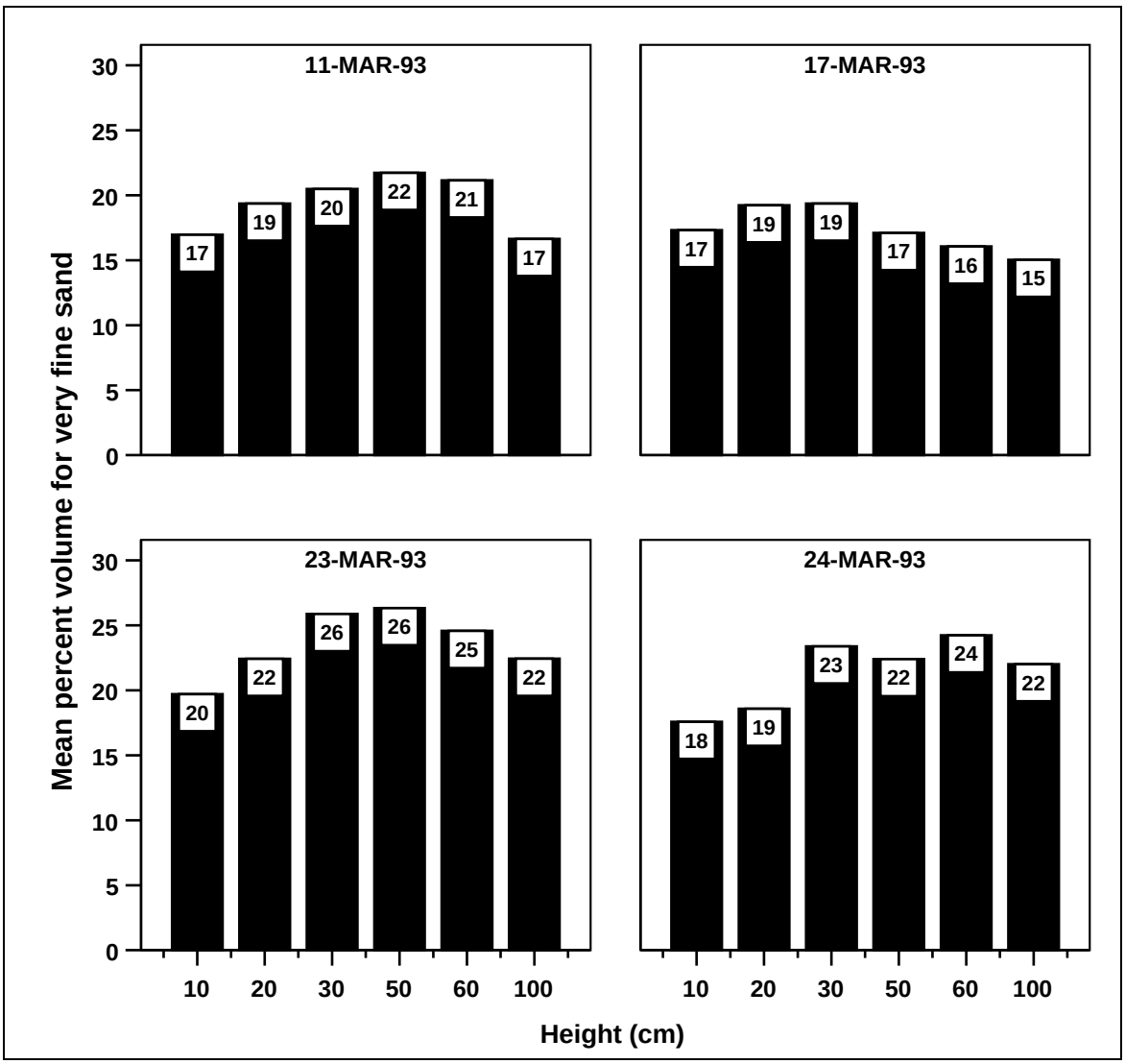

Figure 2.8 Mean percent volume of very fine sand: height and dust events

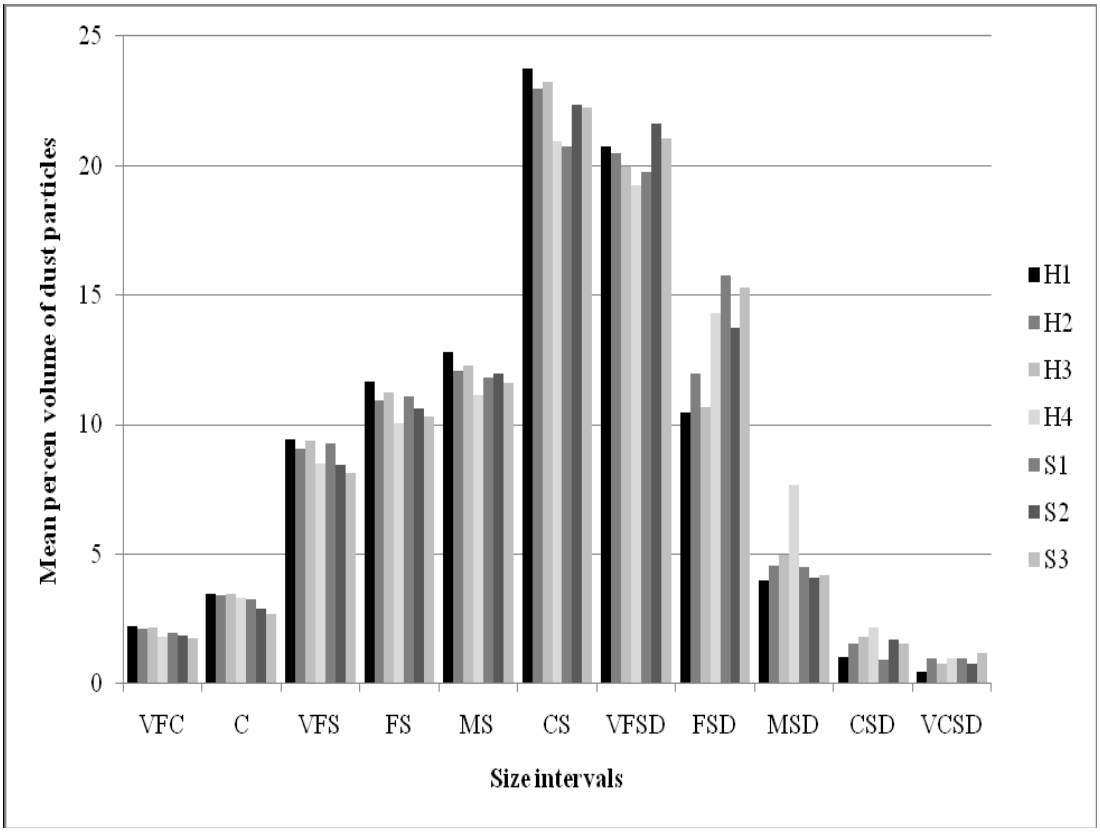

Figure 2.9 Influence of location on the mean percent volume of dust particles: March 1993

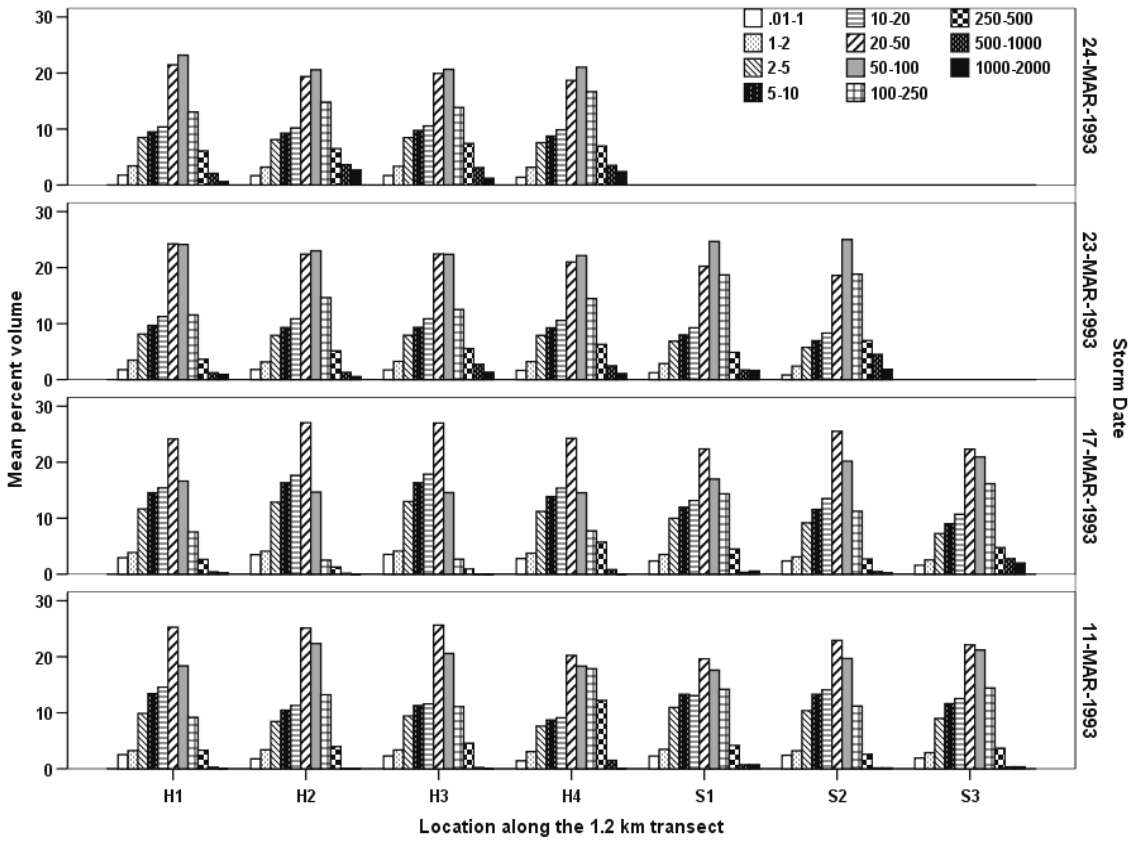

Figure 2.10 Variation of the mean percent volume: location and dust event

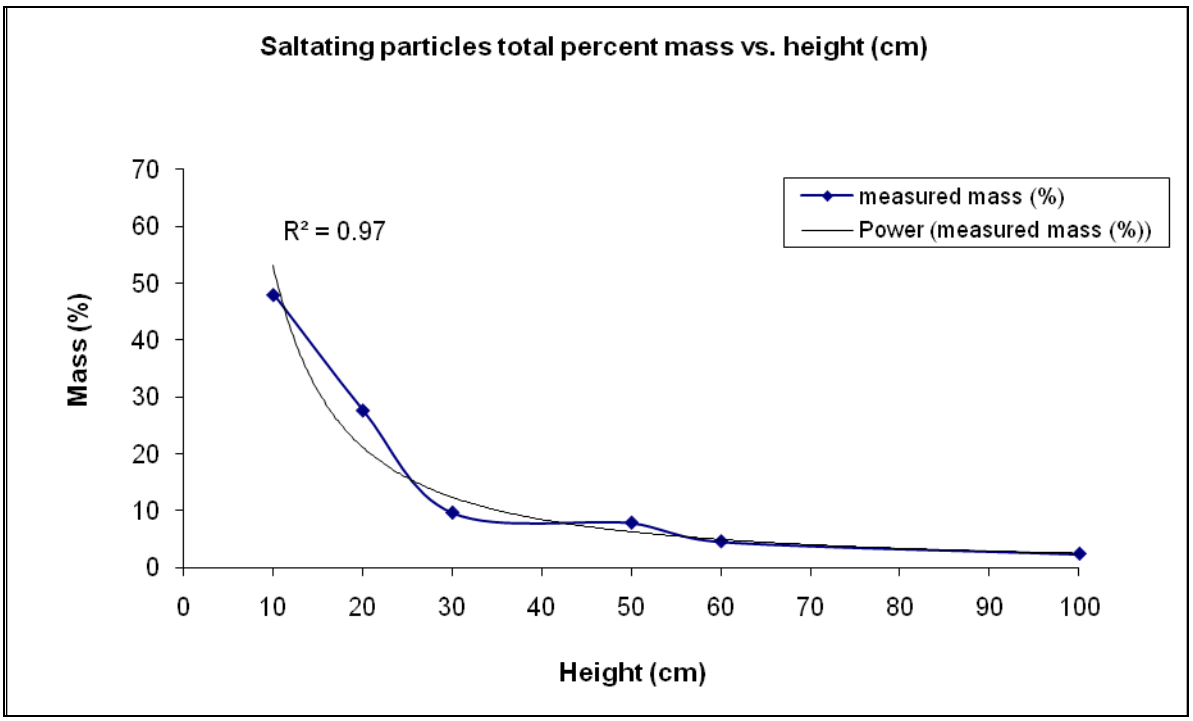

Figure 2.11 Saltating particles: percent mass vs. height (cm) (after Cahill *et al*., 1996)

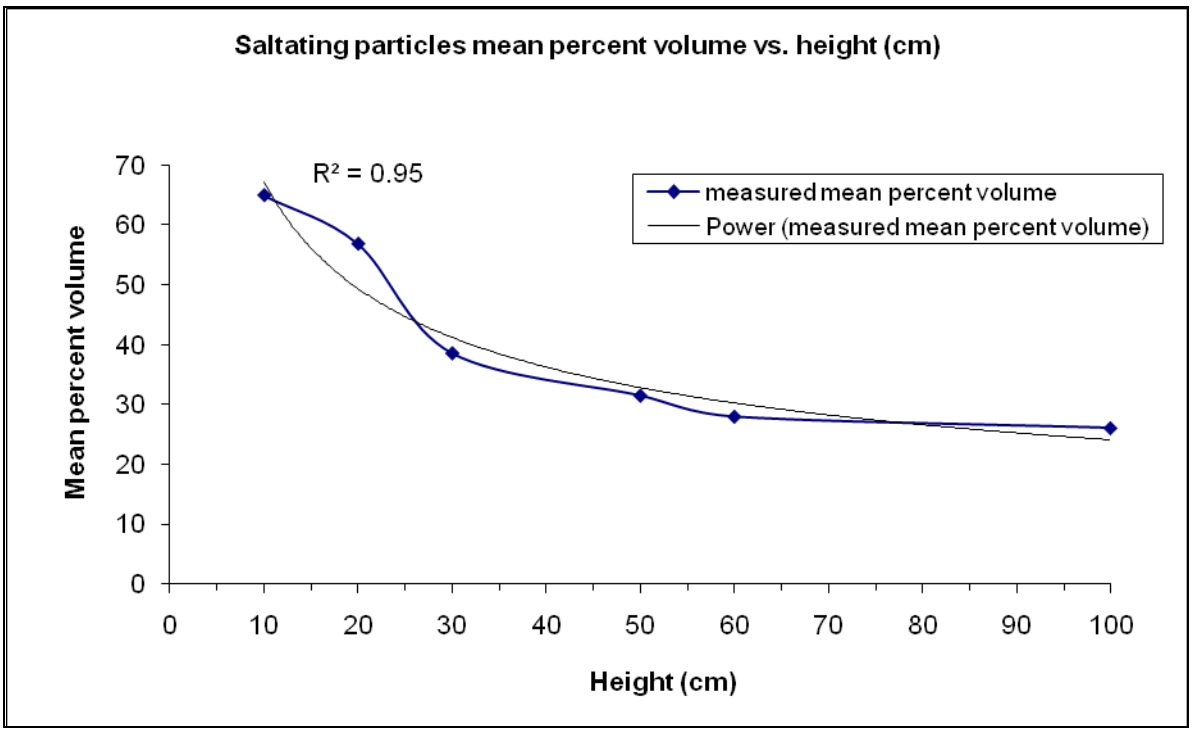

Figure 2.12 Saltating particles: mean percent volume vs. height (cm) (after Cahill *et al.*, 1996)

CHAPTER 3. PARTICLE SIZE/COMPOSITION RELATIONSHIPS OF WIND-ERODING SEDIMENTS, OWENS (DRY) LAKE, CALIFORNIA, USA

Abstract

Major, minor, and trace element concentrations were determined by PIXE in 118 aeolian sediment samples collected at six heights in seven locations along a 1.2 km transect during three sequential dust storms at Owens (dry) Lake, California, USA. Na and S concentrations covaried with each other and inversely with Si and Ca, increased with height, and decreased with distance downwind and time. Mg, Al, Si, K, Mn, Fe, and Sr concentrations at northerly sites varied with height and location as opposed to nearly constant concentrations at southerly locations. Volumetric particle-size distribution (PSD) for each sample was determined via laser diffraction. PSDs of the collected sediment reflected a trimodal distribution: 63% of samples peaked at 20-50 μm (silt), 11% at 50-100 μm very fine sand) and 26% at 100-250 μm (fine sand). Most silty samples occurred during the first two events. Significant differences in element concentrations existed in relation to the PSDs. Na and S concentrations were proportional to the submicron to silt particle fraction during each event. Al, Ti, Mn, K, Fe, and Rb concentrations correlated with 100-500μm (fine/medium sand) particles in the first two events and a wider PSD range 250-1000μm (coarse sand) in the third event. The results suggest sodium sulfate aerosol emission during the first windstorm, while subsequent saltation-dominated events released more aluminosilicate minerals containing higher trace metal concentrations. These combined techniques reveal particle size/chemical fractionation and spatial variability of sediment properties during re-suspension at aeolian "hotspots," with implications to geochemical cycling and aerosol source/receptor relationships.

Introduction

Generation of aeolian dust particles creates a severe air pollution and health and environmental hazard in the regions downwind of dust sources. Fugitive dust and aeolian sand blowing from the anthropogenically desiccated playa (dried bed) of Owens (dry) Lake, California (caused by the diversion of the Owens River) presented a massive environmental problem with extremely high particulate matter concentrations recorded on the playa and in downwind receptor sites (Cahill *et al.* 1996). This dust aerosol and its source sediments are known to contain elevated concentrations of potentially harmful metallic elements including arsenic, copper, chromium, lead, etc (Ryu *et al*. 2002). It is also seasonally rich in salts and sulfur (Gill *et al*. 2002). In this study, elemental composition and particle size distributions of aeolian bulk dust samples collected during the Lake Owens Dust Experiment (LODE) field campaign in spring 1993 were analyzed to determine possible correlations of dust chemistry with particle size, location along the playa surface, height above the playa surface and sequential wind storms.

Experimental

Airborne sediment samples were collected from three sequential wind storms in 1993 (11, 17, and 23 March) at Owens (dry) Lake, California. The sampling site was located on the south sand sheet, one of the primary dust production regions of the playa (Figure 3.1). The sediment samples were collected in Big Spring Number Eight (BSNE) passive samplers (Fryrear 1986). The BSNEs were placed at seven locations along a 1.2-kilometer long transect and oriented from north to south, paralleling the direction of the prevailing wind (Gillette *et al*. 1996) (Fig. 2). At each location, individual BSNE collectors were placed with inlets at elevations of 10, 20, 30, 50, 60, and 100 cm above the initial playa surface (Gillette *et al*. 1996). Figure 3.2 shows the placement of each BSNE along the selected line transect (not drawn to scale).

Elemental composition/concentrations of the aeolian sediment samples were determined via Particle Induced X-ray Emission (PIXE) and volumetric particle size distribution (PSD) via laser diffraction. A total of 118 samples, each representing a unique combination of date, location, and height above the land surface, were analyzed.

The percent volume of the PSD was determined using a Malvern Mastersizer 2000 laser diffraction particle sizer operating in dry (Scirocco) mode. To obtain the volumetric PSD, the measured sample volume via the Malvern was divided into 11 intervals spaced logarithmically between 0.01 and 2000 μm, expressed in percentages. Samples were analyzed dry in order to measure the actual size of the grains/particles moving in the air. The protocols recommended by Sperazza *et al*. (2004) as adapted to dry powder samples were followed for the particle size analyses. For elemental analysis, 0.2- 3.0 gram aliquots of dust samples were pulverized in a corundum mortar and pestle to a particle size of 30- 50 μm or smaller. An aliquot of approximately 0.2 to 1 gram of each powdered sample was pelletized into a 2.5 cm disk between two Kapton films. The surface depth uniformity was at least 100 μm.

Sample elemental analysis was conducted by Elemental Analysis Incorporated (EAI), Lexington, Kentucky, USA. PIXE analysis was performed by a General Ionex 4 MV tandem accelerator with a duoplasmatron source capable of producing beam currents in the range of a few nanoamps to tens of microamps, a dual quadrapole focusing lens, an x-y beam scanner to insure beam homogeneity, a beam pulser with 50 ns response time, and a vacuum/helium chamber with internal dimensions of 50 cm x 40 cm x 20 cm length, (width and height, respectively). The data acquisition system included a computer driving a CAMAC crate front ended with a 150 eV resolution, 30 mm2 Si (Li) detector for X-ray collection and Au surface barrier detector to monitor scattered protons. Samples were irradiated using a 1.6 cm diameter collimator to enhance overall response for elements and reduce potential for homogeneity issues.

Each pellet was irradiated such that it was subjected to a minimum number of proton counts (typically 1 million per sample).

Data reduction was accomplished with a modified version of software developed at the University of Guelph (Campbell *et al*. 1993). The efficacy of the analyses was verified using USA National Institute of Standards and Technology Standard Reference Material 2711, Montana II Soil, which was pelletized and analyzed under the same conditions during the same run.

Results

Variation of elemental concentrations with respect to sequential wind storms

A total of 19 elements were detected by PIXE in the dust samples. They were classified as major (Si, Ca, Na, Mg, S, Al, Fe, K), minor (Cl, Sr, Ti, Mn), and trace (Zn, Rb, As, Br, Cu, Ni, Ga) elements with average concentrations of (1.36E+05, 1.15E+05, 1.15E+05, 4.46E+04, 3.27E+04, 2.11E+04, 1.17E+04, 1.13E+04), (8.26E+03, 1.41E+03, 1.30E+03, 4.14E+02), and (1.07E+02, 5.63E+01, 1.97E+01, 1.51E+01, 1.33E+01, 7.51E+00, 7.32E+00) in parts per million ppm), respectively. All elements except Ni, Ga, and Br were detected in every sample.

Of the 19 detectable elements, only Na, S, and Zn decreased in concentration (ppm) from dust storm to dust storm. On average, Na, S, and Zn decreased in concentrations by 40%, 64%, and 14% from 11 March to 17 March, respectively and decreased by 22%, 28%, and 40% from 17 March to 23 March, respectively. Figure 3.3 demonstrates the decrease for Na. The remaining detected elements increased presented the opposite behavior. On the average, elemental concentrations increased 34% from 11 March to 17 March and 9% from 17 March to 23 March. This is represented for Al only in Figure 3.4.

Variation of elemental concentrations with respect to height and location

In general, Na, S, and Ni concentrations increased with height and decreased with distance downwind. Fig. 3 shows this for Na. Mg, K, Al, Si, Mn, Fe, and Sr concentrations in dust from northerly sites varied with height and location as opposed to relatively constant concentrations at southerly locations as shown in Fig. 4 for Al and Fig. 5 for Fe, where H1 is the northernmost location and S2 the southernmost location. All other elements demonstrated no clear pattern when associating variations in concentrations with respect to height or location.

Variation of elemental concentrations relative to particle size

Volumetric PSDs reflected a trimodal distribution: 63% of the samples peaked at 20-50μm (silt), 11% at 50-100μm (very fine sand) and 26% at 100- 250μm (fine sand) as shown in Fig. 6. Figure 3.6 shows the overall distribution of 118 dust samples analyzed for the three dust events during March 1993. The majority of samples high in silt content occurred during the first and second dust events.

Significant differences in element concentrations existed in relation to the volumetric percentage of particles in a given size range. For example, Na and S concentrations varied proportional to the percent volume of submicron to silt particle fraction during each event. K, Al, Ti, Mn, Fe, and Rb concentrations varied positively with the percent volume of particles in the 100- 500μm size range (fine/medium sand) in the first two dust events and with the percent volume of particles in the 250-1000μm size range coarse sand) in the third dust event. The concentration of these elements varied, however, inversely proportional to the percent volume of particles in the .01–1μm and 20-100μm size range during the three dust events.

Discussion

The results suggest fine sodium sulfate salt aerosol emissions, primarily during the first windstorm, while subsequent saltation-dominated events released more aluminosilicate minerals

containing higher concentrations of most trace metals. These combined techniques reveal particle size/chemical fractionation and small-scale spatial variability of sediments during dust and sand re-suspension at aeolian "hotspots," with implications to geochemical cycling and aerosol source/ receptor relationships. Preliminary analysis of elemental concentration variation as obtained via PIXE (an excellent technique for analysis of dry powders and aeolian dust materials) in relation to percent volume of particles in a given size range provides the opportunity to explore possible confounding factors such as height and location when correlating elemental concentrations to particle size distributions.

We must also note that these data regarding the size and chemistry of the particles analyzed are irrespective of the total amount of sediment collected in each wind storm, at each location, and/or each height. The amount of dust mobilized in each storm or at any point in space and time is a variable related to the playa surface conditions and the strength, orientation, and duration of the wind. For example, the total mass of material collected during these events at heights of 10 and 20 cm above the surface was approximately an order of magnitude higher than the mass collected at 50, 60, and 100 cm (Cahill *et al.* 1996), and the total amount of sediment mobilized during the 11 March to 23 March dust storms was approximately two orders of magnitude higher than that of the 17 March storm.

Future work will investigate the statistical significance of variability and relationships among these factors, and add additional chemical information on the samples obtained via ion chromatography and X-ray diffraction.

References

Cahill, T.A., Gill, T.E., Reid, J.S., Gearhart, E.A,, Gillette, D.A. *Earth Surf. Proc. Landforms* 1996; **21:** 621- 639, DOI: 10.1002/ SICI)1096-9837 199607)21:7<621::AID-ESP661>3.0.CO;2-E

Ryu, J.I.H., Gao, S., Dahlgren, R.A,, Zierenberg, R.A. *Geochim. Cosmochim. Acta* 2002; **66**: 2981-2994, DOI:10.1016/S0016-7037 02)00897-9

Gill, T.E., Gillette, D.A,, Niemeyer, T., Winn, R.T. Nucl. Instr. and Meth. in Phys. Res. B 2002; 189: 209- 213, DOI: 10.1016/S0168-583X 01)01044-8

Fryrear, D.W., *J. Soil Water Conserv.* 1986; **41:** 117- 120.

Gillette, D.A., Herbert, G., Stockton, P.H., Owen, P.R., *Earth Surf. Proc. Landforms* 1996; **21:** 641- 660, DOI: 10.1002/ SICI)1096-9837 199607)21:7<641::AID-ESP662>3.0.CO;2-9

Sperazza, M., Moore, J.N., Hendrix, M.S., *J. Sed. Res.* 2004; **74:** 736- 743, DOI: 10.1306/031104740736

Campbell, J.L., Higuchi, D., Maxwell, J.A., Teesdale, W.J., *Nucl. Instr. and Meth. in Phys. Res. B* 1993; **77:** 95- 109, DOI: 10.1016/0168-583X 93)95530-I.

Figures

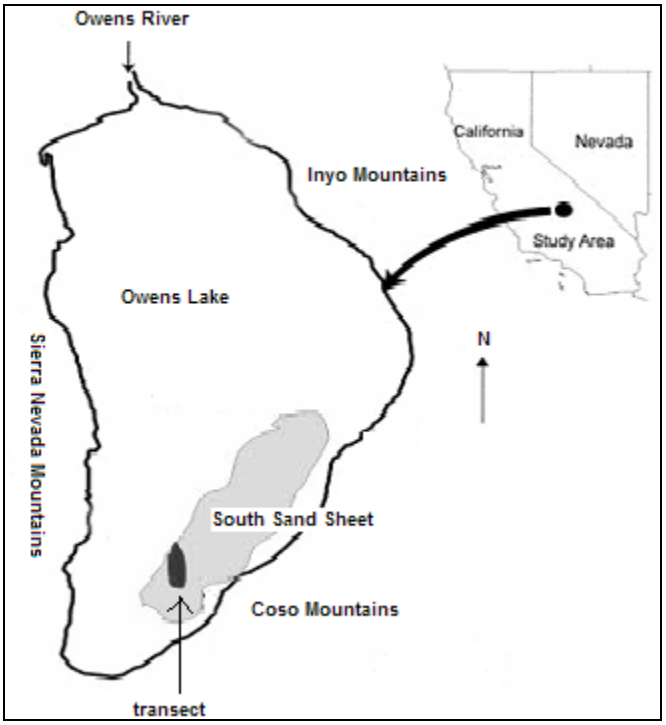

Figure 3.1 Location of study site (not drawn to scale)

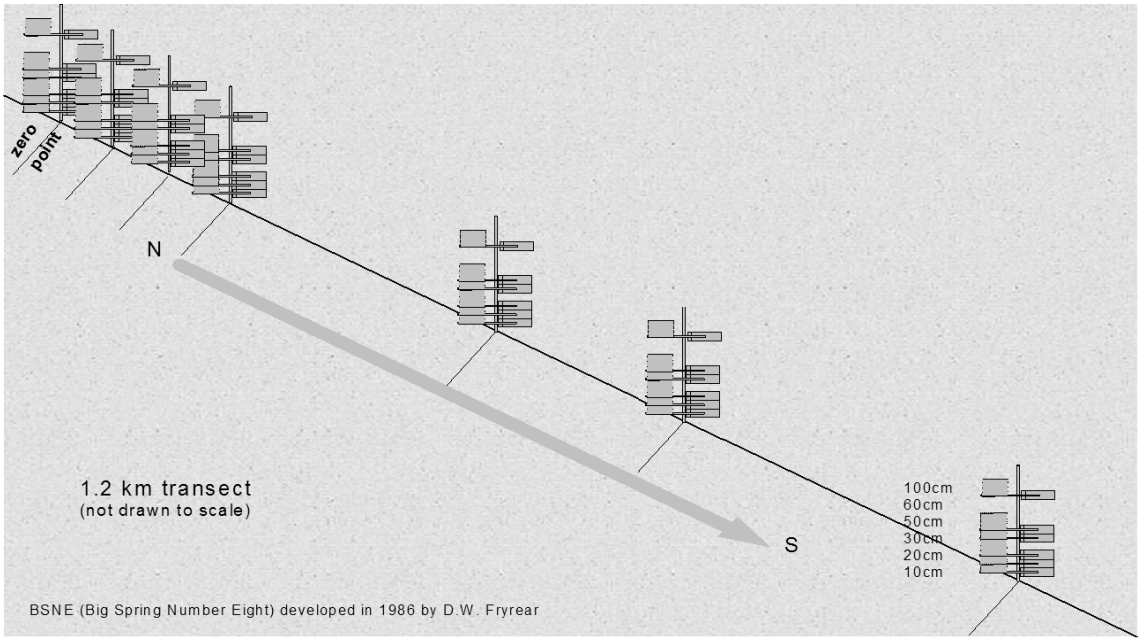

Figure 3.2 Collection method six heights/seven locations (not drawn to scale)

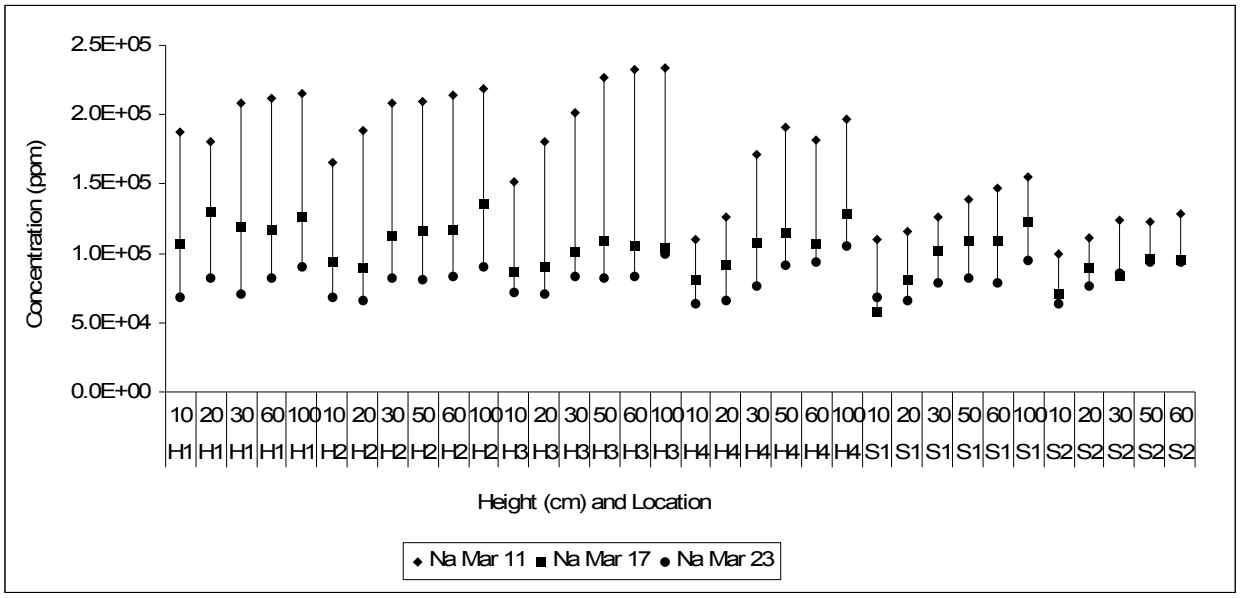

Figure 3.3 Decrease in sodium concentrations per dust event, increase with height.

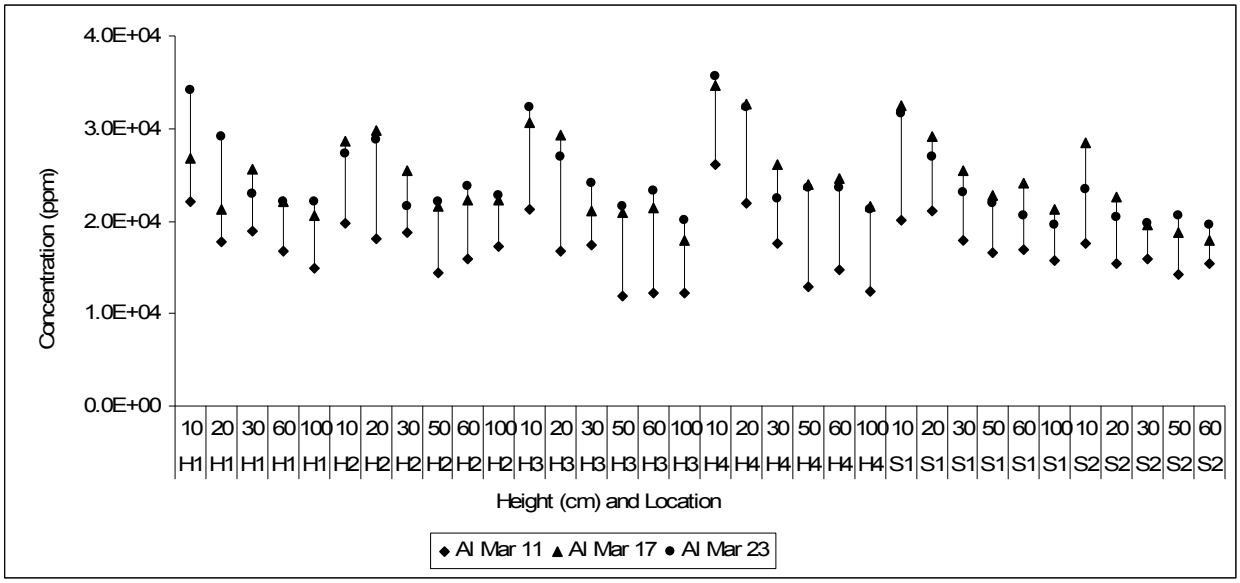

Figure 3.4 Increase in aluminum concentrations per dust event, decrease with height

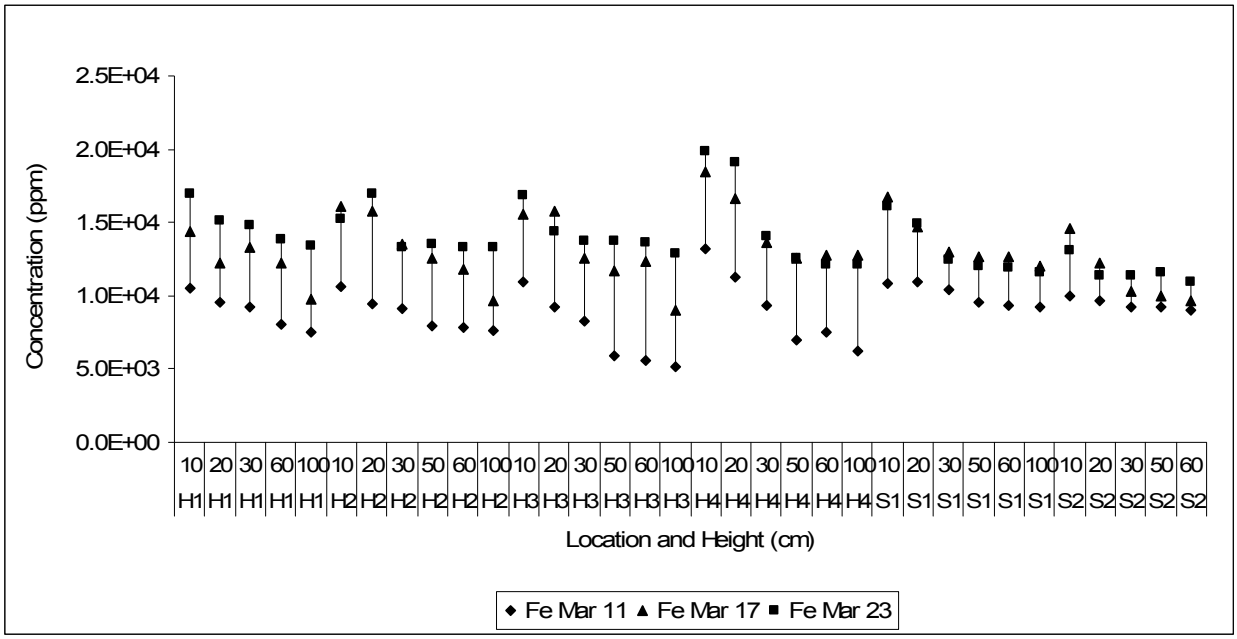

Figure 3.5 Increase of Fe concentration from H1 (north) S2 (south).

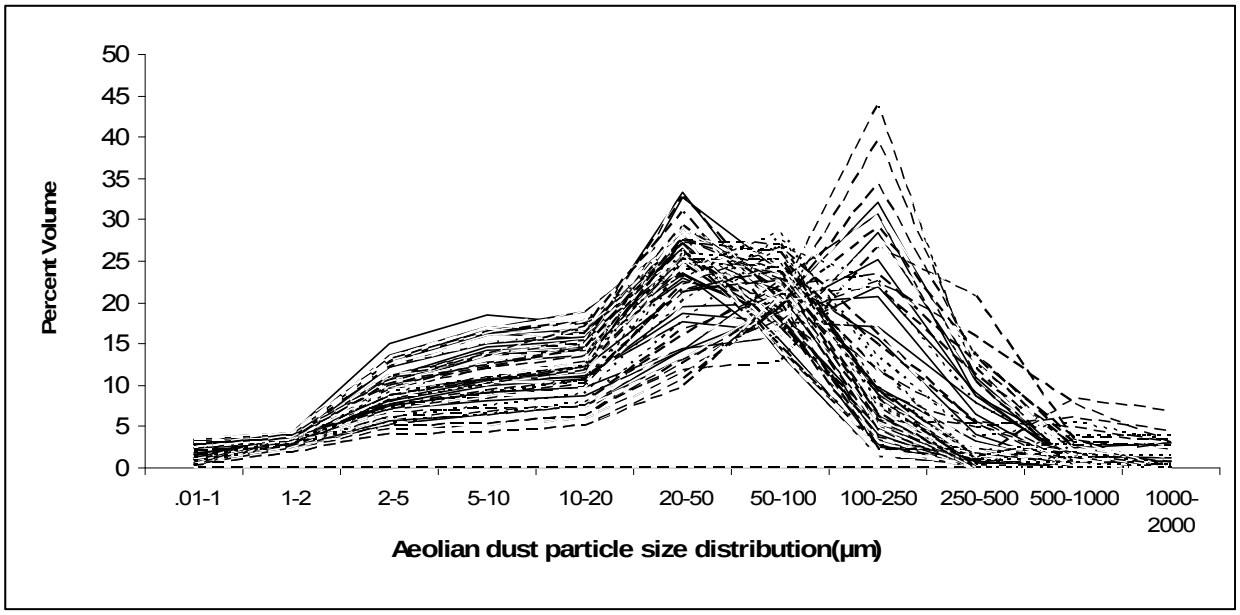

Figure 3.6 Particle size distribution for March 1993 dust events.

CHAPTER 4. INTERCOMPARISON OF PIXE AND ICP-AES ANALYSES OF AEOLIAN DUST FROM OWENS (DRY) LAKE, CALIFORNIA

Abstract

PIXE and ICP-AES can be combined to obtain a wider range of detected elements, augment previous data, and/or to verify measured concentrations of heavy and trace metals in geological samples. Inter-comparison of datasets generated by multiple techniques is challenging due to the differing processes and methods of each technique. Here we compare elemental data obtained by both techniques for aeolian dusts from Owens (dry) Lake, California. Nineteen elements were detected by PIXE, 16 by ICP-AES, and ten elements were detected by both techniques. Statistical analyses of dataset groupings illustrated which parameters significantly differed between PIXE and ICP. Relative variation (%) showed that PIXE gave higher concentrations than ICP-AES for Al, As, Cu, Fe, K, Mn, Ni, Sr, Ti, and Zn in all samples. For As, Cu, Sr, and Zn, relative variation was variable between the techniques. PIXE detection limits exceeded ICP-AES concentrations for Ba, Cd, Co, Cr, Pb, and Mo. Low ICP-AES percent recoveries of Al, Fe, K, Mn, and Ti for NIST SRM 2710 indicated incomplete dissolution during digestion (EPA Method 3050B), since elements were bound in silicate structures. Variability between the two datasets is explained by differences between analytical techniques, sample preparation methods, and/or variability in sample matrices.

Introduction

Inductively coupled plasma atomic emission spectroscopy (ICP-AES) and particle induced X-ray emission spectrometry (PIXE) are two widely used analytical methods to determine the elemental composition and concentrations for soils, sediments, aerosols, and other environmental samples. Both analytical methods have yielded accurate and precise measurements in a range of applications and under varying conditions (i.e. sample size requirements and availability, sample preparation technique, range of elements, etc). (Cruvinel *et al.* 1999; Saitoh *et al.* 2002; Nsouli *et al.* 2004; Zhang *et al.* 2005; Zhang and O'Connor 2005; Almeida *et al.* 2006; Pye *et al.* 2006; Lunderberg *et al.* 2008; Markwitz *et al.* 2008). Other techniques commonly used to determine elemental composition/concentrations in environmental samples include, but are not limited to X-ray fluorescence (XRF), neutron activation analysis (NAA), and atomic absorption spectroscopy (AAS) (Nsouli *et al.* 2004; Pekney and Davidson 2005; Pye *et al.* 2006).

The inter-comparison of elemental composition/concentrations obtained by two or more analytical techniques is important for quality control and quality assurance purposes (Almeida *et al.* 2003). It is understood that some methods are more suitable for measuring higher concentrations whereas others are more precise in measuring low concentrations (Zhang and O'Connor 2005). None of the available analytical techniques have a well defined advantage for a range of applications over another. In fact, these limitations make them complementary rather than competitive techniques. The relative performance of each method is ideally fitted to best detect a range of elements. Hypothetically, ICP-AES has the ability of simultaneously measuring up to 70 elements but is normally used to measure up to 20-30 elements (Grave *et al.* 2005). However, ICP-AES can also analyze samples sequentially (as was the case in this study). As with ICP-AES, PIXE also has the capability to measure elements from Na to U in the periodic table, but is best suited for elements in the medium atomic number (Z) range $19 < Z < 31$ (Nayak and Vijayan 2006). For this reason, when two or more techniques are used in combination with one another the results can yield a wider range of detectable elements and concentrations.

Investigations are usually designed using a specific analytical technique to obtain initial information relevant to the sampled material, but in many cases may later use other analytical techniques to augment previous data, to verify results, or both (Gerab *et al.* 1998; Gidhagen *et al.* 2002; Menzel *et al.* 2002; Reheis *et al.* 2002; Saitoh *et al.* 2002; Nsouli *et al.* 2004; Bellot-Gurlet *et al.* 2005; Pappalardo *et al.* 2005; Pekney and Davidson 2005; Zhang *et al.* 2005; Zhao *et al.* 2006; Breit *et al.* 2007; Marques *et al.* 2007; Zhao *et al.* 2007; Castillo *et al.* 2008; Lunderberg *et al.* 2008; Ruth *et al.* 2008; Strivay *et al.* 2008; Zahid 2009).

Inter-comparison of datasets generated by any two analytical techniques becomes challenging (Grave *et al.* 2005) due to the inherent processes and methods of each technique such as sample preparation, instrumental components and capabilities, operating conditions and elemental sensitivities (Gatti *et al.* 1999). In this study, we present and inter-compare the elemental compositions and concentrations of 118 aeolian dust samples from Owens (dry) Lake, California analyzed by both PIXE and ICP-AES. Analyses by PIXE were conducted at Elemental Analysis Incorporated (EAI) in Lexington, Kentucky, USA in 2001 and analyses by ICP-AES were conducted in laboratories of the departments of Geosciences and Environmental Toxicology at Texas Tech University, Lubbock, Texas, USA in 2002. It was important to compare the data generated by PIXE with that determined by ICP-AES in terms of evaluating the concentrations obtained for the same elements. These samples present additional challenges in the comparison of these two datasets including detection limits of the analytical techniques, and design of sample collection which resulted in variability of sample matrices and particle size.

PIXE and ICP-AES: Complementary Techniques

PIXE and ICP-AES are two analytical techniques that are ideal for the determination of multi-elemental concentrations. PIXE can simultaneously detect elements from sodium to uranium in a short time and, depending on analytical conditions and procedures, is able to detect major to trace elements at the concentration level of parts per million (μg g-1) (Saitoh *et al.*

2002). An advantage of PIXE is its ability to simultaneously analyze for dozens of elements without the need for sample dissolution or digestion prior to analysis (Smodis 2007). ICP-AES also has the ability to analyze a wide range of elements and is used for the analysis of light elements such as Na and Mg (Zhang *et al.* 2005). These two methods have been used by numerous investigators to complement one another where ICP-AES is used for the analysis of light elements and PIXE for the analysis of elements heavier than Na (e.g., Zhang *et al.* 2005; Almeida *et al.* 2006; Stihi *et al.* 2006).

Successful elemental analysis by any technique requires an understanding of the capabilities and limitations of the instrument as well as previous knowledge of the analyzed material when at all possible. The analytical procedures and experimental set-ups used for PIXE and/or ICP-AES may differ from study to study or application to application. Descriptions of the typical procedures and set-ups are beyond the scope of this paper, but widely described elsewhere (Maxwell *et al.* 1995; Gerab *et al.* 1998; Prati *et al.*1998; Aldape *et al.*1999; Cruvinel *et al.* 1999; Gatti *et al.* 1999; Menzel *et al.* 2002; Nsouli *et al.* 2004; Bellot-Gurlet *et al.* 2005; Grave *et al.* 2005; Zhang *et al.* 2005; Zhang and O'Connor 2005; Bolormaa *et al.* 2007; Markwitz *et al.* 2008).

For elemental analysis by PIXE, special attention is focused on the detection of light elements, normally described in the literature as elements in the $Z \leq (11)$ Na range. Most PIXE analyses are not sufficiently sensitive to detect or quantify light elements of $Z \leq (11)$ (Cruvinel *et al.* 1999; Ma *et al.* 2001; Dias da Cunha and Barros Leite 2002; Aburaya *et al.* 2006; Bolormaa *et al.* 2007). Other complementary techniques such as RBS (Strivay *et al.* 2008) or PIGE (Nayak and Vijayan 2006) may be coupled with PIXE in order to normalize X-ray spectra and to analyze the major light elements of the sample. The absolute quantity of the lighter elements like Na, Mg, Al and Si, can also be sometimes underestimated because of the X-ray self-absorption inside each individual grain of a sample (Marino *et al.* 2008). Although the detection of trace

concentrations across the periodic table has been successful in some studies using PIXE (Nsouli *et al.* 2004), PIXE is best suited for elements in the lower middle Z elements (i.e. $19 < Z < \sim 35$) from K X-rays, and higher Z elements (such as Ba and Pb) from L X-rays. Other possible drawbacks are that PIXE's detection limits are generally higher than those for ICP-AES and the lack of homogeneous material might produce skewed results (Lunderberg *et al.* 2008).

ICP-AES is a widely used technique for the characterization of trace metal concentrations in sediments (*e.g.*, Rice 1999). This analytical method has low detection limits for most metals, but one of its drawbacks is the need to digest the solid sample material with a strong acid to produce an aqueous sample for analysis (Menzel *et al.* 2002; Lunderberg *et al.* 2008).

The most distinct difference between PIXE and ICP-AES is the underlying technique used in the analysis of elemental composition/concentrations. PIXE is an X-ray spectrometric technique where the X-ray spectrum is initiated by energetic protons exciting the inner shell electrons in the target atoms. It is a sensitive and convenient method to determine relatively low concentrations of elements such as transition metals in samples of limited size (Aldape *et al.* 1999; Menzel *et al.* 2002). The technique utilizes a focused MeV energy proton beam (Budka *et al.* 2002) for the analysis of samples which may be smaller than a milligram. It is nondestructive and essentially accurate (Garman 1999; Bellot-Gurlet *et al.* 2005; Zhang *et al.* 2005). A detailed description of the PIXE analytical technique is given in the United States Environmental Protection Agency (EPA). Compendium Method IO-3.6, "Determination of metals in ambient particulate matter using proton induced x-ray emission spectroscopy" (1999). ICP-AES is a type of emission atomic spectroscopy technique which uses an Ar plasma energy source to produce excited atoms and ions capable of emitting light (wavelengths). ICP-AES is commonly used when funds are limited since it presents a significant advantage of less costly instrumentation as compared to other multi-element techniques (Zachariadis and Michos 2007). A possible disadvantage of ICP technique is the destructive sample preparation method prior to actual

analysis (Smodis 2007). Improper preparation could lead to contamination of samples (Ruth *et al.* 2008), incomplete digestion, and/ or loss of material by evaporation (Menzel *et al.* 2002; Smodis 2007). The attainable precision of ICP-AES for most elements falls between 1–3%, which is as good as AAS and better than ICP-MS (Pye *et al.* 2006). Both analytical methods have the ability to determine elemental concentrations in samples as small as 0.05 g. Detection limits for both techniques are highly dependent on the matrix properties of each sample (Lunderberg *et al.* 2008) and the quantity of the sample. The smaller the sample, the higher the likelihood of introduced error (Pye *et al.* 2006).

Owens (dry) Lake Study Area

Aeolian dust samples were collected from Owens (dry) Lake, California in March 1993. Owens (dry) Lake is located in the Basin and Range physiographic province of the Western USA and is surrounded by the Sierra Nevada to the west, the Inyo Mountains to the east and Coso Mountains to the southeast (Levy *et al.* 1999; Ryu *et al.* 2002. (Figure 4.1) The surrounding geology plays a direct role in the composition of the playa (dry lake bed) sediment and thus, the dusts generated from the playa (Tyler *et al.* 1997). The exposed bedrock of the Sierra Nevada is dominated by granodioritic plutons (Bischoff and Cummins 2001), with limestone and dolomite dominating the sedimentary rocks of the Inyo Mountains and shale, conglomerate, and quartzite present in lesser amounts (Levy *et al.* 1999). Owens Lake is dry, desiccated by water diversions in the first part of the 20th century. The lake accumulated abundant deposits of sulfate and carbonate rich salts from the dissolution and crystallization of minerals and salts as the lake desiccated (Levy *et al.* 1999), as well as from saline groundwater immediately beneath the playa surface. The result is a seasonally-variable, wind-erodible crust of evaporites and clastic sediments which covers much of the lakebed and releases copious amounts of dust under strong winds (Cahill *et al.* 1996).

Studies (Gill *et al.* 2002; Reheis *et al.* 2002; Ryu *et al.* 2002) have shown that the dust generated by the wind storms at Owens (dry) Lake contains high concentrations of a number of potentially toxic elements such as As, Ba, Br, Cr, Cu, Pb, Mo, Ni, Rb, Sr, Th, U, Zn, and Zr. Areas of significant dust emission at Owens (dry) Lake are comprised of seasonally-varying, sometimes efflorescent surface crusts rich in evaporite minerals such as mirabilite (Na_2SO_4•10 H_2O), halite (NaCl), trona ($Na_3H(CO_3)_2$•$2H_2O$), natron (Na_2CO_3•$10H_2O$), and thenardite (Na_2SO_4) (Saint- Amand *et al.* 1987). The temperature and vapor pressure of H_2O (g) in the atmosphere affect the degree of mineral hydration and the mineralogical and chemical composition of the surface crusts (and therefore, the dust) from season to season (Levy *et al.* 1999).

Average winter surface air temperature at Owens (dry) Lake is 3°C and average summer temperature is 27°C (Tyler *et al.* 1997). Early spring (i.e. March) dust storms are the most frequent and tend to generate most of the variation in dust particle size and elemental composition due to the dynamic geomorphology of the dry lake. The initial playa surface consists of an efflorescent crust rich in mirabilite and other evaporites that is deflated by the first early spring wind event followed by the degradation of the salt-silt-clay layers by subsequent storms (Cahill *et al.* 1996; Rojo *et al.* 2008). The first set of samples collected for this study was obtained during the first spring dust storm on 11 March, 1993. The remaining dust samples were collected during each subsequent dust storm which took place on 17 March, and 23 March, 1993, respectively.

Sample details

One hundred forty-four dust samples were collected along a 1.2 km north-south transect (A- B on Figure 4.2) of the dry playa (lake bed) of Owens (dry) Lake for the Lake Owens Dust Experiment (LODE) during this sequence of three separate wind events in March 1993. The sampling site was located on the playa's south sand sheet which is one of the primary dust storm

initiation regions of the playa (Cahill *et al.* 1996). The dust samples were collected in Big Spring Number Eight (BSNE) passive aeolian sediment samplers (Fryrear 1986) (Figure 4.2). The BSNEs were placed at seven locations along the A–B transect which is aligned in the same direction as the prevailing wind (Zhong *et al.* 2008). where A and B represent north and south, respectively (Fig. 2) (Cahill *et al.* 1996; Gillette *et al.* 1997). Individual BSNE collectors were placed with inlets at elevations of 10, 20, 30, 50, 60, and 100 cm above the initial playa surface at each location (Gillette *et al.* 1997) as shown in Figure 4.2. Samples of aeolian sediment (dust and sand) were recovered from the BSNEs after each wind storm and stored in sealed zip-lock plastic bags in a dry environment.

The design of the sample collection had an effect on the particle size distribution (PSD) of the aeolian dust samples from Owens (dry) Lake and the resulting data from their elemental analyses. Each sample had a unique collection point related to height, location along the North-South transect, and time (dust event). This dictated the manner in which the elemental data was examined. Data analyses were based on the inter-comparison of absolute values of corresponding data points (elemental concentrations) generated by PIXE and ICP-AES. For instance, Na and S concentrations (μg g-1) of the Owens (dry) Lake aeolian dust samples decreased from the first dust event (11 March) to the second dust event (17 March) by 40% and 64% respectively, while Si concentrations increased from event to event as presented in Figure 4.3. Na and S concentrations increased with respect to height above the playa surface and the percent volume of finer particles increased. These increases are represented by the peaks in Figure 4.3.

The effects of grain size on the chemical composition of geological samples (Kiminami and Fujii 2007), sediments (Pye *et al.* 2006), soils (Wang *et al.* 2006), and dust samples (Rojo *et al.* 2008) play an important role in the assessment of their elemental compositions and chemical variability. Heavy metal concentrations in soils are mainly controlled by the particle sizes where the accumulation is inversely related to particle size. Finer particles tend to adsorb more heavy

metals due to their high specific surface area (Kiminami and Fujii 2007; Zhang *et al.* 2007). Trace elements in atmospheric particulate matter (APM) samples have been shown to have relatively higher concentrations in the finer particle size fractions than coarser particles (Castillo *et al.* 2008). Furthermore, since the silt and clay-sized particles are preferentially removed from soils during dust events, dust thus has the potential to become further enriched in the concentrations of trace elements relative the parent soils (Lawrence and Neff 2009).

Analytical methods

This study contrasts and compares two independent analytical datasets gathered from the same sample set. The PIXE analytical technique was used to obtain information related to the number and concentration of elements in the dust samples and to investigate the effects of event sequence, height above the land surface, and particle size on chemical composition (Rojo *et al.* 2008). A second analytical data set was acquired using ICP-AES to obtain the bio- or environmentally available components of the samples. The existence of two datasets from the same sample set presented the opportunity to compare and contrast the two analytical techniques and to evaluate how each dataset might be used in the investigation. Different standard reference material (SRM) from the National Institute of Standards and Technology (NIST) was used during the PIXE and ICP-AES elemental analysis. NIST SRM 2711 was used by PIXE analysis and NIST SRM 2710 by ICP-AES. SRM 2711 and SRM 2710, both Montana Soils, are intended mainly for use in the analysis of soils, sediments, or other materials of a similar matrix. The main difference between the two SRMs is that SRM 2711 is a moderately contaminated soil while SRM 2710 is a highly contaminated soil (http://www.nist.gov). The certified elements for SRM 2711 and SRM 2710 are given in Table 4.1 and Table 4.2, respectively.

PIXE

The PIXE system at EAI was calibrated by using a set of seventy-two elemental gravimetric standard targets from Micromatter Corporation in the form of thin films of

evaporated metals certified at a level of ±5%. The instrumental calibration H curves were constructed from this set. The analytical laboratory performs periodic complete calibrations to check for possible changes in characteristics of the X-ray detector as the time progresses. As part of EAC's QA Protocol, the PIXE analytical laboratory uses two detector positions for X-ray collection, one for the K line x-rays and one for the L x-ray. A close-in position with a thick absorber and a back-out position with no absorber are used for spectrum balance and enhancement.

The PIXE laboratory is equipped with a General Ionex 4 MV tandem accelerator equipped with a duoplasmatron source, a dual quadrapole focusing lens, an x-y beam scanner to insure beam homogeneity, a beam pulser with 50 ns response time, and a vacuum/helium chamber with internal dimensions of 50.8 cm w x 40.6 cm l x 20.3 cm h. The accelerator was operated at a constant 1.550 MeV. Protons enter the target chamber via a 0.30 mil Kapton window and the X-rays exit through a 0.1 mil Mylar window at 45 degrees relative to the beam entry. A dual irradiation is carried out on each sample to achieve more uniform detection limits across the entire periodic table. In one position the detector directly views the X-rays emitted from the target. This allows the low atomic numbered elements to be detected. The second position has an absorber placed between the sample and the detector to preferentially filter the emitted X-rays. The background Bremsstrahlung and cross-section effects work to produce a high flux of very low energy X-rays. EAI employs a polypropylene X-ray filter to enable PIXE to achieve better detection limits for the higher atomic number elements.

Samples prepared for PIXE analysis followed the method described by Gill *et al.* (2002). The dusts were pulverized in a synthetic corundum mortar and pestle, with hardness of 9+ on the Mohs scale, resulting in a powder with an average grain size of 30 μm or smaller as measured in dry mode by a Malvern Mastersizer laser diffraction granulometer. The pulverized samples weighing several grams each were prepared by pelletizing a 2.5 cm disk between two Kapton

films. All samples were irradiated using a 5/8" collimator to enhance the overall response for the elements and to reduce the potential for homogeneity issues. Data were acquired using a computer driving a "Computer Aided Measurement And Control" (CAMAC) crate front end with a 150 eV resolution, 30 mm2 Si (Li) detector for X-ray collection and Au surface barrier detector to monitor scattered protons. A modified version of software developed at the University of Guelph was used to convert raw spectral data into elemental concentrations (Campbell *et al.* 1993).

The accuracy of the PIXE measurements at EAI was established using a large number of standards from the National Institute of Standards and Technology (NIST), the U.S. Geological Survey (USGS), and the Japanese National Institute for Environmental Studies (NIES). Instrumental PIXE results are, in almost every case, in agreement with the certified values within one standard deviation. The precision of the PIXE method was checked by simultaneously preparing and analyzing the NIST SRM 2711 along with and by the same techniques as the dust samples. The results obtained from the measurement of seven replicates are displayed in Table 4.1. The certified values for NIST 2711 and the data obtained by PIXE were in all cases in close agreement. The statistical uncertainty for all elements was less than 1% in each run. Therefore, a relative error of 1% is reported. Elements detected in the analyses of the dust samples from Owens (dry) Lake were: Al, As, Br, Ca, Cl, Cu, Fe, Ga, K, Mg, Mn, Na, Ni, Rb, S, Si, Sr, Ti, and Zn.

ICP-AES

ICP-AES analyses were performed in the Texas Tech University GeoAnalytical Lab on a sequential Leeman Labs DRE ICP-AES. Since the elements are analyzed sequentially, the stability of the instrument electronics is monitored every 20 minutes and periodically adjusted by aligning to an Hg lamp wavelength. Each element wavelength has previously been aligned in an x-y relationship to the Hg wavelength using a single element standard and is periodically

checked for alignment. The plasma is aligned by aspirating a 10 μg g^{-1} Fe standard in the same acid matrix as the samples to be analyzed. Calibration curves are constructed for each analytical run by analyzing a set of standards in sequence twice. With a sequential instrument it is important to account for both the drift of the instrument over time and the slight variability in the sample introduction system by replicating the conditions expected during the run when building the calibration curves. If the % RSDs are greater than 10% between the sequential runs of the calibration standards, a third run is performed to verify the accuracy of the calibration. Check standards are used throughout the analytical run to monitor drift over time and evaluate the precision and accuracy of the analysis. Each analysis for each element is an average of three analyses which determines the precision of that specific analysis. For any samples with elemental concentrations above the highest calibration standard there are two choices: 1) rerun the samples with an appropriate set of calibration standards, or 2) dilute the sample to a concentration for the current calibration and rerun.

Calibration and check standards are made from a 100 μg g-1 multi-element certified ICP standard (SPEX CertiPrep Instrument Calibration Standard 2) using calibrated pipettes and volumetric flasks. All glassware has been cleaned with deionized water, soaked at least 24 hours in a 10% HNO_3 bath, and rinsed thoroughly with deionized water. Standards are matrix matched with the samples; in this case the matrix is the final HNO_3/HCl concentration of the EPA Method 3050B which was followed to prepare the digested samples. The blank used in the calibration is the matrix used to make up the standards thus accounting for any possible contamination from the deionized water or acids used. The consistency of the sample digestion via EPA Method 3050B was measured by digesting NIST SRM 2710 with each batch of approximately 40 samples. NIST SRM 2710 was the only appropriate standard available in the lab for comparison with dust samples. Since NIST SRM 2710 is a highly contaminated standard only 0.5 g was used for digestion in order to achieve concentrations closer to the dust samples. Table 4.2 lists certified total and leached (digested) values for NIST 2710 plus percent recoveries for the three

NIST 2710 standards prepared with the samples for this study. Examination of Table 4.2 shows most of the elements analyzed by ICP-AES are within the range of the values for the digested NIST 2710 standard. It is known that some of the elements in NIST SRM 2710 are contained in insoluble phases (Byrne and Benedik 1988; Lindstrom *et al.* 1990). In addition, several method blanks were run to document any contamination from the acids and digestion vessels used. The method blanks indicate possible Cu and Ba contamination at the 0.1µg g-1 levels, most likely from the digestion vessels.

Samples were prepared as per EPA Method 3050B and analyzed per EPA Method 6010B (EPA 1996). As with PIXE, the dust samples were pulverized in a synthetic corundum mortar and pestle, with hardness of 9+ on the Mohs scale, resulting in a powder with an average grain size of 30 µm or smaller as measured via laser diffractometer. Digestion of the dust samples was performed in the laboratories of Dr. George Cobb in the Environmental Toxicology Department at Texas Tech University. Approximately one gram of pulverized dry sample was weighed out (to the nearest 0.01 g) and the exact weight was recorded. Several samples weighed less than one gram and in those cases the total sample was used. After weighing, the samples were placed in labeled Teflon digestion beakers. Samples were wetted with 5 mL water then 5 mL concentrated HNO_3 was added and the beakers covered with Teflon lids. The samples were placed on hot plates set at 95 ºC ± 5 ºC and refluxed for 15 minutes without boiling. Samples were allowed to cool before the addition of 5 mL of HNO_3 followed by 30 minutes of refluxing at 95 ºC ± 5 ºC. The lids were then removed and the solution was allowed to evaporate to approximately 5mL without boiling. Once again the samples were allowed to cool before adding 2 mL of water and 3 mL of 30% H_2O_2 (for several batches of samples this cooling step occurred overnight). The samples were returned to the hot plate for warming and to start the peroxide reaction. If the samples effervesced, 30% H_2O_2 was added in 1 mL aliquots (to a maximum of 10 mL) and the samples were heated until effervescence subsided. Care was taken to avoid excessive effervescence and subsequent sample loss. The acid-peroxide digestate was heated until the

volume was reduced to approximately 5 mL. Samples were allowed to cool for a third time. Once cooled 10 mL concentrated HCl was added to the sample digestate. The samples were covered, returned to the hot plate and refluxed at 95 ºC ± 5 ºC for 15 minutes. The lids were then removed and the digestate evaporated to approximately 5mL. Samples were allowed to cool before being after digestion was completed and the volume of digested sample reduced to approximately 5mL. Each sample was rinsed from the Teflon digestion beaker into a volumetric flask through a funnel with filter paper to catch any undigested sample. The filter paper and undigested residue were rinsed thoroughly to ensure the entire digested sample ended up in the volumetric flask. Each sample was brought up to volume with deionized water and transferred to a labeled sample bottle. The filter paper and undigested residue for each sample were placed in a labeled capped test tube for later reference.

Elements selected for ICP-AES analysis were based on the pre-existing PIXE analytical runs, the matrices of the dust samples, and the limitations of the ICP-AES sample digestion method. As a result, the lists of detected elements between the two analytical techniques are not identical. Si was not analyzed for by ICP-AES because the digestion method would result in incomplete digestion of the silicate minerals. The elements Br, Cl, Ga, Rb, and S were not possible to analyze with the Leeman Labs DRE ICP-AES housed in the GeoAnalytical Labs at TTU. The elements As, Ba, Be, Cd, Co, Cr, Cu, Mn, Mo, Ni, Pb, Se, V, and Zn were analyzed for all samples for all three dust events using a calibration defined by blank, 0.01, 0.05, 0.1, 1 and 4 ppm standard concentrations. The samples were run as two separate batches. In the first batch, V and Se resulted in only qualitative data at best due to excessive drift for these elements during the analytical run. For the second batch of samples, V was more stable and produced quantitative data above 1 ppm. In both analytical runs, many Sr values were outside the calibration (above 4 ppm) and reanalyzed in a third analytical run with appropriate calibration standards. The third analytical run included Al, Ca, Fe, K, Mg, Na, Sr, and Ti using a calibration defined by blank, 1, 4, 10, 20, and 50 ppm standard concentrations. After analyzing a small

batch, a decision was made to not analyze for Ca and Mg since these elements had extremely high concentrations, were out of the calibration, and had been analyzed previously by PIXE. A fourth analytical run was done with diluted samples for Al, K, Na, and Fe. Again one element, Na, was too concentrated and a decision was made to use the PIXE data. Additionally, the decision was made to not analyze the samples from the 17 March event for Al, Fe, K, Sr, Ti, by ICP-AES due to limited consumables and time constraints. It should be noted that only a few 17 March samples analyzed by PIXE were available for analysis by ICP-AES.

Results and Discussion

The overall inter-comparison of the two datasets provided interesting results. The combined multi-elemental analyses reported a total of 25 elements. Nineteen elements were reported by PIXE and sixteen by ICP-AES: ten of the 25 elements were reported by both analytical methods. Ba, Cd, Co, Cr, Pb, and Mo were reported by ICP-AES only. Br, Ca, Cl, Ga, Mg, Na, Rb, S, and Si were reported by PIXE only and Al, As, Cu, Fe, K, Mn, Ni, Sr, Ti, and Zn were reported by both analytical methods. Differences in the detected elements and their respective concentrations may be explained by the different analytical techniques and sample preparation methods, as well as by contributing factors related to Owens (dry) Lake's composition and dust emission processes, the spatiotemporal design of sample collection, and particle size prior to sample preparation. The elemental composition of samples is often influenced by particle size and spatial and temporal scales (Rojo *et al.* 2008). A detailed explanation (Reheis *et al.* 2002) of the influence of these factors on sample chemical composition and their respective concentrations is beyond the scope of this paper. However, statistical analyses, relative variation and percent recoveries are used below to evaluate the concentrations obtained by PIXE and ICP-AES. Ni concentrations were not included in any of the analyses due to limited data points.

SPSS statistical software (SPSS, Chicago, Illinois, USA) was used to test for data (element concentrations) normality and to test the null hypothesis that there was no statistical difference between the two data sets (PIXE and ICP-AES) at a significance level of $\alpha = .05$ (Reheis *et al.* 2002). The relative variation (%) between PIXE and ICP-AES concentrations ($\mu g\ g^{-1}$) for the most common elements (Al, As, Cu, Fe, K, Mn, Ni, Sr, Ti, and Zn) was used to assess the disparity or any variation between the respective concentrations. The median percent recoveries for NIST SRM 2710 were used to assess the efficiency of digestion method EPA Method 3050B as a sample preparation technique for aeolian dusts to be analyzed by ICP-AES.

The One-Sample Kolmogorov-Smirnov test was used to test for data normality and the non-parametric Kruskal-Wallis test was used to test for the differences in distributions of the concentrations obtained from the two analytical methods. The concentrations for Al, Fe, and K obtained by PIXE and ICP-AES were graphed (Figure 4.4) to confirm that the distribution shapes were similar, as the Kruskal-Wallis test assumes that the observations in each group come from populations with similar shapes of their respective distributions. Mn and Ti concentrations, although not shown in Figure 4.4, had distribution shapes similar to Al, Fe, and K.

The datasets were first statistically analyzed as a whole and subsequently were grouped and analyzed by event date, height, location, and elemental composition to assess the potential contributions of playa geomorphology and spatiotemporal differences on the statistical results. The results of the statistical analyses are presented in Table 4.3. Sample concentrations are assumed to be from different populations when significance levels are <5%. The datasets of the whole and datasets grouped by event date (only included 11 March and 23 March) were assumed to be statistically significant with p-values < 0.05 (Table 4.3I-a, b). Datasets grouped by height had statistical significance at 10, 20, and 30 cm above the playa surface with p = .023, .038, and .035, respectively. Heights at 50, 60, and 100 cm above the playa surface had p-values > 0.05 (Table 4.3-c) and are therefore assumed not to be statistically significant. Datasets grouped by

locations (refer to Figure 4.2 for locations and height. were statistically significant for locations S1 and S2 with p = .034 and .044, respectively (Table 4.3-d). Locations H1, H2, H3, H4 and S3 were not statistically significant since these locations had p > 0.05. Datasets grouped by elemental composition were statistically significant for Al, Cu, Fe, K, Mn, Sr, Ti, and Zn with p < 0.05. Arsenic was not significant with p = .794 (Table 4.3-e). Statistically analyzing grouped data provided further insight of the aeolian emission dynamics of Owens (dry) Lake and the elemental variation respect to spatiotemporal variation.

The relative variation (%) between PIXE and ICP-AES with respect to ICP-AES was determined to evaluate the extent of the difference in concentration of each element detected by both analytical techniques (Figure 4.5). Figure 4.5 shows the relative variation in the manner of Bellot-Gurlet *et al.* (2005). The percent relative variation indicates the required increase (or decrease if negative) in ICP-AES concentrations to equal the absolute difference in concentrations between PIXE and ICP-AES. A positive relative variation (> 0%) means that PIXE concentrations were higher than ICP-AES concentrations as was the case for all samples for Al, Fe, K, Mn, and Ti. A negative relative variation (< 0%) means that ICP-AES concentrations were higher than PIXE concentrations as was the case in some samples for As, Cu, Sr, and Zn (Figure 4.5) For instance, Al had the widest relative variation with a maximum of 321%, a minimum of 89% and a mean of 183%. Ti, K, Mn, and Fe followed with a max, min, and mean of (216%, 85%, 136%), (181%, 17%, 63%), (120%, 53%, 88%), and (116%, 19%, 54%), respectively. For the elements As, Cu, Sr, and Zn the relative variation had a max, min, and mean of (37%, -40%, -0.49%), (71%, -26%, 24%), (34%, -3%, 12%), and (86%, -55%, 39%), respectively. Concentrations for these elements were higher in some samples when measured by PIXE and higher in other samples when measured by ICP-AES. It is possible that the range of the percent relative variations seen in Figure 4.5 can be attributed to the combined effects of sample collection design, particle size distribution prior to sample preparation, and playa geomorphology based on the statistical results presented in Table 4.3 on a small scale and

on a larger scale based on studies by Reheis *et al.* (2002), Pye *et al.* (2007), and Lawrence and Neff (2009). These effects play an essential role in the chemical composition and concentrations of the Owens (dry) Lake dust samples.

Median percent recovery values were calculated using NIST SRM 2710 in order to evaluate the contribution of the ICP-AES digestion method to the relative difference (%) between PIXE and ICP-AES. Table 4.2 contains the certified values and the median percent recoveries of the digested NIST SRM 2710 material for Al, As, Ba, Cd, Co, Cr, Cu, Fe, Pb, Mn, Mo, Ni, K, Sr, Ti, and Zn. Co, Cr, Mo, and Sr are non-certified values. NIST SRM 2710 was prepared and digested along with the dust samples to document the precision of the digestion method since the efficiency of sample digestion is a vital aspect impinging on the analytical results of multi-element analysis by any of the ICP techniques (Sucharova and Suchara 2008). Matrices of varying environmental samples (i.e. soils, rocks, atmospheric particulate matter, etc.) that have high silica content may reduce the recovery of some elements in the sample when prepared by digestion. Si was not analyzed for by ICP-AES in the NIST SRM 2710 Montana Soil or the Owens (dry) Lake samples. However, the certified value for Si in NIST SRM 2710 is 28.97 ± 0.18 % mass fraction (http://www.nist.gov). Si concentrations in Owens (dry) Lake samples, measured by PIXE, ranged from a low of 6.8% to a high of 18% and a mean concentration of 14% mass fraction. Elements with positive relative variations such as Al, Fe, K, Mn and Ti, have concentrations that vary proportional to one another (Figure 4.4) Si concentrations also reveal this proportionality which is reflective of the spatial (location and height) and temporal (dust event) variations amongst the samples (Figure 4.3).

Si was the second most abundant element ($\mu g\ g^{-1}$) in the Owens (dry) Lake samples in the first dust event (11 March) as reported by PIXE (Na had higher concentrations than Si). Si, Al, Fe, K, Mn, and Ti concentrations increased from the 11 March dust event to the 23 March dust event as opposed to Na and S, which decreased (Figures 3 and 4). Higher concentrations of Si

were found in samples collected from the lower trays of the BSNEs (Figure 4.2) which contained 40% - 60% volume of sand-sized (100 - 1000 μm diameter) particles suggesting that Si concentrations were higher in the coarser particles than finer particles. Elements such as Al, Fe, K, Mn and Ti, that bind in silicate structures are not completely released or dissolved in digests by common mineral acids (Felt and Georgian 2008; Shafer *et al.* 2008; Sucharova and Suchara 2008) such as hydrochloric acid and nitric acid. Method 3050B is not a total digestion technique (Bacardit and Camarero 2010; He *et al.* 2010), but can provide essential information related to the number of elements which are available in the environment under varying conditions and are potentially toxic (Rao et *al.* 2008). The large difference in concentrations between PIXE and ICP-AES for Al, Fe, K, Mn and Ti can be most likely explained by the incomplete digestion of these elements under EPA Method 3050B.

Table 4.2 shows that the percent recovery for Al is ~19% based on one run. The certified value for Al from Table 4.2 is 6.44±0.08% (mass fraction) which indicates that the digestion efficiency by EPA Method 3050B is only ~19% of the certified value. The relative variation for Al ranged from 89% to 320% indicating that ICP-AES concentrations were ~20 to 40% that of PIXE concentrations as also indicated by the percent recovery value. NIST percent recoveries were used here for assessment purposes only since the elemental matrix and Si content of the NIST SRM 2710 would not be exactly the same as for the Owens (dry) Lake samples. The recoveries do show, however, the effect of Si on the percent recovery of elements that bind to a silicate matrix. These elements include Fe, K, and Ti which have median percent recoveries (based on one analysis) of ~52%, 14%, and 39%, respectively. Median percent recovery for Mn (from three analyses) was ~ 57%. Figure 4.5 shows that Fe and K concentrations were 45 to 85% that of PIXE, Mn was 46 to 66%, and Ti was 32 to 52% that of PIXE concentrations. The percent recovery from NIST SRM 2710 values for these elements provide sufficient evidence to support the argument that the differences between reported PIXE and ICP-AES concentrations are mainly related to the sample preparation (digestion) method for ICP-AES. Additional

confirmation can be seen in Figure 4.4 where Al, Fe, and K show the same spatial and temporal pattern, even though the concentrations are different between PIXE and ICP-AES and have a slightly upward trend similar to the trend for Si (Figure 4.3) Although not shown in Figure 4.3, Mn and Ti have similar trends. This explanation is supported by the high content of Si in the Owens (dry) Lake samples and the low percent recoveries obtained from the NIST SRM 2710 analyses.

The relative variation of As, Cu, Sr, and Zn was considerably lower than the group of elements that are predominantly present in the silicate matrix. Some samples showed higher concentrations for these elements when measured by PIXE and others when measured by ICP-AES as reflected by their respective max, min, and mean of (37%, -40%, -0.49%), (71%, -26%, 24%), (37%, -40%, -0.49%), and (86%, -55%, 39) (Figure 4.5). The NIST 2710 percent recovery values show that As had a median percent recovery efficiency of 99% which does not fully explain the variation between PIXE and ICP-AES concentrations for As (Figure 4.5). Cu had a median percent recovery of 73%: this is consistent with the relative variation for Cu (Figure 4.5). For Cu, ~86% of the total samples had higher concentration when analyzed by PIXE and the remaining 14% had higher concentrations when analyzed by ICP-AES. Samples with higher concentrations reported by ICP-AES for As and Cu came from the first two (11 March and 17 March) dust events. The 11 March dust samples were predominantly comprised of eroded efflorescent sodium sulfate and carbonate salts (Tyler *et al.* 1997, Rojo *et al.* 2008), while the 17 March dust samples were comprised of a mixture of evaporites and clastic materials derived from the erosion of the underlying salt-silt-clay crust (Cahill *et al.* 1996, Rojo *et al.* 2008). Sr had the least relative variation ranging from -3% to 34% where most of the sample concentrations measured by ICP-AES were on the average 90% that of PIXE concentrations. The median percent recovery for Sr was only 30% based on one run. The percent recovery for Sr does not coincide with the relative variation because NIST SRM 2710, a clastic matrix, may not be exactly comparable to evaporite/carbonate matrices. Sr concentrations were considerably

higher in the S1, S2, S3 locations relative to the H1, H2, H3, and H4 locations for the 17 March dust event. The same pattern was observed in the 23 March dust event, but at a much lesser extent. The S-locations were covered by sand-textured sediments more predominately than efflorescent evaporites; the higher Sr concentrations therein may be due to presence of sand-sized calcite grains. By 23 March, most of the efflorescent salts had been removed by the wind, and the entire transect was more clastic- and carbonate-dominated (Rojo *et al.* 2008). Zn had a percent recovery of 67% and a relative variation ranging from -55% to 86%. Although PIXE and ICP-AES concentrations followed a similar distribution, the data was difficult to assess since it appeared to have extreme concentrations for certain samples of no specific pattern for the 11 March dust event. Zn concentrations decreased from the 11 March to the 23 March dust event, but increased slightly with height. These variations in Zn are likely an artifact of the BSNE dust collector itself, which is made of zinc-galvanized sheet steel (Van Pelt and Zobeck 2007).

It is possible that the grain size of the sediment particles, both as sampled in the field and after grinding (comminution) will affect both the efficiency of digestion for samples analyzed by ICP-AES and the potential auto-absorption of X-rays (especially for light elements) for samples analyzed by PIXE. Different sample preparation methods for analytical techniques can result in differences in reported elemental concentrations; for example, Ruth *et al.* (2008) reported higher PIXE-detected concentrations of aluminum in ice core dust samples than ICP-MS-detected concentrations, and ascribed the differences to issues in the ICP-MS acid digestion method.

Of the 25 elements reported by both techniques, Ba, Cd, Co, Cr, Mo, and Pb were not detected by PIXE, but were detected by ICP-AES. These elements belong to the transition metals group and are also well known heavy metals with the exception of Ba. Elements not detected by either analytical technique are most likely due to a combination of atomic number (high Z), analytical conditions (in the case of PIXE, irradiation time and/or peak analysis software), matrix interferences, detection limits, and/or low concentrations in the dust samples compared to

detection limits. Table 4.1 shows that Ba, Cd, Co, Cr, Mo, and Pb also formed part of the elemental matrix for NIST SRM 2711 (Co, Cr, and Mo show non-certified values) Cd, Co, and Mo were also not detected by PIXE in the NIST SRM 2711 soil material. Ba was detected with a mean of 615.92 ± 256.38 μg g^{-1} as compared to the certified value of 726 ±38 μg g^{-1}. However, Ba concentrations in the Owens (dry) Lake samples measured by ICP-AES were much lower, ranging from a low of 13.9 to a high of 242.0 μg g^{-1} with corresponding DL established by PIXE of 97.64 and 212.1 μg g^{-1}, respectively (Table 4.4). Cr and Pb were also detected by PIXE in the NIST SRM 2711 soil material with a mean mass concentration of 43.67 ± 8.22 μg g^{-1} compared to the non-certified value of 47 μg g^{-1} and a mean concentration of 0.117% ± 0.003% as compared to the certified value of 0.1162% ± 31%, respectively. The NIST SRM 2711 certified value for Cd is 41.70 ± 0.25 μg g^{-1} and the non-certified values for Co and Mo are 10 μg g^{-1} and 1.6 μg g^{-1}, respectively. A review of ICP-AES results showed that in the Owens (dry) Lake samples, Ba, Cd, Co, Cr, Mo, and Pb were present in trace amounts generally below the detection limits of the PIXE analyses under the aforementioned analytical conditions. The PIXE limit of detection (LOD) value for an element is calculated on the basis of 3 standard deviations (σ) of the background area (B) over one full-width-at-half-maximum (FWHM) of the principal X-ray peak centroid. For higher-Z elements such as Ba and Pb, PIXE detection with the experimental setup used would be via their L X-rays rather than their more intense K x-rays, strongly increasing detection limits and decreasing ability to detect these elements via PIXE.

Table 4.4 shows the detection limits established by PIXE and the concentrations detected by ICP-AES in μg g^{-1}. Table 4.4 also shows the absolute difference between the detection limits and ICP-AES concentration. The detection limits established by PIXE were at least 90% of the time considerably higher than the concentrations reported by ICP-AES. The detection limits for Cd, Co, and Mo (NIST SRM 2711) were at all times higher than the certified/non-certified values with at an average of 48.83, 23.40, and 14.89 μg g^{-1} respectively.

Ba, Cd, Co, Cr, Mo, and Pb were present in the dust in trace amounts. It is possible, however, that the concentrations reported by ICP-AES were under-reported, if they were present in the silicate matrix of the samples, as was the case with Al, Fe, K, Mn, and Ti. The mean percent recovery values for Ba, Cd, Co, Cr, Mo, and Pb are 46%, 80.3%, 99.2%, 51.0%, 81.4%, and 79.7%, respectively (Table 4.2). The percent recoveries provide sufficient information to support the idea that these elements were present in trace amounts. Knowing the concentration of these samples is important since X-ray spectral intensities measured by PIXE are proportional to the concentrations of the elements in the samples (Pajek *et al.* 1999). In some instances, the intensity of Kα X-rays for transition elements has been corrected for contribution of Kβ X-Rays from adjacent elements (Bolormaa *et al.* 2007). It is possible to also use a filter to attenuate the x-ray lines corresponding to major elements for improved detection of other elements (Roelandts and Weber 1999). The type of absorber material and thickness is directly dependent on the sample matrix and the elements of interest (Kuisma-Kursula, 2000). Spectrum fitting, the detection efficiency, and values of X-ray transmission through the absorber can account for the majority of errors in the analytical results by PIXE (Saitoh *et al.*, 2002). Although PIXE is capable of detecting elements from Na to U, detection limits are largely dependent on atomic number Z of the target element, irradiation time, matrix interferences, detector efficiency, and proton beam intensity (Demortier 1999; Papp *et al.* 2002). In PIXE, X-ray production cross-sections decrease with increasing atomic number for a given target element (Neelmeijer and Mader 2002), thus higher atomic numbered elements produce fewer X-rays per unit proton charge than do lower atomic numbered elements. Very light elements ($Z < 11$) cannot be detected by PIXE, and since characteristic X-ray energies of light elements such as Na are very low, they will have high minimum limits of detection by PIXE. These factors combine to make the PIXE technique not generally as well suited as the ICP-AES technique for the analysis of heavy elements or very light elements. Furthermore, for small concentrations of trace elements, the particle size of the sample becomes an essential determining factor of how many individual particles may be present in the sampled volume.

Table 4.4 compares the maximum and minimum detection limits established by PIXE to the maximum and minimum concentrations measured by ICP-AES for Ba, Cd, Co, Cr, Mo, and Pb, respectively. Thus, the relatively high PIXE detection limits for these elements under the analytical conditions experienced coupled with low actual concentrations of the elements in the samples as determined by ICP-AES can explain the non-detection of Ba, Cd, Co, Cr, Mo, and Pb by PIXE. For elements Ba, Cr, and Pb the detection limits established by PIXE were not much higher than the concentrations reported by ICP-AES and thus a longer time of exposure to the proton beam could have lowered the detection limits in the PIXE analyses and resulted in the detection of these elements by PIXE. Ba and Pb detection in PIXE, which must be accomplished via L lines, is hampered by K/L line interferences with lighter elements. Thus, low intrinsic concentrations and/or high atomic numbers present the most likely explanation of the non-detection of Ba , Cd, Co, Cr, Mo, and Pb in these samples by PIXE.

Conclusions

We presented and inter-compared the elements detected and their concentrations in a suite of aeolian dust samples analyzed by ICP-AES and PIXE. We encountered two main anomalies: (1) differences in elements detected by the two techniques and (2) variations in concentrations for certain elements detected by both PIXE and ICP-AES as presented in the previous sections. The intrinsic differences of each technique and analytical method appear to be major contributing factors to the differences in concentrations and/or detection of elements between the two analytical techniques. Other contributing factors may be related to matrix effects, limits of detection, and/or sample preparation.

The difference in concentrations between the two analytical techniques may be related to matrix effects which are reflected in the sample preparation method used for ICP-AES analysis. Samples of solid material need to be converted to aqueous form for analysis by ICP-AES. This can be achieved by a fusion and subsequent dissolution or an acid digestion either by hot plate or

microwave (Cook *et al.* 1997; Perez-Santana *et al.* 2007). The method chosen was digestion by hot plate. This sample preparation method uses a combination of strong acids to digest the sample as described above in the Experimental section. Elements bound in silicate structures- typical of soils and sediments- may not be completely dissolved by this type of acid digestion, therefore leaving traces of undissolved samples behind (Gasparics *et al.* 1997; Hoenig 2001; Smodis 2007). Silicon concentrations in samples reported by PIXE were on the average 1.39 x 10^5 µg g-1. This likely explains some of the observed differences between elemental concentrations obtained by PIXE and ICP-AES, since PIXE analyzes the solid sample. An analysis of the undissolved residues remaining after digestion should provide results that could be used for a mass balance calculation to reduce the apparent discrepancy between the PIXE and ICP-AES results (Lunderberg *et al.* 2008; Peaslee *et al.* 2008). It is also possible that the use of a hot plate rather than a microwave for the digestions increased the variability between the two sets of analyses. Microwave digestion is found to result in more consistent recoveries because the possibility of boiling a sample is greatly reduced, however the greater influence on the analytical differences is the completeness of the digestion, which will be directly related to the matrix of the sample (Cook *et al.* 1997; Perez-Santana *et al.* 2007).

This study clearly shows how two different analytical techniques can provide different apparent analytical results when the same materials are analyzed. When a given element is present at concentrations close to the limit of detection of one technique or the other, disparities are likely to manifest in elements reported by the two techniques. The use of X-ray spectrometric methods such as PIXE reduces the need for extensive sample preparation (dissolution in acids), but may sacrifice accuracy in the detection and quantification of elements especially at low concentrations or low or high atomic numbers. ICP techniques can detect elements at low concentrations, but incomplete dissolution of samples- especially silica-rich materials- can impart error in the results, especially for elements bound into the silicate matrix. Therefore, when choosing analytical techniques, sample preparation techniques, and interpreting analytical results

for geological samples, care should be taken to consider the impacts on analysis from samples of different mineralogies / compositions resulting from different geological processes (in this example, sediments comprised primarily of evaporites vs. clastic sediments).

When economically feasible, the use of more than one technique (such as an X-ray spectrometric technique and an ICP technique) may serve as quality assurance and may yield valuable results to improve understanding of potential sources of error in analysis, better assess the actual concentrations and partitioning of elements present, and to provide high confidence in the concentrations of certain elements which are more accurately quantified by one technique or another. The exploration of possible causes of variability and inter-comparison of data results helps establish quality assurance techniques that will further assist in data interpretation and will provide a stronger understanding of the differences in analytical techniques. This evaluation has also exposed the importance of proper data manipulation to assure data integrity and proper data comparison to include uncertainties, adequate concentration units, and consideration of detection limits. It is of essence however, to clearly define the scope and purpose of a particular study and to become familiar with the capabilities and limitations of each analytical technique prior to sample analysis.

References

Aburaya J., Added N., Tabacniks M., de Almeida Rizzutto M. and Lopes Barbosa M.D. 2006. X-ray production yield in standardized thick target PIXE. Nuclear Instruments and Methods in Physics Research B, 249, 792–795.

Aldape, F., Hernandez-Mendez B. and Flores M. J. 1999. Manganese survey in airborne particulate matter from a mining area at Hidalgo State, Mexico. Nuclear Instruments and Methods in Physics Research Section B- Beam Interactions with Materials and Atoms, 150, 363-369.

Almeida, S.M., Reis M.A., Freitas M.C. and Pio C.A. 2003. Quality assurance in elemental analysis of airborne particles. Nuclear Instruments and Methods in Physics Research Section B- Beam Interactions with Materials and Atoms, 207, 434- 446.

Almeida, S.M., Freitas M.C., Reis M.A., Pio C.A. and Trancoso M.A. 2006. Combined application of multielement analysis—k0-INAA and PIXE—and classical techniques for source apportionment in aerosol studies. Nuclear Instruments and Methods in Physics Research Section A- Accelerators, Spectrometers, Detectors And Associated Equipment, 564, 752–760.

Bacardit, M.and Camarero L. 2010. Atmospherically deposited major and trace elements in the winter snowpack along a gradient of altitude in the Central Pyrenees: The seasonal record of long-range fluxes over SW Europe. Atmospheric Environment, 44, 582–595.

Barreiros, M.A., Pinheiro T., Araújo M.F., Costa M.M., Palha M. and DaSilva R.C., 2001. Quality assurance of X-ray spectrometry for chemical analysis. Spectrochimica Acta, B 56, 2095–2106.

Bellot-Gurlet, L., Poupeau G., Salomon J., Calligaro T., Moignard B., Dran J.C., Barrat J.A. and Pichon L., 2005. Obsidian provenance studies in archaeology, a comparison between PIXE, ICP-AES and ICP-MS. Nuclear Instruments and Methods in Physics Research Section B- Beam Interactions with Materials and Atoms, 240, 583– 588.

Bischoff, J.L. and Cummins K. 2001. Wisconsin glaciation of the Sierra Nevada, 79,000-15,000 yr B.P. as recorded by rock flour in sediments of Owens Lake, California. Quaternary Research, 55, 14- 24.

Bolormaa, O., Baasansurena J., Kawasaki K., Watanabe M. and Hattroi T. 2007. Total elemental composition analysis of soil samples using the PIXE technique. Nuclear Instruments and Methods in Physics Research Section B- Beam Interactions with Materials and Atoms, 262, 385–390.

Breit, G.N., Yount J.C., Uddin M.N., Muneem A.A., Lowers H.A., Berry C.J. and Whitney, J.W. 2007. Compositional data for Bengal Delta sediment collected from a borehole at Rajoir, Bangladesh. U.S. Geological Survey Open-File Report, 2007-1022, 46 pp.

Budka, D., Przybyowicz W.J., Mesjasz-Przybyowicz J. and Sawicka-Kapusta K. 2002. Elemental distribution in lichens transplanted to polluted forest sites near Kraków, Poland. Nuclear Instruments and Methods in Physics Research Section B- Beam Interactions with Materials and Atoms, 189, 499-505.

Byrne, A.R. and Benedik, L. 1988. Determination of uranium at trace levels by radiochemical neutron activation analysis employing radioisotopic yield determination. Talanta, 35, 161- 166.

Cahill, T.A., Gill T.E., Reid J.S., Gearhart E.A. and Gillette D.A. 1996. Saltating particles, playa crusts and dust aerosols at Owens (Dry) Lake, California. Earth Surface Processes and Landforms, 21, 621- 639.

Campbell, J.L., Higuchi D., Maxwell J.A. and Teesdale W.J. 1993. Quantitative PIXE microanalysis of thick specimens. Nuclear Instruments and Methods in Physics Research Section B- Beam Interactions with Materials and Atoms, 77, 95- 109.

Castillo, S., Moreno T., Querol X., Alastuey A., Cuevas E., Herrmann L., Mounkailac M. and Gibbons W. 2008. Trace element variation in size-fractionated African desert dusts. Journal of Arid Environments, 72, 1034–1045.

Cook, J.M., Gardner M.J., Griffiths A.H., Jessep M.A., Ravenscroft J.E. and Yates, R. 1997. The comparability of sample digestion techniques for the determination of metals in sediments. Marine Pollution Bulletin, 34, 637-644.

Cruvinel, P.E., Flocchini R.G., Artaxo P., Crestana S. and Herrmann P.S.P. Jr. 1999. Elemental analysis of agricultural soil samples by particle induced X-ray emission , PIXE. technique. Nuclear Instruments and Methods in Physics Research Section B- Beam Interactions with Materials and Atoms, 150, 478- 483.

Demortier, G. 1999. PIXE analysis of high Z complex matrices. Nuclear Instruments and Methods in Physics Research Section B- Beam Interactions with Materials and Atoms, 150, 520- 531.

Dias da Cunha, K. and Barros Leite C.V. 2002. Metal trace analysis by PIXE and PDMS techniques. Nuclear Instruments and Methods in Physics Research Section B- Beam Interactions with Materials and Atoms, 187, 401–407.

Felt, D. R., Bednara A. J. and Georgian T. 2008. The effects of grinding methods on metals concentrations in soil. Talanta, 77 380–387.

Fryrear, D.W. 1986. A field dust sampler. Journal of Soil and Water Conservation, 41, 117-120.

Garman, E. 1999. Leaving no element of doubt, analysis of proteins using microPIXE. Structure, 7, R291–R299.

Gasparics, T., Csato I. and Zaray Gy. 1997. Analysis of Antarctic marine sediment by inductively coupled plasma atomic emission and total reflection X-ray fluorescence spectrometry. Microchemical Journal, 55, 56- 63.

Gatti, L. V., Mozeto A. A. and Artaxo P. 1999. Trace elements in lake sediments measured by the PIXE technique. Nuclear Instruments and Methods in Physics Research Section B- Beam Interactions with Materials and Atoms, 150, 298-305.

Gerab, F., Artaxo P., Gillett R. and Ayers G. 1998. PIXE, PIGE and ion chromatography of aerosol particles from northeast Amazon Basin. Nuclear Instruments and Methods in Physics Research Section B- Beam Interactions with Materials and Atoms, 136-138, 955-960.

Gidhagen, L., Kahelin H., Schmidt-Thomé P. and Johansson C. 2002. Anthropogenic and natural levels of arsenic in PM10 in Central and Northern Chile. Atmospheric Environment, 36, 3803-3817.

Gill, T.E. 1996. Eolian sediments generated by anthropogenic disturbance of playas: human impacts on the geomorphic system and geomorphic impacts on the human system. Geomorphology, 17, 207- 228.

Gill, T.E., Gillette D.A., Niemeyer T. and Winn R.T., 2002. Elemental geochemistry of wind-erodible playa sediments, Owens Lake, California. Nuclear Instruments and Methods in Physics Research Section B- Beam Interactions with Materials and Atoms, 189, 209–213.

Gillette, D.A., Fryrear D.W., Gill T.E., Ley T., Cahill T.A. and Gearhart, E.A. 1997. Relation of vertical flux of particles smaller than 10 μm to total aeolian horizontal mass flux at Owens Lake. Journal of Geophysical Research, 102, 26009- 26015.

Grave, P., Lisle L. and Maccheroni M. 2005. Multivariate comparison of ICP-OES and PIXE/PIGE analysis of east Asian storage jars. Journal of Archaeological Science, 32, 885-896.

He, Y. T., Fitzmaurice A. G., Bilgin A., Choi S., O'Day P., Horst J., Harrington J., Reisinger H. J., Burris D. R. and Hering J. G. 2010. Geochemical processes controlling arsenic mobility in groundwater: A case study of arsenic mobilization and natural attenuation. Applied Geochemistry, 25, 69–80.

Hill, S.J., Arowolo T.A., Butler O.T., Chenery S.R.N., Cook J.M., Cresser M.S. and Miles, D.L. 2002. Atomic spectrometry update. Environmental analysis. Journal of Analytical Atomic Spectrometry, 17, 284- 317.

Hoenig, M. 2001. Preparation steps in environmental trace element analysis -- facts and traps. Talanta, 54, 1021-1038.

Kiminami, K. and Fujii K. 2007. The relationship between major element concentration and grain size within sandstones from four turbidite sequences in Japan. Sedimentary Geology, 195, 203–215.

Kuisma-Kursula, P. 2000. Accuracy, precision and detection limits of SEM–WDS, SEM–EDS and PIXE in the multi-elemental analysis of medieval glass. X-Ray Spectrometry, 29, 111–118.

Lawrence, C. R. and Neff J. C. 2009. The contemporary physical and chemical flux of aeolian dust: A synthesis of direct measurements of dust deposition. Chemical Geology, 267, 46–63.

Levy, D.B., Schramke J.A., Esposito K.J., Erickson T.A. and Moore J.C. 1999. The shallow ground water chemistry of arsenic, fluorine, and major elements, eastern Owens Lake, California. Applied Geochemistry, 14, 53- 65.

Lindstrom, R.M., Byrne A.R., Becker D.A., Smodis B. and Garrity, K.M. 1990. Characterization of the mineral fraction in botanical reference materials and its influence on homogeneity and analytical results. Fresenius Journal of Analytical Chemistry, 338, 569- 571.

Lunderberg, J.M., Bartlett R.J., Behm A.M., Contreras C., DeYoung P.A., Hoogeveen N.L., Huisman A.J., Peaslee G.F. and Postma J.K. 2008. PIXE as a complement to trace metal analysis of sediments by ICP-OES. Nuclear Instruments and Methods in Physics Research Section B- Beam Interactions with Materials and Atoms, 266, 4782- 4787.

Ma, C., Kasahara M., Holler R. and Kamiya T. 2001. Characteristics of single particles sampled in Japan during the Asian dust-storm period. Atmospheric Environment, 35, 2707-2714.

Marino, F., Calzolai G., Caporali S., Castellano E., Chiari M., Lucarelli F., Maggi V., Nava S., Sala M. and Udisti R. 2008. PIXE and PIGE techniques for the analysis of Antarctic ice dust and continental sediments. Nuclear Instruments and Methods in Physics Research Section B- Beam Interactions with Materials and Atoms, 266, 2396-2400.

Markwitz, A., Barry B. and Shagjjamba, D. 2008. PIXE analysis of sand and soil from Ulaanbaatar and Karakurum, Mongolia. Nuclear Instruments and Methods in Physics Research Section B- Beam Interactions with Materials and Atoms, 266, 4010- 4019.

Maxwell, J.A., Teesdale W.J. and Campbell J.L. 1995. The Guelph PIXE software package II. Nuclear Instruments and Methods in Physics Research Section B- Beam Interactions with Materials and Atoms, 95, 407-421.

Menzel, N., Schramel P. and Wittmaack K. 2002. Elemental composition of aerosol particulate matter collected on membrane filters, a comparison of results by PIXE and ICP-AES. Nuclear Instruments and Methods in Physics Research Section B- Beam Interactions with Materials and Atoms, 189, 94- 99.

Mouli, C. P., Venkata Mohan S., Balaram V., Praveen Kumar M. and Jayarama Reddy S. 2006. A study on trace elemental composition of atmospheric aerosols at a semi-arid urban site using ICP-MS technique. Atmospheric Environment, 40, 136-146.

Nayak, P.K. and Vijayan, V. 2006. Complementary PIGE, PIXE, EDXRF and γ-ray spectroscopic investigation on natural chromites. Nuclear Instruments and Methods in Physics Research Section B- Beam Interactions with Materials and Atoms, 245, 505–510.

Neelmeijer, C. and Mader, M. 2002. The merits of particle induced X-ray emission in revealing painting techniques. Nuclear Instruments and Methods in Physics Research Section B- Beam Interactions with Materials and Atoms, 189, 293– 302.

Nsouli, B., Darwish T., Thomas J.P., Zahraman K. and Roumie M. 2004. Ni, Cu, Zn and Pb background values determination in representative Lebanese soil using the thick target PIXE technique. Nuclear Instruments and Methods in Physics Research Section B- Beam Interactions with Materials and Atoms, 219–220, 181–186.

Ono, D. 2006. Application of the Gillette model for windblown dust at Owens Lake, CA. Atmospheric Environment, 40, 3011- 3021.

Pajek, M., Jaskola M., Czyzewski T., Glowacka L., Banas D., Braziewicz J., Kretschmer W., Lapicki Trautmann G., D. 1999. M-shell X-ray production cross sections for PIXE applications. Nuclear Instruments and Methods in Physics Research Section B- Beam Interactions with Materials and Atoms, 150, 33-39.

Papp, T., Lakatos T., Nejedly Z. and Campbell, J.L. 2002. Improvement in limit of detection in particle induced X-ray emission by means of rise time and pulse shape discrimination. Nuclear Instruments and Methods in Physics Research Section B- Beam Interactions with Materials and Atoms, 189, 66–71.

Pappalardo, L., Karydas A.G., Kotzamani N., Pappalardo G., Romano F.P. and Zarkadas Ch. 2005. Complementary use of PIXE-alpha and XRF portable systems for the non-destructive and in situ characterization of gemstones in museums. Nuclear Instruments

and Methods in Physics Research Section B: Beam Interactions with Materials and Atoms, 239, 1-2, 114-121.

Peaslee, G.F., DeYoung P.A., Lunderberg J.M., Rojo L., Gill T.E. and Barnes M.A. 2008. PIXE analysis of lake sediment, as a complementary technique for ICP analysis. Geological Society of America Abstracts and Programs, 40, 6, 131.

Pekney, N.J. and Davidson C.I. 2005. Determination of trace elements in ambient aerosol samples. Analytica Chimica Acta, 540, 269-277.

Perez-Santana, S., Pomares Alfonso M., Villanueva Tagle M., Pena Icart M., Brunori C. and Morabito R. 2007. Total and partial digestion of sediments for the evaluation of trace element environmental pollution. Chemosphere, 66, 1545-1553.

Pillay, A.E. 2001. Analysis of archaeological artefacts, PIXE, XRF or ICP-MS? Journal of Radioanalytical and Nuclear Chemistry, 247, 593- 595.

Prati, P., Lucarelli F., Mandò P. A., Tonus S., Zucchiatti A. and Calastrini F. 1998. PIXE measurements of particulate concentrations in atmosphere near a steel smelter in Genova, Italy. Nuclear Instruments and Methods in Physics Research Section B: Beam Interactions with Materials and Atoms, 139, 258-263.

Pye, K., Blott S.J. and Wray D.S. 2006. Elemental analysis of soil samples for forensic purposes by inductively coupled plasma spectrometry — precision considerations. Forensic Science International, 160, 178–192.

Rao, C. R. M., Sahuquillo A. and Lopez-Sanchez J. F. 2008. A review of the different methods applied in environmental geochemistry for single and sequential extraction of trace elements in soils and related materials. Water Air and Soil Pollution, 189, 291–333.

Reheis, M.C., Budahn J.R. and Lamothe P.J. 2002. Geochemical evidence for diversity of dust sources in the southwestern United States. Geochimica et Cosmochimica Acta, 66, 1569-1587.

Rice, K.C. 1999. Trace-element concentrations in streambed sediment across the conterminous United States. Environmental Science and Technology, 33, 2499- 2504.

Roelandts, I. and Weber G. 1999. Two decades with PIXE spectrometry at the University of Liege. Journal of Radioanalytical and Nuclear Chemistry, 240, 413-424.

Rojo, L., Gill T.E. and Gillette D.A. 2008. Particle size/composition relationships of wind-eroding sediments, Owens (Dry) Lake, California, USA. X-Ray Spectrometry, 37, 111-115.

Ruth, U., Barbante C., Bigler M., Delmonte B., Fischer H., Gabrielli P., Gaspari V., Kaufmann P., Lambert F., Maggi W., Marino F., Petit J.-R., Udisti R., Wagenbach D., Wegner A. and Wolff E.W. 2008. Proxies and measurement techniques for mineral dust in Antarctic ice cores. Environmental Science and Technology, 42, 5675- 5681.

Ryu, J.H., Gao S., Dahlgren R.A. and Zirenberg, R.A. 2002. Arsenic distribution, speciation and solubility in shallow groundwater of Owens Dry Lake, California. Geochimica et Cosmochimica Acta, 66, 2981– 2994.

Saint- Amand, P., Gaines C. and Saint- Amand D. 1987. Owens Lake, an ionic soap opera staged on a natric playa. Geological Society of America Centennial Field Guide-Cordilleran Section, 113- 118.

Saitoh, K., Sera K., Gotoh T. and Nakamura M. 2002. Comparison of elemental quantity by PIXE and ICP-MS and/or ICP-AES for NIST standards. Nuclear Instruments and Methods in Physics Research Section B- Beam Interactions with Materials and Atoms, 189, 86- 93.

Santos, W.P.C., Hatje V., Lima L.N., Trignano S.V., Barros F., Castro J.T. and Korn M.G.A. 2008. Evaluation of sample preparation , grinding and sieving of bivalves, coffee and cowpea beans for multi-element analysis. Microchemical Journal, 89, 123- 130.

Smodis, B. 2007. Investigation of trace element atmospheric pollution by nuclear analytical techniques at a global scale: Harmonised approaches supported by the IAEA. Journal of Environmental Management, 85, 121-128.

Stihi, C., Bancuta A., Popescu I.V., Virgolici M., Cimpoca V., Gugiu M. and Vlaicu Gh. 2006. Air pollution studies using PIXE and ICP methods. Journal of Physics- Conference Series, 41, 565- 568.

Strivay, D., Ramboz C., J.P. Gallien, D. Grambole, Sauvage T., Kouzmanov K. 2008. Micro-crystalline inclusions analysis by PIXE and RBS. Nuclear Instruments and Methods in Physics Research Section B- Beam Interactions with Materials and Atoms, 266, 2375–2378.

Sucharova, J. and Suchara I. 2006. Determination of 36 elements in plant reference materials with different Si contents by inductively coupled plasma mass spectrometry: Comparison of microwave digestions assisted by three types of digestion mixtures. Analytica Chimica Acta, 576, 163–176.

Tyler, S.W., Kranz S., Parlange M.B., Albertson J., Katul G.G., Cochran G.F., Lyles B.A. and Holder, G. 1997. Estimation of groundwater evaporation and salt flux from Owens Lake, California, USA. Journal of Hydrology, 200, 110- 135.

United States Environmental Protection Agency 1996. Method 3050B, Acid digestion of sediments, sludges, and soils, and Method 6010B, Inductively Coupled Plasma- Atomic Emission Spectrometry.

United States Environmental Protection Agency 1999. Compendium Method IO-3.6, Determination of metals in ambient particulate matter using proton induced x-ray emission spectroscopy. Center for Environmental Research Information, Office of Research and Development, U.S. Environmental Protection Agency, Cincinnati, OH, Document Number EPA/625/R-96/010a, online at http://www.epa.gov/ttnamti1/files/ambient/inorganic/mthd-3-6.pdf

Van Pelt, R.S. and Zobeck T.M. 2007. Chemical constituents of fugitive dust. Environmental Monitoring and Assessment, 130, 3- 16.

Wang, J., Nakazato T., Sakanishi K.,Yamada O., Tao H. and Saito I. 2004. Microwave digestion with HNO_3/H_2O_2 mixture at high temperatures for determination of trace elements in coal by ICP-OES and ICP-MS. Analytica Chimica Acta, 514, 115–124.

Zachariadis, G.A. and Michos, C.E. 2007. Development of a slurry introduction method for multi-element analysis of antibiotics by inductively coupled plasma atomic emission spectrometry using various types of spray chamber and nebulizer configurations. Journal of Pharmaceutical and Biomedical Analysis, 43, 951-958.

Zahid, A., Hassan M. Q., Breit G. N., Balke K.D. and Flegr M. 2009. Accumulation of iron and arsenic in the Chandina alluvium of the lower delta plain, Southeastern Bangladesh. Environmental Geochemistry and Health, 31, 69–84.

Zhang, B., Cheng H.S., Ma B., Li Q.H., Zhang P., Gan F.X. and Yang F.J., 2005. PIXE and ICP-AES analysis of early glass unearthed from Xinjiang, China. Nuclear Instruments and Methods in Physics Research Section B- Beam Interactions with Materials and Atoms, 240, 559-564.

Zhang, C. and O'Connor P. 2005. Comparison between heavy metal concentrations in sediments analysed by two methods, analyses on detection limits and data quality. Applied Geochemistry, 20, 1737-1745.

Zhang, W., Yu L., Lu M., Hutchinson S. M., Feng H. 2007. Magnetic approach to normalizing heavy metal concentrations for particle size effects in intertidal sediments in the Yangtze Estuary, China. Environmental Pollution, 147, 238-244.

Zhao, P., Feng Y., Zhu T. and Wu J. 2006. Characterizations of resuspended dust in six cities of North China. Atmospheric Environment, 40, 5807- 5814.

Zhao, X., Zhuang G., Wang Z., Sun Y., Wang Y. and Yuan H. 2007. Variation of sources and mixing mechanism of mineral dust with pollution aerosol- revealed by the two peaks of a super dust storm in Beijing. Atmospheric Research, 84, 265- 279.

Zhong, S., Li J., Whiteman C.F., Bian X. and Yao W. 2008. Climatology of high wind events in the Owens Valley, California. Monthly Weather Review, 136, 3536- 3552.

Tables

Table 4.1 Comparison of NIST certified values to analytical results for PIXE

NIST 2711 certified values				NIST 2711 values analyzed by PIXE															
Element	Units	value	*uncert	Energy (keV)	first run value	first run *uncert	second run value	second run *uncert	third run value	third run *uncert	fourth run value	fourth run *uncert	fifth run value	fifth run *uncert	sixth run value	sixth run *uncert	seventh run value	seventh run *uncert	mean	*uncert
Al	%	6.53	0.09	1.485	5.89	0.06	6.48	0.07	6.44	0.06	6.70	0.07	6.04	0.06	6.26	0.06	7.21	0.07	6.43	0.06
As	µg g^{-1}	105	8	10.544	65	14	78	14	134	14	90	14	102	15	91	15	101	15	95	14
Ba	µg g^{-1}	726	38	4.466	487	233	506	248	706	263	525	256	829	261	622	259	636	275	616	256
Cd	µg g^{-1}	41.7	0.25	23.173	ND		ND		ND		ND		ND		ND		ND		ND	
Ca	%	2.88	0.08	3.692	2.78	0.03	3.15	0.04	3.29	0.04	3.49	0.04	3.30	0.03	3.29	0.04	3.97	0.04	3.33	0.04
Co**	µg g^{-1}	10	NA	6.930	ND		ND		ND		ND		ND		ND		ND		ND	
Cu	µg g^{-1}	114	2	8.048	98	4	112	4	115	4	104	4	122	4	115	4	119	4	112	4
Cr**	µg g^{-1}	47	NA	5.415	37	8	38	8	56	8	39	8	41	9	48	8	46	9	44	8
Fe	%	2.89	0.06	6.404	2.63	0.03	2.89	0.03	2.91	0.03	2.84	0.03	3.08	0.03	2.90	0.03	3.06	0.03	2.90	0.03
Pb	µg g^{-1}	1162	31	10.551	1150	30	1180	30	1050	30	1150	30	1250	30	1180	30	1230	30	1170	30
Mg	%	1.05	0.03	1.254	1.18	0.05	1.21	0.05	1.15	0.05	1.33	0.05	1.08	0.05	1.12	0.06	1.36	0.05	1.20	0.05
Mn	µg g^{-1}	638	28	5.899	588	10	629	10	645	11	645	11	682	11	628	11	688	11	643	11
Mo**	µg g^{-1}	1.6	NA	17.480	ND		ND		ND		ND		ND		ND		ND		ND	
Ni	µg g^{-1}	20.6	1.1	7.478	12.9	2.7	16.3	2.9	13.0	3.0	12.2	3.0	8.6	3.3	15.4	3.2	10.0	3.2	12.6	3.0
P	%	0.09	0.01	2.014	0.11	0.03	0.13	0.03	0.15	0.03	0.18	0.04	0.14	0.03	0.16	0.04	0.18	0.04	0.15	0.03
K	%	2.45	0.08	3.314	2.14	0.03	2.46	0.03	2.49	0.03	2.77	0.03	2.45	0.03	2.62	0.04	3.17	0.04	2.58	0.03
Si	%	30.44	0.19	1.740	25.38	0.25	28.48	0.29	28.52	0.29	29.79	0.30	26.36	0.26	28.01	0.28	33.12	0.33	28.52	0.29
Na	%	1.14	0.03	1.041	1.12	0.12	1.13	0.13	0.91	0.13	1.21	0.12	0.68	0.12	0.85	0.15	1.17	0.13	1.01	0.13
Sr	µg g^{-1}	245.3	0.7	14.165	237.0	13.9	218.9	13.0	240.0	14.2	197.3	14.0	254.0	14.7	258.3	14.7	198.8	13.2	229.2	14.0
S	%	0.042	0.001	2.308	0.067	0.011	0.067	0.014	0.080	0.013	0.094	0.012	0.083	0.012	0.097	0.016	0.109	0.015	0.085	0.013
Ti	%	0.306	0.023	4.511	0.279	0.005	0.304	0.005	0.323	0.005	0.305	0.005	0.317	0.005	0.301	0.005	0.333	0.006	0.309	0.005
V	µg g^{-1}	81.6	2.9	4.952	81.8	20.9	80.4	21.4	61.9	23.1	104.2	22.9	111.5	23.9	62.7	23.0	100.5	24.4	86.1	22.8
Zn	µg g^{-1}	350.4	4.8	8.639	323.7	6.0	336.8	6.0	347.3	6.5	335.9	6.4	378.8	7.0	358.1	6.7	360.9	6.5	348.8	6.4

*Statistical uncertainty in the elemental mass fraction
**Non-certified values
ND: not detected
NA: not applicable

Table 4.2 Comparison of NIST certified values to analytical results for ICP-AES

		NIST 2710 cert values			NIST 2710 leached values					NIST 2710 values analyzed by ICP-AES				
Element	*Method	units	values	uncert	runs	range			median % recovery	Values				median % recovery
						low	high	median		1st	2nd#	3rd	median	
Al		mass %	6.44	0.08	6	1.2	2.6	1.8	28	1.22			1.22	19
As		µg g^{-1}	626	38	3	490	600	590	94	674	622	561	622	99
Ba	Xrf	µg g^{-1}	707	51	3	300	400	360	51	336	342	297	336	48
Cd	Icpms	µg g^{-1}	21.8	0.2	8	13	26	20	92	16.1	18.6	17.8	17.8	82
Co**		µg g^{-1}	10		7	6.3	12	8.2	82	10	10	9	10	103
Cr**		µg g^{-1}	39		6	15	23	19	49	20	21	19	20	51
Cu		µg g^{-1}	2950	130	8	2400	3400	2700	92	2551	2163	978	2163	73
Fe		mass %	3.38	0.10	9	2.2	3.2	2.7	80	1.75			1.75	52
Pb		µg g^{-1}	5532	80	8	4300	7000	5100	92	4769	4905	3545	4769	86
Mn	Xrf	mass %	1.01	0.04	8	0.62	0.9	0.77	76	0.58	0.69	0.49	0.58	57
Mo**	Icpms	µg g^{-1}	19		2	13	27	20	100	16	15	15	15	81
Ni	Icpms	µg g^{-1}	14.3	1.0	8	8.8	15	10.1	71	14.0	15.1	12.8	14.0	98
K		mass %	2.11	0.11	6	0.37	0.5	0.45	21	0.29			0.29	14
Sr**		µg g^{-1}	330		3	94	110	100	42	100			100	30
Ti	Xrf	mass %	0.283	0.010	3	0.092	0.11	0.1	35	0.110			0.110	39
Zn		µg g^{-1}	6952	91	9	5200	6900	5900	85	5467	4635	3088	4635	67

* ICP was used for certified values unless noted

**non-certified values

#50 ml dilution

median % recovery = 100 x [median value/cert value]

Table 4.3 Kruskal-Wallis statistical analysis: comparison of PIXE and ICP-AES

a. Test Statistics(a,b)

		Concentra
Combined dust events	Chi-Square	23.47
	df	1
	Asymp. Sig.	0.00

a. Kruskal Wallis Test
b. Grouping Variable:

b. Test Statistics(a,b)

Date		Concentra
34039.00	Chi-Square	10.29
	df	1
	Asymp. Sig.	0.00
34051.00	Chi-Square	16.36
	df	1
	Asymp. Sig.	0.00

c. Test Statistics(a,b)

Height		Concentra
10	Chi-	5.20
	df	1
	Asymp.	0.02
20	Chi-	4.31
	df	1
	Asymp.	0.04
30	Chi-	4.44
	df	1
	Asymp.	0.04
50	Chi-	3.73
	df	1
	Asymp.	0.05
60	Chi-	2.88
	df	1
	Asymp.	0.09
100	Chi-	3.36
	df	1
	Asymp.	0.07

d. Test Statistics(a,b)

Loc		Concentr
H1	Chi-	3.59
	df	1
	Asymp.	0.06
H2	Chi-	3.78
	df	1
	Asymp.	0.05
H3	Chi-	3.22
	df	1
	Asymp.	0.07
H4	Chi-	3.64
	df	1
	Asymp.	0.06
S1	Chi-	4.49
	df	1
	Asymp.	0.03
S2	Chi-	4.06
	df	1
	Asymp.	0.04
S3	Chi-	1.62
	df	1
	Asymp.	0.20

e. Test Statistics(a,b)

PIXE/ICP		Concentr
Al	Chi-	101.26
	df	1
	Asymp.	0.00
As	Chi-	0.07
	df	1
	Asymp.	0.79
Cu	Chi-	22.90
	df	1
	Asymp.	0.00
Fe	Chi-	65.46
	df	1
	Asymp.	0.00
K	Chi-	92.02
	df	1
	Asymp.	0.00
Mn	Chi-	98.65
	df	1
	Asymp.	0.00
Sr	Chi-	16.86
	df	1
	Asymp.	0.00
Ti	Chi-	101.00
	df	1
	Asymp.	0.00
Zn	Chi-	19.36
	df	1
	Asymp.	0.00

a. Kruskal Wallis Test
b. Grouping Variable: Method

Table 4.4 Comparison of NIST certified values to analytical results from ICP-AES

		PIXE detection limits (μg g^{-1})			ICP-AES analytical values (μg g^{-1})		
Element	**Date**	**Median**	**Min**	**Max**	**Median**	**Min**	**Max**
Ba	11-Mar	121	98	138	36	14	234
Cd	11-Mar	31.2	18.3	41.2	0.22	0.15	0.29
Co	11-Mar	10	8	12	3	2	4
Cr	11-Mar	5	4	5	4	3	5
Pb	11-Mar	8	7	9	10	8	14
Mo	11-Mar	7.7	5.6	9.9	0.56	0.32	0.91
Ba	17-Mar	172	129	212	152	47	242
Cd	17-Mar	37.0	20.4	58.2	0.34	0.25	0.44
Co	17-Mar	10	8	15	4	3	6
Cr	17-Mar	7	5	8	5	4	7
Pb	17-Mar	11	8	13	13	12	15
Mo	17-Mar	9.3	6.3	14.8	0.65	0.51	9.8
Ba	23-Mar	156	134	190	84	25	238
Cd	23-Mar	31.9	21.7	50.8	0.32	0.22	0.46
Co	23-Mar	14	11	22	4	3	6
Cr	23-Mar	6	5	8	5	4	7
Pb	23-Mar	11	9	13	13	12	16
Mo	23-Mar	8.1	5.0	14.1	1.0	0.9	1.8

Figures

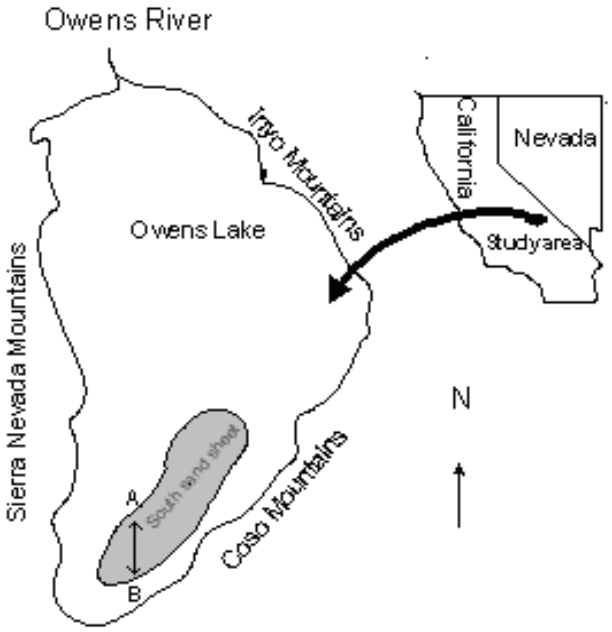

Figure 4.1 Location of study site (after Rojo *et al.* 2008)

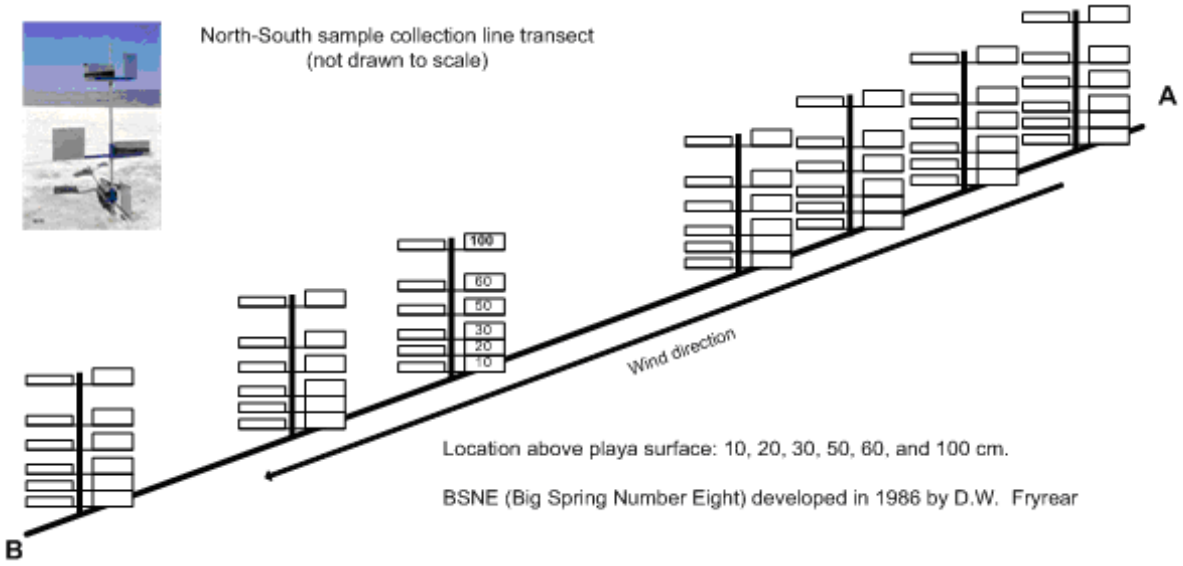

Figure 4.2 BSNE aeolian sediment sampler (after Rojo *et al.* 2008).

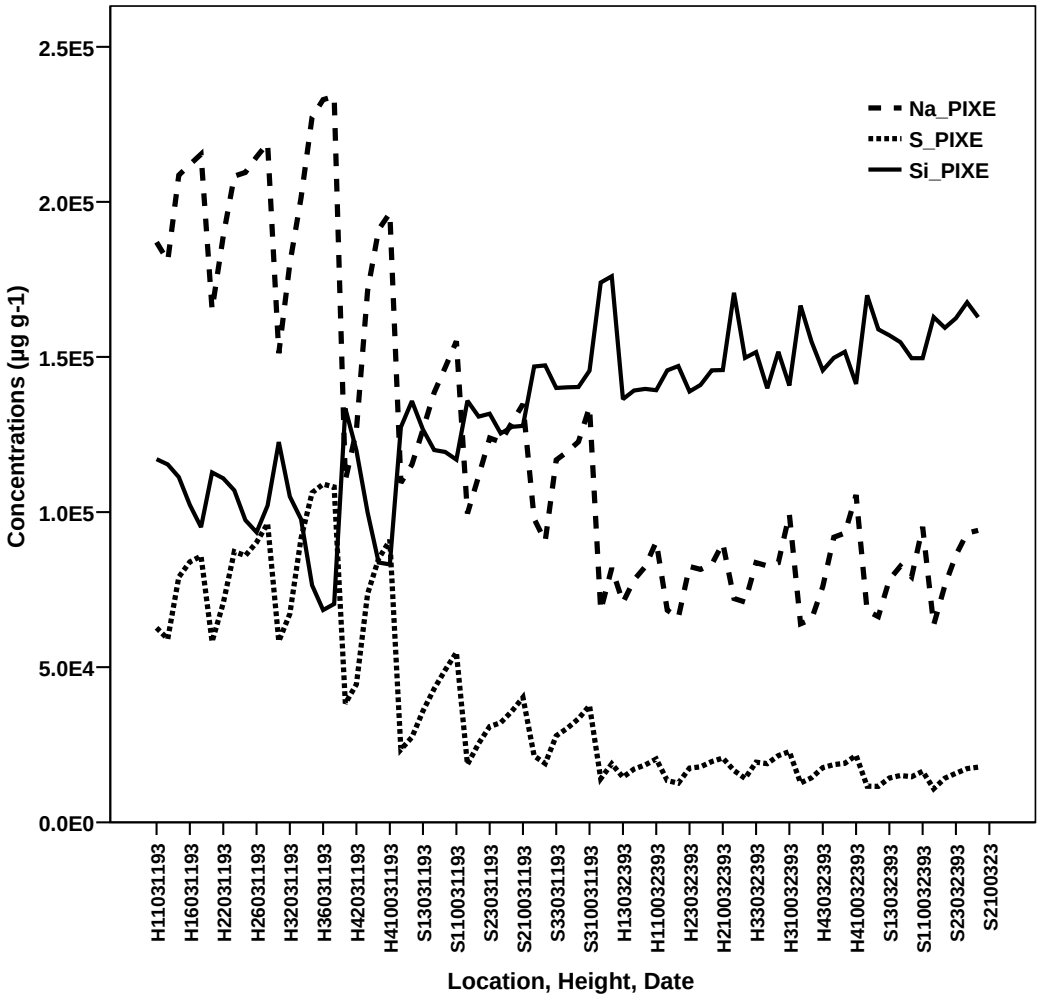

Figure 4.3 Spatial and temporal variation of Na, S, and Si

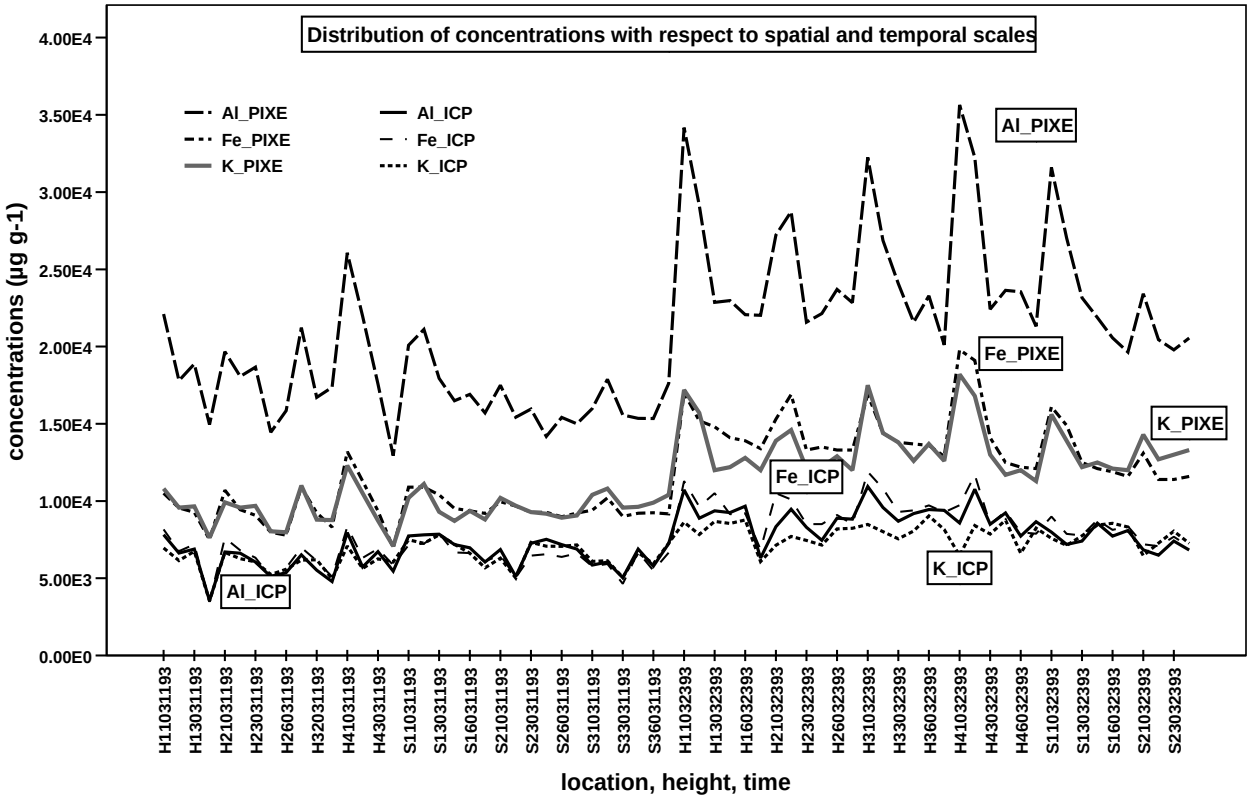

Figure 4.4 Al, Fe, and K concentration variations for PIXE and ICP-AES

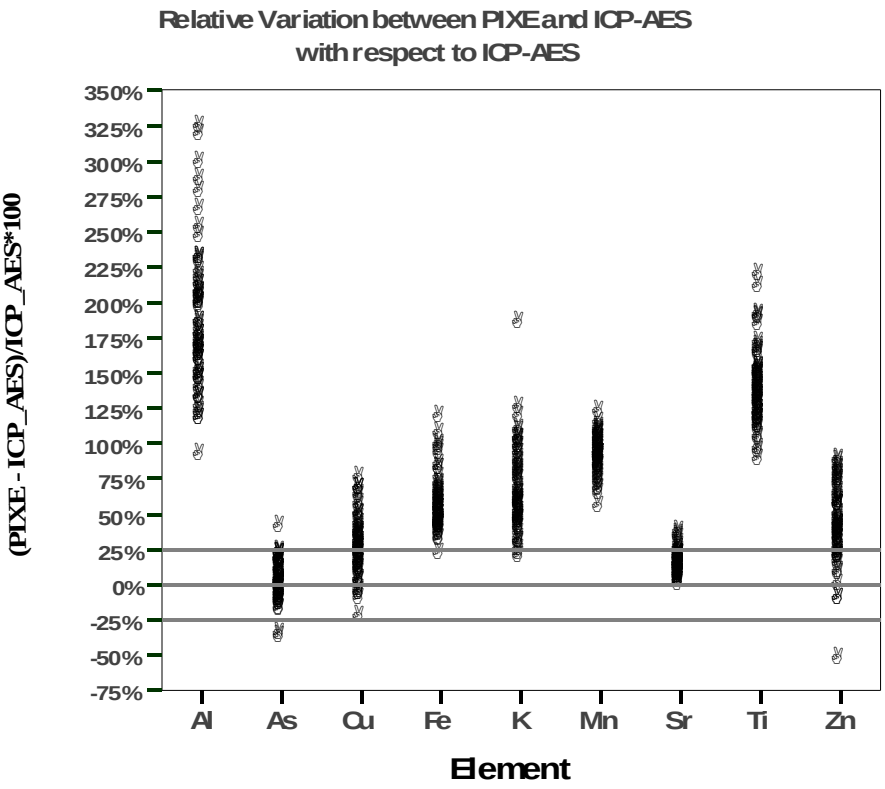

Figure 4.5 Relative variation between PIXE and ICP-AES with respect to ICP-AES

CHAPTER 5. CONCLUSION

This dissertation illustrates the interplay of factors influencing the volumetric particle size distribution (PSD) and elemental chemistry of aeolian dust and sand at Owens (dry) Lake, California during a sequence of four wind events over a time period of less than two weeks, as well as differences encountered between elemental chemistry of splits of the same samples of this material by two different analytical techniques.

The particle size distribution was evaluated by laser diffraction on bulk, dry samples of aeolian material collected during four separate wind storms and categorized by textural category from the finest clay to the coarsest sand to gain knowledge and further understanding of the range of particle sizes of the aeolian sediments moving directly above the surface of the dry playa. PSDs of the collected sediment reflected a trimodal distribution: 63% of samples peaked at 20-50 μm (silt), 11% at 50-100 μm (very fine sand) and 26% at 100-250 μm (fine sand). Most silty samples occurred during the first two events. The particle size distributions reflected the influence of spatial and temporal changes of atmospheric conditions, wind speed and direction, and the playa's composition (transition from a playa covered by efflorescent salts to a degrading salt-silt-clay crust), as well as position in relation to height above the playa surface and location along the 1.2 km transect. This investigation presented the opportunity to therefore infer that these factors do not act independently of one another, but instead influence each other with respect to the distribution of the aeolian dust and sand particles in space and time and the volumetric size distribution of those particles. Other factors influencing the particle size distribution of the sediments, not strictly considered here, would include the rate of aeolian sediment production; the total amount of dust and aeolian sand generated; spatial and temporal variations in the particle size of the playa surface material itself; and variations in dust or sand size and mass produced by deflation, abrasion (including autoabrasion); and saltation-sandblasting. The volumetric distribution of the different grain sizes has provided further insight of the potential influence of wind speed and direction of vertical and horizontal flux of dust and

sand particles, and has offered the opportunity to estimate the transition layer/zone from saltating mode to suspension mode. Particles captured in aeolian saltation or suspension can be further analyzed for elemental composition and evaluate the potential risks to the environment and public health. The correlation of the percent volume of the PSD with respect to location has provided a new opportunity to further investigate the trajectories, characteristics, and variations of these grains at heights of 1m and below. Such understandings of the variations of aeolian transport and dust emission processes at short scales of space and time (from event to event and point to point) shed light on basic sediment transport processes and may provide tools for aeolian dust and sand control and management.

Most of the above samples were analyzed for elemental concentration by Particle-Induced X-Ray Emission Spectrometry (PIXE). Significant differences ($\alpha = 0.05$) in elemental concentrations existed in relation to the PSDs. Na and S concentrations were proportional to the submicron to silt particle fraction during each event. Na and S concentrations covaried with each other and inversely with Si and Ca, increased with height, and decreased with distance downwind and time. On the other hand, Al, Ti, Mn, K, Fe, and Rb concentrations correlated with 100-500µm (fine/medium sand) particles in the first two events and a wider PSD range 250-1000µm (medium/coarse sand) in the third event. Mg, Al, Si, K, Mn, Fe, and Sr concentrations at northerly sites varied with height and location as opposed to nearly constant concentrations at southerly locations. The results of the PIXE analysis of the Owens (Dry) Lake dust and sand samples, when combined with the particle size analyses, suggest fine sodium sulfate salt aerosol emissions, primarily during the first windstorm, while subsequent saltation-dominated events released more aluminosilicate minerals containing higher concentrations of most trace metals. These combined techniques reveal particle size/chemical fractionation and small-scale spatial variability of sediments during dust and sand re-suspension at aeolian "hotspots," with implications to geochemical cycling and aerosol source/ receptor relationships.

We presented and inter-compared the elements detected and their concentrations in a suite of these Owens (dry) Lake aeolian dust and sand samples analyzed by ICP-AES and PIXE. We encountered two main anomalies: (1) differences in elements detected by the two techniques and (2) variations in concentrations for certain elements detected by both PIXE and ICP-AES. The intrinsic differences of each technique and analytical method appear to be major contributing factors to the differences in concentrations and/or detection of elements between the two analytical techniques. Other contributing factors may be related to matrix effects, limits of detection, and/or sample preparation.

The difference in concentrations between the two analytical techniques may be related to matrix effects which are reflected in the sample preparation method used for ICP-AES analysis. Samples of solid material need to be converted to aqueous form for analysis by ICP-AES. This can be achieved by a fusion and subsequent dissolution or an acid digestion either by hot plate or microwave. The method chosen was digestion by hot plate. This sample preparation method uses a combination of strong acids to digest the sample as described above in the Experimental section. Elements bound in silicate structures- typical of soils and sediments- may not be completely dissolved by this type of acid digestion, therefore leaving traces of undissolved samples behind. Silicon concentrations in samples reported by PIXE were on the average 1.39 x 10^5 μg g^{-1}. This likely explains some of the observed differences between elemental concentrations obtained by PIXE and ICP-AES, since PIXE analyzes the solid sample. An analysis of the un-dissolved residues remaining after digestion should provide results that could be used for a mass balance calculation to reduce the apparent discrepancy between the PIXE and ICP-AES results. It is also possible that the use of a hot plate rather than a microwave for the digestions increased the variability between the two sets of analyses. Microwave digestion is found to result in more consistent recoveries because the possibility of boiling a sample is greatly reduced, however the greater influence on the analytical differences is the completeness of the digestion, which will be directly related to the matrix of the sample.

This study clearly shows how two different analytical techniques can provide different apparent analytical results when the same materials are analyzed. When a given element is present at concentrations close to the limit of detection of one technique or the other, disparities are likely to manifest in elements reported by the two techniques. The use of X-ray spectrometric methods such as PIXE reduces the need for extensive sample preparation (dissolution in acids), but may sacrifice accuracy in the detection and quantification of elements especially at low concentrations or low or high atomic numbers. ICP techniques can detect elements at low concentrations, but incomplete dissolution of samples- especially silica-rich materials- can impart error in the results, especially for elements bound into the silicate matrix. Therefore, when choosing analytical techniques, sample preparation techniques, and interpreting results, care should be taken to consider the impacts on analysis from samples of different mineralogies / compositions resulting from different geological processes (in this example, sediments comprised primarily of evaporites vs. clastic sediments).

When economically feasible, the use of more than one technique (such as an X-ray spectrometric technique and an ICP technique) may serve as a quality assurance check and may yield valuable results to improve understanding of potential sources of error in analysis, better assess the actual concentrations and partitioning of elements present, and to provide high confidence in the concentrations of certain elements which are more accurately quantified by one technique or another. The exploration of possible causes of variability and inter-comparison of data results helps establish quality assurance techniques that will further assist in data interpretation and will provide a stronger understanding of the differences in analytical techniques. This evaluation has also exposed the importance of proper data manipulation to assure data integrity and proper data comparison to include uncertainties, adequate concentration units, and consideration of detection limits. It is of essence however, to clearly define the scope and purpose of a particular study and to become familiar with the capabilities and limitations of each analytical technique prior to sample analysis.

I must also note that these data regarding the size and chemistry of the particles analyzed are irrespective of the total amount of sediment collected in each wind storm, at each location, and/or each height. The amount of dust mobilized in each storm or at any point in space and time is a variable related to the playa surface conditions and the strength, orientation, and duration of the wind. For example, the total mass of material collected during these events at heights of 10 and 20 cm above the surface was approximately an order of magnitude higher than the mass collected at 50, 60, and 100 cm, and the total amount of sediment mobilized during the 11 March and 23 March dust storms was approximately two orders of magnitude higher than that of the 17 March storm.

Future work on these samples can investigate the statistical significance of variability and relationships among these factors, and add additional chemical information on the samples obtained via ion chromatography, electron microscopy, and X-ray diffraction, amongst other techniques.

APPENDIX A

Particle size distribution for aeolian samples from Owens (dry) Lake, California (size intervals in percent volume)

Sample ID	Location	Height	Date	.01-1	1-2	2-5	5-10	10-20	20-50	50-100	100-250	250-500	500-1000	1000-2000
H11031193	H1	10	11-Mar-93	0.97	3.35	7.44	9.25	9.66	14.37	15.94	28.46	10.56	0.00	0.00
H21031193	H2	10	11-Mar-93	1.13	3.81	8.06	10.16	11.22	17.72	16.41	22.03	9.23	0.23	0.00
H31031193	H3	10	11-Mar-93	0.47	3.19	6.90	7.53	7.82	12.41	14.79	30.67	15.66	0.56	0.00
H41031193	H4	10	11-Mar-93	0.34	2.56	5.95	6.09	6.12	9.40	12.34	31.77	22.58	2.86	0.00
S11031193	S1	10	11-Mar-93	0.37	2.68	6.36	7.01	7.49	10.91	16.49	34.28	11.87	1.20	1.34
S21031193	S2	10	11-Mar-93	0.33	2.38	5.59	6.52	7.55	13.18	19.95	32.11	10.90	0.68	0.83
S31031193	S3	10	11-Mar-93	0.33	2.29	5.29	6.44	7.52	14.28	22.78	30.75	8.82	0.63	0.87
H12031193	H1	20	11-Mar-93	2.51	3.16	9.89	13.69	14.49	22.54	20.57	11.90	1.26	0.00	0.00
H22031193	H2	20	11-Mar-93	1.09	3.51	7.66	9.97	10.81	19.60	19.96	20.79	6.60	0.01	0.00
H42031193	H4	20	11-Mar-93	0.46	3.10	6.79	7.73	7.82	12.74	14.04	27.83	18.58	0.90	0.00
S12031193	S1	20	11-Mar-93	0.57	3.07	7.11	8.23	8.81	14.15	18.89	25.21	8.65	2.34	2.98
S22031193	S2	20	11-Mar-93	1.89	2.79	8.36	10.67	12.11	21.36	22.87	15.66	4.16	0.13	0.00
S32031193	S3	20	11-Mar-93	0.30	2.15	5.09	6.08	6.98	13.11	19.84	31.48	12.51	1.29	1.18
H13031193	H1	30	11-Mar-93	2.84	3.21	10.24	14.66	16.44	25.76	18.21	6.28	2.16	0.19	0.00
H33031193	H3	30	11-Mar-93	3.23	3.74	11.36	14.08	14.65	26.47	18.31	5.26	2.58	0.32	0.00
H43031193	H4	30	11-Mar-93	0.48	2.98	5.55	5.83	6.41	19.77	21.25	23.11	14.63	0.00	0.00
S13031193	S1	30	11-Mar-93	2.37	3.15	10.27	12.94	12.59	22.06	19.94	11.66	4.24	0.79	0.00
S23031193	S2	30	11-Mar-93	2.77	3.22	10.86	14.14	14.66	25.09	21.64	7.61	0.00	0.00	0.00
S33031193	S3	30	11-Mar-93	2.37	2.92	9.69	12.72	13.57	25.49	23.56	8.85	0.70	0.13	0.00
H15031193	H1	50	11-Mar-93	2.72	3.03	9.74	14.04	16.04	28.54	20.17	4.06	1.43	0.22	0.00
H25031193	H2	50	11-Mar-93	2.19	2.83	8.47	10.31	10.31	31.91	28.82	5.17	0.00	0.00	0.00
H35031193	H3	50	11-Mar-93	2.97	3.37	10.33	12.95	13.42	29.39	22.76	4.80	0.00	0.00	0.00
H45031193	H4	50	11-Mar-93	2.94	3.37	10.17	12.98	13.47	26.57	20.16	3.90	3.38	3.05	0.00
S15031193	S1	50	11-Mar-93	3.25	3.77	13.03	16.18	15.65	23.45	18.17	6.24	0.26	0.00	0.00
S25031193	S2	50	11-Mar-93	3.00	3.45	11.74	15.23	15.68	25.93	19.74	5.23	0.00	0.00	0.00
S35031193	S3	50	11-Mar-93	2.70	3.18	10.65	14.04	14.79	25.94	22.27	6.42	0.00	0.00	0.00
H16031193	H1	60	11-Mar-93	3.08	3.43	11.36	15.14	15.17	27.05	17.10	2.04	4.43	1.18	0.00
H26031193	H2	60	11-Mar-93	2.63	3.32	9.55	11.31	12.83	31.25	24.22	4.87	0.00	0.00	0.00
H36031193	H3	60	11-Mar-93	2.51	3.12	9.11	10.54	10.40	34.26	26.44	3.62	0.00	0.00	0.00
H46031193	H4	60	11-Mar-93	2.90	3.30	9.64	10.84	11.65	32.70	23.84	2.66	1.81	0.66	0.00
S16031193	S1	60	11-Mar-93	3.35	3.90	13.67	16.98	16.31	23.56	17.40	4.84	0.00	0.00	0.00
S26031193	S2	60	11-Mar-93	3.14	3.58	12.49	16.23	16.64	25.89	18.04	4.00	0.00	0.00	0.00
S36031193	S3	60	11-Mar-93	2.76	3.20	10.94	14.55	15.46	26.68	20.99	5.42	0.00	0.00	0.00
H110031193	H1	100	11-Mar-93	2.94	3.20	10.59	13.69	15.59	33.35	18.26	2.39	0.00	0.00	0.00
S110031193	S1	100	11-Mar-93	3.70	4.20	15.12	18.44	17.44	23.60	14.68	2.84	0.00	0.00	0.00
S210031193	S2	100	11-Mar-93	3.32	3.83	13.21	17.03	17.82	25.95	15.81	2.53	0.48	0.01	0.00
S310031193	S3	100	11-Mar-93	3.07	3.43	12.16	15.99	16.81	27.20	17.82	3.52	0.00	0.00	0.00

Sample ID	Location	Height	Date	.01-1	1-2	2-5	5-10	10-20	20-50	50-100	100-250	250-500	500-1000	1000-2000
H11031793	H1	10	17-Mar-93	1.53	3.64	8.82	10.73	10.97	18.73	17.70	17.13	7.98	1.52	1.25
H41031793	H4	10	17-Mar-93	0.43	3.00	6.66	7.17	7.38	11.86	12.77	26.57	20.79	3.36	0.00
S11031793	S1	10	17-Mar-93	0.32	2.37	5.30	5.46	6.08	9.72	16.26	40.81	13.65	0.03	0.00
S21031793	S2	10	17-Mar-93	0.30	2.17	4.77	5.09	5.80	11.28	19.05	39.58	11.96	0.00	0.00
S31031793	S3	10	17-Mar-93	0.19	1.79	4.14	4.28	5.10	9.72	20.79	43.64	10.35	0.01	0.00
H12031793	H1	20	17-Mar-93	2.92	3.60	11.12	13.66	14.17	23.01	18.28	9.66	3.18	0.40	0.00
S12031793	S1	20	17-Mar-93	0.47	3.18	6.51	6.93	7.39	12.95	17.08	30.54	10.18	1.47	3.30
S22031793	S2	20	17-Mar-93	2.12	2.92	8.58	10.66	11.99	23.69	22.62	11.36	2.48	2.12	1.46
S32031793	S3	20	17-Mar-93	0.30	2.19	5.01	5.71	6.61	13.27	18.95	32.77	11.58	1.16	2.45
H13031793	H1	30	17-Mar-93	3.25	3.97	12.29	15.07	15.83	24.97	17.62	6.20	0.74	0.07	0.00
H23031793	H2	30	17-Mar-93	3.42	4.08	12.56	15.58	16.17	25.15	16.26	5.07	1.63	0.07	0.00
H33031793	H3	30	17-Mar-93	3.32	3.97	12.12	15.11	16.27	26.14	16.91	4.84	1.21	0.12	0.00
H43031793	H4	30	17-Mar-93	3.03	3.69	11.08	13.75	15.07	24.68	16.94	5.70	5.31	0.74	0.00
S13031793	S1	30	17-Mar-93	3.09	3.68	11.09	13.45	14.25	25.99	20.91	7.32	0.23	0.00	0.00
S23031793	S2	30	17-Mar-93	2.70	3.21	9.72	12.28	13.94	27.95	22.71	6.04	0.96	0.50	0.00
S33031793	S3	30	17-Mar-93	2.01	2.77	8.03	10.08	11.62	24.86	24.15	9.27	1.33	3.35	2.53
H15031793	H1	50	17-Mar-93	3.41	3.98	12.76	16.34	17.74	27.10	15.37	2.49	0.79	0.01	0.00
H25031793	H2	50	17-Mar-93	3.39	3.98	12.66	16.01	17.16	25.84	14.94	2.51	2.97	0.52	0.00
H35031793	H3	50	17-Mar-93	3.51	4.12	13.01	16.44	17.51	26.24	14.29	2.35	2.53	0.02	0.00
H45031793	H4	50	17-Mar-93	3.47	4.03	12.95	16.39	17.77	27.01	14.72	2.66	0.99	0.01	0.00
S15031793	S1	50	17-Mar-93	3.37	3.86	12.09	15.20	16.78	28.03	17.29	3.37	0.00	0.00	0.00
S25031793	S2	50	17-Mar-93	2.98	3.42	10.62	13.55	15.50	28.76	20.36	4.80	0.00	0.00	0.00
S35031793	S3	50	17-Mar-93	2.45	3.01	9.06	11.53	13.43	27.57	22.72	5.37	2.13	2.72	0.00
H16031793	H1	60	17-Mar-93	3.59	4.15	13.28	16.95	18.27	26.88	14.15	2.25	0.47	0.01	0.00
H26031793	H2	60	17-Mar-93	3.52	4.01	12.75	16.81	18.82	28.31	13.92	1.38	0.47	0.01	0.00
H36031793	H3	60	17-Mar-93	3.61	4.28	13.37	16.82	18.16	26.85	14.51	2.39	0.00	0.00	0.00
H46031793	H4	60	17-Mar-93	3.45	4.03	12.53	15.61	17.61	28.75	15.56	2.47	0.00	0.00	0.00
S16031793	S1	60	17-Mar-93	3.45	3.95	12.42	15.07	16.76	29.60	16.55	2.20	0.00	0.00	0.00
S26031793	S2	60	17-Mar-93	3.02	3.41	10.73	13.91	16.71	30.45	18.63	3.15	0.00	0.00	0.00
S36031793	S3	60	17-Mar-93	1.99	2.54	7.86	10.51	12.45	25.86	19.09	3.66	0.87	8.27	6.90
H210031793	H2	100	17-Mar-93	3.61	4.30	13.45	16.85	18.40	28.87	13.48	1.04	0.00	0.00	0.00
H310031793	H3	100	17-Mar-93	3.64	4.15	13.37	16.88	19.47	28.72	12.59	1.17	0.00	0.00	0.00
H410031793	H4	100	17-Mar-93	3.54	3.97	12.79	16.32	18.95	28.88	12.73	1.30	1.52	0.01	0.00
S110031793	S1	100	17-Mar-93	3.45	3.95	12.50	15.62	17.59	27.89	13.82	1.86	2.88	0.44	0.00
S210031793	S2	100	17-Mar-93	3.00	3.34	10.62	13.83	17.08	30.91	17.74	2.42	0.92	0.13	0.00
S310031793	S3	100	17-Mar-93	2.66	3.01	9.42	11.90	14.95	32.70	19.86	2.18	2.19	1.12	0.00

Sample ID	Location	Height	Date	.01-1	1-2	2-5	5-10	10-20	20-50	50-100	100-250	250-500	500-1000	1000-2000
H11032393	H1	10	23-Mar-93	0.60	3.13	6.10	6.80	7.73	16.65	20.97	21.72	11.18	2.56	2.55
H21032393	H2	10	23-Mar-93	0.45	3.06	5.90	6.24	7.37	14.89	21.06	26.83	12.50	1.29	0.41
H31032393	H3	10	23-Mar-93	0.37	2.56	5.12	5.38	6.32	13.11	17.93	22.46	15.88	7.76	3.12
H41032393	H4	10	23-Mar-93	0.34	2.39	4.95	5.07	5.83	11.23	17.23	27.44	13.62	6.80	5.10
S11032393	S1	10	23-Mar-93	0.27	1.94	4.10	4.24	5.15	10.49	20.60	36.49	12.32	1.97	2.42
S21032393	S2	10	23-Mar-93	0.07	1.44	3.46	3.55	4.45	9.05	20.44	41.98	12.56	1.47	1.53
H12032393	H1	20	23-Mar-93	1.07	3.54	7.04	8.47	9.77	22.17	26.56	16.11	5.21	0.06	0.00
H22032393	H2	20	23-Mar-93	0.36	2.54	5.09	5.34	6.32	12.63	19.55	29.05	13.72	3.15	2.25
H32032393	H3	20	23-Mar-93	0.45	3.01	5.82	6.35	7.58	16.12	21.96	23.31	12.55	2.43	0.41
H42032393	H4	20	23-Mar-93	0.46	3.05	5.90	6.43	7.65	15.52	20.21	21.99	15.53	3.27	0.00
S12032393	S1	20	23-Mar-93	0.26	1.87	4.05	4.21	5.03	10.54	19.38	34.25	13.14	3.75	3.53
S22032393	S2	20	23-Mar-93	0.42	2.76	5.59	6.54	7.94	17.60	26.89	22.44	7.73	1.79	0.31
H13032393	H1	30	23-Mar-93	1.05	3.56	7.05	8.28	9.85	21.61	23.79	11.64	5.40	4.80	2.97
H23032393	H2	30	23-Mar-93	2.19	3.16	8.30	9.99	11.53	25.28	26.57	11.66	1.21	0.11	0.00
H33032393	H3	30	23-Mar-93	1.41	3.37	7.45	9.00	10.17	21.62	22.49	9.10	4.82	6.17	4.40
H43032393	H4	30	23-Mar-93	1.42	3.49	7.74	9.28	10.51	21.14	24.34	14.91	5.40	1.59	0.19
S13032393	S1	30	23-Mar-93	1.01	3.44	6.98	8.48	9.52	21.38	30.29	16.76	2.01	0.13	0.00
S23032393	S2	30	23-Mar-93	0.77	2.84	6.10	7.54	8.94	20.18	27.75	13.38	3.70	5.51	3.30
H15032393	H1	50	23-Mar-93	2.28	3.27	8.68	10.55	12.24	27.50	27.11	8.38	0.00	0.00	0.00
H25032393	H2	50	23-Mar-93	2.29	3.29	8.80	10.47	11.79	25.18	25.28	9.09	1.44	1.79	0.57
H35032393	H3	50	23-Mar-93	2.48	3.18	8.83	10.91	12.80	27.20	25.97	8.63	0.00	0.00	0.00
H45032393	H4	50	23-Mar-93	2.40	3.41	9.30	11.15	12.57	25.76	24.48	8.29	1.80	0.84	0.00
S15032393	S1	50	23-Mar-93	1.32	3.26	7.37	8.96	10.52	23.25	26.70	9.79	1.13	3.88	3.82
S25032393	S2	50	23-Mar-93	1.50	2.88	7.44	9.24	10.75	23.80	28.43	12.42	0.88	1.26	1.40
H16032393	H1	60	23-Mar-93	2.59	3.48	9.31	11.27	13.06	28.26	25.17	6.85	0.00	0.00	0.00
H26032393	H2	60	23-Mar-93	2.56	3.27	9.24	11.54	13.54	27.61	23.35	5.55	1.95	1.38	0.00
H36032393	H3	60	23-Mar-93	2.74	3.65	9.99	11.91	13.49	27.74	23.87	6.60	0.00	0.00	0.00
H46032393	H4	60	23-Mar-93	2.43	3.40	9.35	11.11	12.33	24.78	23.91	7.91	1.35	2.26	1.18
S16032393	S1	60	23-Mar-93	2.21	3.27	9.15	10.71	12.11	27.22	26.30	7.82	0.58	0.62	0.00
S26032393	S2	60	23-Mar-93	1.86	2.76	8.04	10.17	12.25	26.01	24.86	7.94	0.48	3.08	2.56
H110032393	H1	100	23-Mar-93	3.06	3.85	10.65	12.64	14.83	29.22	21.22	4.53	0.00	0.00	0.00
H210032393	H2	100	23-Mar-93	2.90	3.64	10.10	12.26	14.50	28.76	22.20	5.63	0.00	0.00	0.00
H310032393	H3	100	23-Mar-93	2.95	3.71	10.30	12.50	14.77	28.84	22.01	4.92	0.00	0.00	0.00
H410032393	H4	100	23-Mar-93	2.85	3.55	10.12	12.50	14.43	27.56	22.73	6.26	0.00	0.00	0.00
S110032393	S1	100	23-Mar-93	2.38	3.35	9.52	11.26	13.16	28.57	24.73	7.04	0.00	0.00	0.00
S210032393	S2	100	23-Mar-93	0.26	1.84	3.89	4.63	5.52	14.94	21.72	14.80	16.55	14.00	1.84

Sample ID	Location	Height	Date	.01-1	1-2	2-5	5-10	10-20	20-50	50-100	100-250	250-500	500-1000	1000-2000
H11032493	H1	10	24-Mar-93	0.38	2.64	5.26	5.40	6.11	12.51	17.39	26.53	20.71	3.08	0.00
H21032493	H2	10	24-Mar-93	0.36	2.57	5.17	5.21	5.93	11.60	17.12	24.19	14.95	7.55	5.35
H31032493	H3	10	24-Mar-93	0.44	3.08	6.31	6.28	6.69	12.17	16.37	26.47	19.14	3.06	0.00
H41032493	H4	10	24-Mar-93	0.48	3.29	6.44	6.41	7.10	12.34	19.44	33.10	11.33	0.06	0.00
H12032493	H1	20	24-Mar-93	0.95	3.48	6.92	7.61	8.61	18.48	24.27	15.63	6.62	4.50	2.94
H22032493	H2	20	24-Mar-93	0.36	2.56	5.10	5.00	6.03	10.68	17.78	31.93	16.37	2.56	1.64
H32032493	H3	20	24-Mar-93	0.43	3.01	6.25	6.41	6.85	12.90	17.69	22.56	15.97	6.37	1.55
H42032493	H4	20	24-Mar-93	0.41	2.93	6.18	6.03	6.24	10.91	14.57	24.27	19.62	6.75	2.09
H13032493	H1	30	24-Mar-93	1.88	3.66	8.71	9.47	10.07	21.07	24.44	14.67	5.68	0.34	0.00
H23032493	H2	30	24-Mar-93	1.34	3.41	8.00	8.93	9.10	19.21	21.55	10.51	5.31	6.75	5.90
H33032493	H3	30	24-Mar-93	1.37	3.50	7.94	9.43	10.51	20.27	22.90	12.63	6.71	3.13	1.62
H43032493	H4	30	24-Mar-93	1.02	3.56	7.42	8.84	9.90	19.36	24.63	17.19	7.34	0.73	0.00
H15032493	H1	50	24-Mar-93	2.33	3.56	9.61	10.67	11.54	24.81	26.52	8.78	0.24	1.18	0.75
H25032493	H2	50	24-Mar-93	2.17	3.24	9.20	10.64	11.36	21.88	22.34	8.51	2.46	5.00	3.20
H35032493	H3	50	24-Mar-93	2.16	3.14	9.00	10.69	11.52	21.82	21.59	7.74	2.11	6.12	4.12
H45032493	H4	50	24-Mar-93	1.88	2.79	7.86	9.32	10.17	19.14	19.16	7.29	1.85	10.08	10.47
H16032493	H1	60	24-Mar-93	2.42	3.57	9.84	11.33	12.38	26.66	25.93	7.87	0.00	0.00	0.00
H26032493	H2	60	24-Mar-93	2.81	3.59	10.24	12.35	13.84	26.37	23.40	7.40	0.00	0.00	0.00
H36032493	H3	60	24-Mar-93	2.94	3.69	10.78	12.80	13.73	25.97	23.16	6.91	0.00	0.00	0.00
H46032493	H4	60	24-Mar-93	2.16	3.09	8.41	10.43	12.10	23.79	24.48	9.01	1.18	3.52	1.84
H110032493	H1	100	24-Mar-93	2.71	3.67	10.48	12.43	13.58	25.23	20.52	4.80	3.25	3.34	0.00
H210032493	H2	100	24-Mar-93	3.03	3.79	10.96	13.43	14.90	26.42	21.27	6.20	0.00	0.00	0.00
H310032493	H3	100	24-Mar-93	2.90	3.66	10.50	12.80	13.94	26.43	22.26	6.85	0.59	0.08	0.00
H410032493	H4	100	24-Mar-93	2.34	3.35	9.06	11.35	13.65	26.57	24.01	9.17	0.51	0.00	0.00

APPENDIX B

PIXE (particle induced x-ray emission) elemental concentration for aeolian dust samples from Owens (dry) Lake, California

11 Mar 1993 (μg g^{-1})																			
Sample ID	**Al**	**As**	**Br**	**Ca**	**Cl**	**Cu**	**Ga**	**Fe**	**Mg**	**Mn**	**Ni**	**K**	**Rb**	**Si**	**Na**	**Sr**	**S**	**Ti**	**Zn**
H11031193	2.211E+04	1.680E+01	1.505E+01	8.796E+04	7.340E+03	1.208E+01	0.000E+00	1.054E+04	3.468E+04	3.487E+02	0.000E+00	1.077E+04	5.558E+01	1.171E+05	1.870E+05	1.030E+03	6.267E+04	1.200E+03	1.402E+02
H12031193	1.780E+04	1.615E+01	8.942E+00	9.871E+04	8.520E+03	9.662E+00	0.000E+00	9.550E+03	3.711E+04	3.584E+02	0.000E+00	9.570E+03	4.819E+01	1.154E+05	1.810E+05	1.180E+03	5.909E+04	1.150E+03	1.020E+02
H13031193	1.887E+04	1.608E+01	1.153E+01	9.284E+04	8.070E+03	9.827E+00	0.000E+00	9.270E+03	3.580E+04	3.310E+02	0.000E+00	9.660E+03	4.408E+01	1.113E+05	2.086E+05	1.010E+03	7.908E+04	1.060E+03	1.344E+02
H16031193	1.673E+04	1.023E+01	6.893E+00	9.167E+04	8.670E+03	8.152E+00	0.000E+00	8.020E+03	3.482E+04	2.950E+02	0.000E+00	8.270E+03	3.285E+01	1.023E+05	2.120E+05	9.760E+08	8.395E+04	9.658E+02	2.557E+02
H110031193	1.495E+04	1.415E+01	7.776E+00	9.162E+04	8.390E+03	1.148E+01	0.000E+00	7.500E+03	3.521E+04	2.797E+02	0.000E+00	7.630E+03	4.601E+01	9.514E+04	2.154E+05	1.010E+03	8.580E+04	8.787E+02	1.975E+02
H21031193	1.967E+04	1.570E+01	0.000E+00	9.003E+04	7.400E+03	1.218E+01	0.000E+00	1.065E+04	3.234E+04	3.606E+02	0.000E+00	9.910E+03	6.619E+01	1.128E+05	1.653E+05	1.070E+03	5.820E+04	1.210E+03	5.842E+01
H22031193	1.807E+04	1.624E+01	8.164E+00	9.698E+04	7.520E+03	1.042E+01	0.000E+00	9.440E+03	3.594E+04	3.399E+02	0.000E+00	9.570E+03	3.739E+01	1.109E+05	1.890E+05	1.110E+03	7.067E+04	1.060E+03	5.874E+01
H23031193	1.867E+04	1.306E+01	0.000E+00	8.996E+04	7.190E+03	9.327E+00	0.000E+00	9.080E+03	3.417E+04	3.155E+02	0.000E+00	9.690E+03	3.989E+01	1.070E+05	2.083E+05	1.020E+03	8.726E+04	1.080E+03	6.664E+01
H25031193	1.445E+04	1.671E+01	1.279E+01	8.771E+04	7.100E+03	1.428E+01	0.000E+00	7.980E+03	3.391E+04	2.922E+02	1.676E+01	8.040E+03	4.010E+01	9.741E+04	2.095E+05	1.070E+03	8.596E+04	9.446E+02	1.243E+02
H26031193	1.585E+04	1.683E+01	8.607E+00	8.318E+04	6.670E+03	8.636E+00	0.000E+00	7.790E+03	3.149E+04	2.711E+02	4.809E+00	7.980E+03	3.242E+01	9.349E+04	2.145E+05	9.597E+02	9.026E+04	8.614E+02	8.731E+01
H210031193	1.730E+04	1.409E+01	0.000E+00	9.208E+04	6.900E+03	8.569E+00	0.000E+00	7.650E+03	3.644E+04	2.911E+02	0.000E+00	8.260E+03	4.746E+01	1.021E+05	2.189E+05	9.477E+02	9.631E+04	9.411E+02	2.350E-03
H31031193	2.122E+04	1.398E+01	0.000E+00	1.003E+05	5.960E+03	1.204E+01	0.000E+00	1.093E+04	3.467E+04	3.863E+02	0.000E+00	1.097E+04	4.890E+01	1.226E+05	1.512E+05	1.190E+03	5.837E+04	1.300E+03	6.496E+01
H32031193	1.671E+04	1.031E+01	7.250E+00	9.252E+04	6.570E+03	9.131E+00	0.000E+00	9.240E+03	3.289E+04	3.474E+02	7.633E+00	8.800E+03	4.755E+01	1.050E+05	1.801E+05	1.120E+03	6.719E+04	9.895E+02	3.780E+01
H33031193	1.736E+04	1.615E+01	0.000E+00	8.128E+04	5.390E+03	1.075E+01	0.000E+00	8.310E+03	3.028E+04	3.004E+02	8.557E+00	8.770E+03	4.402E+01	9.771E+04	2.013E+05	8.998E+02	9.155E+04	9.895E+02	6.055E+01
H35031193	1.184E+04	1.844E+01	0.000E+00	7.265E+04	5.060E+03	7.759E+00	0.000E+00	5.900E+03	2.788E+04	2.258E+02	0.000E+00	6.330E+03	2.559E+01	7.643E+04	2.273E+05	8.478E+02	1.062E+05	6.469E+02	1.307E+02
H36031193	1.224E+04	1.118E+01	0.000E+00	6.052E+04	5.290E+03	1.366E+01	0.000E+00	5.560E+03	2.518E+04	1.983E+02	1.116E+01	5.980E+03	2.520E+01	6.842E+04	2.330E+05	7.255E+02	1.090E+05	6.345E+02	9.151E+01
H310031193	1.221E+04	1.667E+01	1.213E+01	6.457E+04	5.790E+03	1.090E+01	0.000E+00	5.130E+03	2.953E+04	1.971E+02	1.297E+01	5.890E+03	2.091E+01	7.039E+04	2.340E+05	7.551E+02	1.081E+05	6.044E+02	2.540E+02
H41031193	2.607E+04	1.683E+01	9.825E+00	9.652E+04	5.500E+03	1.395E+01	6.689E+00	1.324E+04	3.414E+04	4.472E+02	5.743E+00	1.227E+04	7.038E+01	1.334E+05	1.102E+05	1.230E+03	3.833E+04	1.530E+03	5.568E+01
H42031193	2.196E+04	1.783E+01	1.288E+01	9.463E+04	5.610E+03	1.440E+01	8.442E+00	1.129E+04	3.381E+04	3.799E+02	5.533E+00	1.053E+04	5.849E+01	1.199E+05	1.264E+05	1.180E+03	4.452E+04	1.270E+03	3.600E+01
H43031193	1.757E+04	1.676E+01	8.205E+00	8.360E+04	4.350E+03	1.384E+01	0.000E+00	9.350E+03	3.144E+04	3.198E+02	8.353E+00	8.730E+03	3.922E+01	9.990E+04	1.714E+05	1.040E+03	7.363E+04	1.030E+03	4.896E+01
H45031193	1.294E+04	1.472E+01	0.000E+00	7.899E+04	5.000E+03	9.147E+00	0.000E+00	6.960E+03	2.903E+04	2.621E+02	4.654E+00	7.080E+03	3.751E+01	8.375E+04	1.911E+05	1.010E+03	8.499E+04	8.267E+02	1.110E+02
H46031193	1.471E+04	1.414E+01	7.542E+00	7.559E+04	4.500E+03	1.255E+01	0.000E+00	7.470E+03	3.146E+04	2.647E+02	8.914E+00	7.320E+03	3.118E+01	8.817E+04	1.823E+05	9.930E+02	8.469E+04	8.178E+02	1.022E+02
H410031193	1.235E+04	1.342E+01	6.300E+00	7.994E+04	5.750E+03	1.113E+01	0.000E+00	6.230E+03	3.119E+04	2.222E+02	9.244E+00	6.730E+03	2.890E+01	8.314E+04	1.964E+05	9.306E+02	9.093E+04	7.297E+02	1.104E+02
S11031193	2.008E+04	1.724E+01	8.063E+00	1.108E+05	4.670E+03	1.166E+01	5.977E+00	1.085E+04	4.075E+04	3.889E+02	0.000E+00	1.018E+04	4.095E+01	1.274E+05	1.094E+05	1.450E+03	2.343E+04	1.220E+03	6.883E+01
S12031193	2.111E+04	1.778E+01	7.444E+00	1.189E+05	4.640E+03	1.545E+01	0.000E+00	1.092E+04	4.541E+04	3.919E+02	0.000E+00	1.107E+04	6.798E+01	1.358E+05	1.153E+05	1.490E+03	2.740E+04	1.250E+03	7.789E+01
S13031193	1.794E+04	1.201E+01	8.740E+00	1.166E+05	4.840E+03	9.316E+00	0.000E+00	1.037E+04	4.467E+04	3.816E+02	0.000E+00	9.300E+03	5.218E+01	1.266E+05	1.266E+05	1.500E+03	3.587E+04	1.130E+03	1.073E+02
S15031193	1.649E+04	1.640E+01	0.000E+00	1.161E+05	4.890E+03	9.848E+00	0.000E+00	9.520E+03	4.342E+04	3.397E+02	0.000E+00	8.710E+03	5.346E+01	1.200E+05	1.385E+05	1.470E+03	4.306E+04	1.080E+03	4.140E+01
S16031193	1.691E+04	1.533E+01	0.000E+00	1.162E+05	4.920E+03	1.114E+01	0.000E+00	9.360E+03	4.380E+04	3.480E+02	0.000E+00	9.370E+03	4.547E+01	1.194E+05	1.466E+05	1.370E+03	4.908E+04	1.040E+03	1.514E+02
S110031193	1.570E+04	1.372E+01	7.292E+00	1.157E+05	4.160E+03	1.040E+01	8.595E+00	9.200E+03	4.309E+04	3.356E+02	0.000E+00	8.810E+03	4.625E+01	1.169E+05	1.551E+05	1.460E+03	5.475E+04	1.030E+03	6.029E+02
S21031193	1.750E+04	1.724E+01	1.125E+01	1.347E+05	6.580E+03	1.119E+01	0.000E+00	9.950E+03	5.052E+04	3.960E+02	0.000E+00	1.022E+04	6.189E+01	1.359E+05	9.951E+04	1.660E+03	1.866E+04	1.100E+03	4.685E+01
S22031193	1.542E+04	1.530E+01	1.100E+01	1.293E+05	6.720E+03	1.373E+01	0.000E+00	9.680E+03	4.911E+04	3.755E+02	7.249E+00	9.700E+03	4.041E+01	1.308E+05	1.116E+05	1.650E+03	2.539E+04	1.100E+03	1.954E+02
S23031193	1.595E+04	1.535E+01	0.000E+00	1.305E+05	6.930E+03	1.090E+01	0.000E+00	9.270E+03	5.194E+04	3.643E+02	0.000E+00	9.280E+03	4.439E+01	1.317E+05	1.239E+05	1.680E+03	3.084E+04	1.060E+03	4.768E+01
S25031193	1.418E+04	1.991E+01	1.125E+01	1.288E+05	5.690E+03	1.348E+01	0.000E+00	9.270E+03	4.714E+04	3.534E+02	0.000E+00	9.180E+03	3.736E+01	1.254E+05	1.226E+05	1.680E+03	3.211E+04	1.030E+03	3.761E+01
S26031193	1.541E+04	1.540E+01	7.200E+00	1.277E+05	5.500E+03	9.811E+00	0.000E+00	8.980E+03	5.108E+04	3.501E+02	0.000E+00	8.920E+03	4.316E+01	1.275E+05	1.289E+05	1.620E+03	3.583E+04	9.671E+02	4.393E+01
S210031193	1.500E+04	2.033E+01	1.237E+01	1.305E+05	5.480E+03	1.230E+01	5.777E+00	9.220E+03	5.009E+04	3.677E+02	0.000E+00	9.070E+03	4.498E+01	1.278E+05	1.348E+05	1.680E+03	4.027E+04	1.050E+03	3.383E+01
S31031193	1.598E+04	1.592E+01	1.553E+01	1.478E+05	8.600E+03	7.570E+00	4.751E+00	9.410E+03	5.713E+04	3.817E+02	0.000E+00	1.036E+04	3.622E+01	1.469E+05	9.780E+04	1.780E+03	2.136E+04	1.070E+03	6.971E+01
S32031193	1.788E+04	1.770E+01	1.206E+01	1.475E+05	8.890E+03	7.887E+00	0.000E+00	1.024E+04	5.340E+04	4.035E+02	0.000E+00	1.075E+04	5.736E+01	1.473E+05	9.060E+04	1.790E+03	1.898E+04	1.180E+03	3.481E+01
S33031193	1.557E+04	1.610E+01	1.106E+01	1.408E+05	6.960E+03	7.497E+00	0.000E+00	9.000E+03	5.677E+04	3.670E+02	0.000E+00	9.570E+03	4.698E+01	1.400E+05	1.168E+05	1.750E+03	2.790E+04	9.980E+02	1.172E+02
S35031193	1.535E+04	1.563E+01	7.101E+00	1.414E+05	6.770E+03	9.140E+00	0.000E+00	9.210E+03	5.504E+04	3.734E+02	0.000E+00	9.620E+03	3.962E+01	1.402E+05	1.195E+05	1.750E+03	3.037E+04	1.000E+03	3.727E+01
S36031193	1.534E+04	1.824E+01	1.023E+01	1.427E+05	7.080E+03	1.145E+01	0.000E+00	9.240E+03	5.678E+04	3.566E+02	0.000E+00	9.890E+03	4.846E+01	1.403E+05	1.227E+05	1.730E+03	3.343E+04	1.020E+03	7.968E+01
S310031193	1.762E+04	1.507E+01	0.000E+00	1.473E+05	7.630E+03	1.058E+01	0.000E+00	9.170E+03	6.046E+04	3.800E+02	0.000E+00	1.038E+04	4.473E+01	1.456E+05	1.339E+05	1.790E+03	3.763E+04	1.110E+03	4.144E+01

17 March 1993 (μg g^{-1})																			
Sample ID	**Al**	**As**	**Br**	**Ca**	**Cl**	**Cu**	**Ga**	**Fe**	**Mg**	**Mn**	**Ni**	**K**	**Rb**	**Si**	**Na**	**Sr**	**S**	**Ti**	**Zn**
H11031793	2.676E+04	2.008E+01	1.240E+01	1.014E+05	6.760E+03	1.276E+01	8.109E+00	1.442E+04	4.039E+04	4.799E+02	5.572E+00	1.292E+04	6.298E+01	1.437E+05	1.060E+05	1.290E+03	2.542E+04	1.610E+03	6.494E+01
H12031793	2.121E+04	1.635E+01	1.495E+01	1.127E+05	7.030E+03	1.386E+01	0.000E+00	1.228E+04	4.355E+04	4.203E+02	0.000E+00	1.178E+04	3.631E+01	1.374E+05	1.293E+05	1.350E+03	3.246E+04	1.400E+03	5.930E+01
H13031793	2.566E+04	2.247E+01	1.518E+01	1.127E+05	7.820E+03	1.557E+01	6.741E+00	1.330E+04	4.484E+04	4.694E+02	0.000E+00	1.265E+04	6.484E+01	1.456E+05	1.194E+05	1.400E+03	3.144E+04	1.480E+03	5.727E+01
H15031793	2.046E+04	2.471E+01	1.615E+01	1.137E+05	7.140E+03	1.656E+01	7.015E+00	1.200E+04	4.367E+04	4.200E+02	0.000E+00	1.130E+04	7.364E+01	1.357E+05	1.227E+05	1.380E+03	3.148E+04	1.320E+03	1.183E+02
H16031793	2.215E+04	1.896E+01	1.558E+01	1.187E+05	7.610E+03	1.535E+01	5.079E+00	1.223E+04	4.549E+04	4.353E+02	0.000E+00	1.223E+04	6.624E+01	1.408E+05	1.173E+05	1.440E+03	3.154E+04	1.430E+03	1.017E+02
H110031793	2.053E+04	1.944E+01	1.549E+01	9.392E+04	5.750E+03	1.154E+01	5.145E+00	9.780E+03	5.009E+04	3.290E+02	0.000E+00	8.360E+03	4.328E+01	1.300E+05	1.261E+05	1.200E+03	2.474E+04	1.090E+03	5.172E+01
H21031793	2.860E+04	2.087E+01	0.000E+00	1.084E+05	6.740E+03	1.581E+01	6.231E+00	1.609E+04	3.956E+04	5.277E+02	0.000E+00	1.528E+04	8.308E+01	1.581E+05	9.319E+04	1.270E+03	2.329E+04	1.720E+03	4.966E+01
H22031793	2.975E+04	1.727E+01	0.000E+00	1.195E+05	8.830E+03	2.088E+01	9.460E+00	1.582E+04	4.246E+04	5.509E+02	5.714E+00	1.521E+04	9.216E+01	1.638E+05	8.863E+04	1.350E+03	2.123E+04	1.750E+03	5.457E+01
H23031793	2.549E+04	1.707E+01	0.000E+00	1.228E+05	7.580E+03	1.652E+01	8.578E+00	1.352E+04	4.389E+04	4.751E+02	0.000E+00	1.435E+04	7.297E+01	1.533E+05	1.128E+05	1.440E+03	3.101E+04	1.530E+03	6.006E+01
H25031793	2.160E+04	1.682E+01	1.707E+01	1.214E+05	8.060E+03	1.134E+01	6.150E+00	1.258E+04	4.571E+04	4.476E+02	0.000E+00	1.211E+04	5.751E+01	1.432E+05	1.162E+05	1.490E+03	3.000E+04	1.390E+03	7.472E+01
H26031793	2.228E+04	2.058E+01	1.125E+01	1.288E+05	9.610E+03	1.599E+01	8.747E+00	1.180E+04	4.764E+04	4.410E+02	0.000E+00	1.254E+04	5.673E+01	1.460E+05	1.164E+05	1.500E+03	3.118E+04	1.300E+03	5.879E+01
H210031793	2.221E+04	1.473E+01	2.404E+01	9.725E+04	8.000E+03	1.304E+01	0.000E+00	9.670E+03	5.218E+04	3.664E+02	0.000E+00	8.950E+03	4.634E+01	1.357E+05	1.352E+05	1.280E+03	2.655E+04	1.050E+03	9.173E+01
H31031793	3.067E+04	2.172E+01	1.204E+01	1.076E+05	7.530E+03	1.703E+01	8.557E+00	1.561E+04	4.164E+04	5.246E+02	0.000E+00	1.430E+04	7.805E+01	1.590E+05	8.663E+04	1.320E+03	1.991E+04	1.680E+03	5.066E+01
H32031793	2.935E+04	2.337E+01	1.434E+01	1.067E+05	8.350E+03	1.691E+01	5.772E+00	1.580E+04	4.078E+04	5.187E+02	0.000E+00	1.435E+04	6.587E+01	1.556E+05	8.972E+04	1.290E+03	1.918E+04	1.770E+03	4.750E+01
H33031793	2.105E+04	1.684E+01	1.379E+01	1.102E+05	7.920E+03	1.374E+01	0.000E+00	1.259E+04	4.202E+04	4.331E+02	0.000E+00	1.211E+04	6.001E+01	1.393E+05	1.002E+05	1.390E+03	2.448E+04	1.330E+03	5.565E+01
H35031793	2.089E+04	1.505E+01	1.498E+01	1.119E+05	8.170E+03	1.299E+01	0.000E+00	1.168E+04	4.530E+04	4.225E+02	0.000E+00	1.102E+04	4.621E+01	1.373E+05	1.084E+05	1.410E+03	2.518E+04	1.300E+03	4.791E+01
H36031793	2.134E+04	2.240E+01	1.111E+01	1.168E+05	6.810E+03	1.549E+01	6.983E+00	1.233E+04	4.498E+04	4.415E+02	0.000E+00	1.198E+04	4.954E+01	1.419E+05	1.051E+05	1.430E+03	2.561E+04	1.400E+03	5.557E+01
H310031793	1.789E+04	1.047E+01	0.000E+00	8.229E+04	5.900E+03	2.228E+01	0.000E+00	9.010E+03	4.361E+04	3.514E+02	0.000E+00	6.950E+03	3.223E+01	1.059E+05	1.046E+05	1.190E+03	1.689E+04	9.330E+02	6.209E+01
H41031793	3.462E+04	1.640E+01	1.637E+01	1.071E+05	7.830E+03	1.916E+01	7.198E+00	1.850E+04	3.931E+04	5.686E+02	7.679E+00	1.675E+04	8.033E+01	1.721E+05	8.138E+04	1.300E+03	1.774E+04	2.010E+03	6.210E+01
H42031793	3.262E+04	1.850E+01	1.110E+01	1.139E+05	8.460E+03	1.495E+01	1.002E+01	1.660E+04	4.166E+04	5.395E+02	0.000E+00	1.548E+04	7.429E+01	1.658E+05	9.198E+04	1.370E+03	2.099E+04	1.850E+03	5.676E+01
H43031793	2.605E+04	1.643E+01	1.372E+01	1.109E+05	7.410E+03	1.764E+01	9.516E+00	1.359E+04	4.296E+04	4.785E+02	0.000E+00	1.266E+04	6.873E+01	1.495E+05	1.074E+05	1.350E+03	2.633E+04	1.460E+03	4.713E+01
H45031793	2.396E+04	1.640E+01	7.836E+00	1.156E+05	7.410E+03	1.524E+01	6.863E+00	1.253E+04	4.601E+04	4.470E+02	0.000E+00	1.181E+04	5.574E+01	1.433E+05	1.143E+05	1.420E+03	2.768E+04	1.350E+03	5.767E+01
H46031793	2.453E+04	1.919E+01	0.000E+00	1.231E+05	8.340E+03	1.805E+01	5.725E+00	1.279E+04	4.896E+04	4.333E+02	0.000E+00	1.218E+04	5.311E+01	1.518E+05	1.068E+05	1.400E+03	2.577E+04	1.410E+03	5.109E+01
H410031793	2.155E+04	2.558E+01	2.385E+01	1.184E+05	8.680E+03	1.341E+01	5.845E+00	1.282E+04	4.700E+04	4.367E+02	0.000E+00	1.204E+04	6.495E+01	1.449E+05	1.287E+05	1.490E+03	3.197E+04	1.440E+03	5.643E+01
S11031793	3.255E+04	2.579E+01	2.026E+01	1.353E+05	7.920E+03	2.043E+01	7.076E+00	1.679E+04	4.588E+04	5.648E+02	0.000E+00	1.613E+04	9.162E+01	1.777E+05	5.841E+04	1.630E+03	1.041E+04	1.880E+03	9.257E+01
S12031793	2.914E+04	2.244E+01	1.109E+01	1.385E+05	7.130E+03	1.457E+01	7.882E+00	1.475E+04	5.072E+04	5.318E+02	0.000E+00	1.464E+04	6.048E+01	1.721E+05	8.144E+04	1.610E+03	1.471E+04	1.650E+03	8.008E+01
S13031793	2.543E+04	1.437E+01	2.133E+01	1.271E+05	8.130E+03	1.688E+01	0.000E+00	1.298E+04	5.187E+04	4.548E+02	0.000E+00	1.321E+04	4.804E+01	1.596E+05	1.021E+05	1.530E+03	1.942E+04	1.390E+03	1.578E+02
S15031793	2.281E+04	1.747E+01	1.439E+01	1.353E+05	8.110E+03	1.032E+01	0.000E+00	1.262E+04	5.230E+04	4.683E+02	0.000E+00	1.297E+04	6.468E+01	1.576E+05	1.087E+05	1.680E+03	2.202E+04	1.400E+03	4.895E+01
S16031793	2.410E+04	1.755E+01	1.142E+01	1.373E+05	8.780E+03	9.866E+00	0.000E+00	1.270E+04	5.475E+04	4.531E+02	0.000E+00	1.273E+04	5.671E+01	1.631E+05	1.093E+05	1.720E+03	2.312E+04	1.480E+03	4.484E+02
S110031793	2.121E+04	2.455E+01	1.930E+01	1.311E+05	7.240E+03	1.247E+01	1.205E+01	1.204E+04	5.360E+04	4.394E+02	0.000E+00	1.198E+04	5.073E+01	1.514E+05	1.222E+05	1.530E+03	2.488E+04	1.300E+03	6.284E+02
S21031793	2.847E+04	1.786E+01	9.360E+00	1.599E+05	1.018E+04	1.675E+01	1.139E+01	1.456E+04	5.577E+04	5.186E+02	0.000E+00	1.567E+04	6.260E+01	1.841E+05	7.110E+04	1.760E+03	1.304E+04	1.690E+03	6.304E+01
S22031793	2.266E+04	2.417E+01	2.058E+01	1.530E+05	9.210E+03	1.122E+01	0.000E+00	1.219E+04	6.237E+04	4.645E+02	0.000E+00	1.374E+04	6.449E+01	1.741E+05	8.864E+04	1.820E+03	1.788E+04	1.410E+03	3.068E+02
S23031793	1.952E+04	1.623E+01	1.697E+01	1.213E+05	6.890E+03	9.102E+00	5.338E+00	1.030E+04	5.542E+04	3.918E+02	0.000E+00	1.031E+04	6.283E+01	1.455E+05	8.388E+04	1.580E+03	1.491E+04	1.150E+03	4.371E+01
S25031793	1.882E+04	2.040E+01	1.583E+01	1.214E+05	7.800E+03	9.274E+00	6.691E+00	9.960E+03	5.679E+04	3.683E+02	0.000E+00	1.002E+04	4.337E+01	1.453E+05	9.557E+04	1.540E+03	1.689E+04	1.140E+03	5.080E+01
S26031793	1.799E+04	2.179E+01	1.110E+01	1.195E+05	8.170E+03	1.148E+01	4.196E+00	9.620E+03	5.362E+04	3.718E+02	0.000E+00	9.730E+03	4.040E+01	1.417E+05	9.441E+04	1.540E+03	1.587E+04	1.090E+03	3.986E+01
S210031793	1.774E+04	2.198E+01	1.059E+01	1.188E+05	8.040E+03	1.402E+01	0.000E+00	1.021E+04	5.581E+04	3.911E+02	0.000E+00	9.860E+03	4.526E+01	1.405E+05	1.068E+05	1.540E+03	1.877E+04	1.100E+03	4.765E+01
S31031793	2.277E+04	2.025E+01	1.605E+01	1.421E+05	8.510E+03	1.458E+01	0.000E+00	1.204E+04	5.270E+04	4.598E+02	7.436E+00	1.230E+04	8.359E+01	1.598E+05	6.009E+04	1.680E+03	9.920E+03	1.320E+03	5.899E+01
S32031793	2.340E+04	1.848E+01	1.586E+01	1.280E+05	8.930E+03	1.026E+01	5.788E+00	1.205E+04	5.282E+04	4.404E+02	0.000E+00	1.209E+04	7.563E+01	1.595E+05	7.425E+04	1.580E+03	1.262E+04	1.390E+03	4.025E+01
S33031793	1.813E+04	1.962E+01	1.296E+01	1.240E+05	9.440E+03	9.936E+00	0.000E+00	1.073E+04	5.628E+04	4.091E+02	6.902E+00	1.055E+04	6.488E+01	1.492E+05	8.282E+04	1.680E+03	1.579E+04	1.160E+03	3.236E+02
S35031793	1.912E+04	2.027E+01	1.070E+01	1.267E+05	8.810E+03	1.170E+01	0.000E+00	1.045E+04	5.604E+04	4.047E+02	7.046E+00	1.068E+04	4.399E+01	1.508E+05	9.775E+04	1.640E+03	1.695E+04	1.150E+03	4.863E+01
S36031793	1.923E+04	2.036E+01	1.028E+01	1.274E+05	9.510E+03	8.529E+00	7.479E+00	1.047E+04	5.929E+04	3.968E+02	6.892E+00	1.063E+04	5.637E+01	1.541E+05	9.714E+04	1.580E+03	1.803E+04	1.120E+03	1.018E+02
S310031793	1.788E+04	2.629E+01	2.262E+01	1.175E+05	1.143E+04	1.076E+01	0.000E+00	1.089E+04	5.718E+04	4.118E+02	0.000E+00	1.024E+04	5.546E+01	1.433E+05	1.226E+05	1.530E+03	2.184E+04	1.190E+03	7.094E+01

23 March 1993 (μg g^{-1})																			
Sample ID	**Al**	**As**	**Br**	**Ca**	**Cl**	**Cu**	**Ga**	**Fe**	**Mg**	**Mn**	**Ni**	**K**	**Rb**	**Si**	**Na**	**Sr**	**S**	**Ti**	**Zn**
H11032393	3.417E+04	2.339E+01	2.028E+01	1.107E+05	1.137E+04	2.176E+01	6.566E+00	1.699E+04	3.818E+04	5.415E+02	5.820E+00	1.721E+04	8.783E+01	1.740E+05	6.825E+04	1.240E+03	1.408E+04	1.890E+03	8.637E+01
H12032393	2.914E+04	2.759E+01	2.772E+01	1.384E+05	1.343E+04	1.634E+01	1.003E+01	1.515E+04	4.715E+04	5.162E+02	8.455E+00	1.566E+04	6.784E+01	1.760E+05	8.193E+04	1.590E+03	1.887E+04	1.700E+03	5.702E+01
H13032393	2.286E+04	2.676E+01	1.519E+01	1.098E+05	9.310E+03	1.545E+01	7.611E+00	1.481E+04	3.908E+04	5.018E+02	6.007E+00	1.203E+04	9.198E+01	1.364E+05	7.084E+04	1.510E+03	1.453E+04	1.600E+03	6.726E+01
H15032393	2.298E+04	2.642E+01	2.264E+01	1.155E+05	1.003E+04	1.840E+01	5.921E+00	1.406E+04	4.382E+04	4.971E+02	6.277E+00	1.217E+04	6.760E+01	1.392E+05	7.813E+04	1.510E+03	1.715E+04	1.500E+03	6.616E+01
H16032393	2.207E+04	2.448E+01	2.189E+01	1.185E+05	9.800E+03	1.374E+01	8.071E+00	1.387E+04	4.275E+04	4.849E+02	8.288E+00	1.275E+04	6.450E+01	1.397E+05	8.239E+04	1.590E+03	1.849E+04	1.470E+03	8.592E+01
H110032393	2.203E+04	2.730E+01	1.801E+01	1.213E+05	1.018E+04	1.432E+01	7.747E+00	1.337E+04	4.437E+04	4.684E+02	8.951E+00	1.199E+04	7.073E+01	1.393E+05	9.043E+04	1.580E+03	2.039E+04	1.480E+03	4.592E+01
H21032393	2.722E+04	2.442E+01	1.579E+01	1.044E+05	9.430E+03	1.824E+01	9.972E+00	1.528E+04	3.776E+04	4.978E+02	5.937E+00	1.391E+04	7.160E+01	1.457E+05	6.834E+04	1.350E+03	1.343E+04	1.710E+03	5.229E+01
H22032393	2.874E+04	2.297E+01	1.962E+01	9.669E+04	1.096E+04	1.722E+01	7.436E+00	1.691E+04	3.556E+04	5.372E+02	6.627E+00	1.457E+04	6.339E+01	1.471E+05	6.595E+04	1.210E+03	1.261E+04	1.810E+03	5.707E+01
H23032393	2.158E+04	2.436E+01	1.885E+01	1.130E+05	9.800E+03	1.699E+01	6.345E+00	1.333E+04	4.215E+04	4.620E+02	6.024E+00	1.209E+04	6.342E+01	1.389E+05	8.247E+04	1.470E+03	1.748E+04	1.460E+03	4.197E+01
H25032393	2.214E+04	2.675E+01	2.146E+01	1.207E+05	1.005E+04	1.326E+01	1.079E+01	1.352E+04	4.387E+04	4.486E+02	0.000E+00	1.215E+04	5.989E+01	1.410E+05	8.156E+04	1.540E+03	1.786E+04	1.440E+03	4.403E+01
H26032393	2.370E+04	2.452E+01	3.012E+01	1.220E+05	1.054E+04	1.642E+01	4.857E+00	1.332E+04	4.350E+04	4.676E+02	0.000E+00	1.291E+04	5.416E+01	1.457E+05	8.311E+04	1.590E+03	1.958E+04	1.470E+03	5.350E+01
H210032393	2.284E+04	2.033E+01	2.304E+01	1.239E+05	1.098E+04	1.480E+01	5.593E+00	1.330E+04	4.523E+04	4.613E+02	0.000E+00	1.197E+04	5.249E+01	1.458E+05	8.998E+04	1.640E+03	2.070E+04	1.440E+03	5.372E+01
H31032393	3.224E+04	2.637E+01	2.010E+01	1.184E+05	1.231E+04	2.248E+01	1.031E+01	1.689E+04	4.142E+04	5.398E+02	0.000E+00	1.745E+04	8.704E+01	1.707E+05	7.214E+04	1.310E+03	1.668E+04	1.830E+03	5.708E+01
H32032393	2.687E+04	2.382E+01	1.770E+01	1.175E+05	1.068E+04	1.380E+01	8.000E+00	1.440E+04	4.151E+04	4.796E+02	0.000E+00	1.437E+04	7.682E+01	1.497E+05	7.102E+04	1.350E+03	1.414E+04	1.470E+03	4.706E+01
H33032393	2.407E+04	2.521E+01	1.270E+01	1.262E+05	1.101E+04	1.514E+01	0.000E+00	1.376E+04	4.422E+04	4.728E+02	0.000E+00	1.378E+04	6.091E+01	1.516E+05	8.370E+04	1.540E+03	1.935E+04	1.470E+03	4.329E+01
H35032393	2.157E+04	2.579E+01	1.613E+01	1.223E+05	1.019E+04	1.711E+01	0.000E+00	1.369E+04	4.100E+04	4.729E+02	0.000E+00	1.264E+04	6.738E+01	1.399E+05	8.269E+04	1.570E+03	1.891E+04	1.460E+03	5.050E+01
H36032393	2.329E+04	2.620E+01	2.180E+01	1.322E+05	1.106E+04	1.440E+01	5.133E+00	1.361E+04	4.467E+04	4.863E+02	6.166E+00	1.372E+04	7.013E+01	1.517E+05	8.369E+04	1.600E+03	2.146E+04	1.460E+03	4.215E+01
H310032393	2.011E+04	2.829E+01	2.022E+01	1.297E+05	1.074E+04	1.387E+01	5.248E+00	1.292E+04	4.585E+04	4.654E+02	0.000E+00	1.264E+04	6.067E+01	1.408E+05	9.926E+04	1.590E+03	2.279E+04	1.380E+03	4.884E+01
H41032393	3.564E+04	2.918E+01	2.116E+01	1.029E+05	1.091E+04	2.318E+01	8.963E+00	1.984E+04	3.414E+04	5.834E+02	0.000E+00	1.819E+04	1.005E+02	1.666E+05	6.400E+04	1.280E+03	1.266E+04	2.110E+03	6.381E+01
H42032393	3.223E+04	2.599E+01	2.023E+01	1.006E+05	1.135E+04	1.628E+01	6.546E+00	1.913E+04	3.297E+04	5.744E+02	0.000E+00	1.679E+04	9.168E+01	1.549E+05	6.548E+04	1.310E+03	1.437E+04	1.940E+03	5.854E+01
H43032393	2.242E+04	2.214E+01	1.231E+01	1.291E+05	9.610E+03	1.588E+01	8.156E+00	1.408E+04	4.235E+04	4.810E+02	0.000E+00	1.297E+04	7.041E+01	1.457E+05	7.602E+04	1.650E+03	1.760E+04	1.540E+03	4.230E+01
H45032393	2.364E+04	2.107E+01	2.274E+01	1.185E+05	8.910E+03	1.369E+01	0.000E+00	1.251E+04	4.849E+04	4.386E+02	0.000E+00	1.174E+04	5.192E+01	1.497E+05	9.187E+04	1.460E+03	1.858E+04	1.380E+03	4.427E+01
H46032393	2.355E+04	2.712E+01	1.956E+01	1.181E+05	9.240E+03	1.262E+01	0.000E+00	1.215E+04	5.092E+04	4.352E+02	0.000E+00	1.200E+04	5.405E+01	1.517E+05	9.325E+04	1.480E+03	1.900E+04	1.390E+03	4.268E+01
H410032393	2.131E+04	2.345E+01	1.855E+01	1.126E+05	9.590E+03	1.474E+01	0.000E+00	1.212E+04	4.991E+04	4.207E+02	0.000E+00	1.126E+04	5.925E+01	1.413E+05	1.055E+05	1.500E+03	2.158E+04	1.280E+03	4.165E+01
S11032393	3.159E+04	2.180E+01	1.907E+01	1.214E+05	1.370E+04	1.634E+01	0.000E+00	1.606E+04	4.647E+04	5.304E+02	0.000E+00	1.555E+04	6.065E+01	1.699E+05	6.816E+04	1.430E+03	1.164E+04	1.830E+03	7.270E+01
S12032393	2.702E+04	2.192E+01	2.160E+01	1.225E+05	1.232E+04	1.550E+01	0.000E+00	1.490E+04	4.346E+04	5.092E+02	0.000E+00	1.387E+04	7.207E+01	1.589E+05	6.632E+04	1.500E+03	1.159E+04	1.630E+03	8.526E+01
S13032393	2.316E+04	2.630E+01	2.044E+01	1.319E+05	1.237E+04	1.334E+01	0.000E+00	1.248E+04	5.131E+04	4.344E+02	0.000E+00	1.224E+04	6.439E+01	1.570E+05	7.823E+04	1.600E+03	1.425E+04	1.340E+03	8.287E+01
S15032393	2.188E+04	2.851E+01	2.055E+01	1.340E+05	1.113E+04	1.398E+01	0.000E+00	1.206E+04	5.269E+04	4.480E+02	0.000E+00	1.249E+04	5.846E+01	1.548E+05	8.255E+04	1.620E+03	1.507E+04	1.370E+03	4.538E+01
S16032393	2.056E+04	2.587E+01	2.147E+01	1.289E+05	9.760E+03	1.205E+01	0.000E+00	1.186E+04	5.135E+04	4.253E+02	0.000E+00	1.209E+04	6.778E+01	1.496E+05	7.912E+04	1.600E+03	1.466E+04	1.350E+03	7.965E+01
S110032393	1.964E+04	2.325E+01	2.509E+01	1.327E+05	9.790E+03	1.184E+01	0.000E+00	1.157E+04	5.413E+04	4.277E+02	0.000E+00	1.197E+04	5.847E+01	1.496E+05	9.523E+04	1.640E+03	1.644E+04	1.290E+03	1.184E+02
S21032393	2.342E+04	2.525E+01	1.919E+01	1.429E+05	1.453E+04	1.128E+01	0.000E+00	1.313E+04	4.920E+04	4.665E+02	0.000E+00	1.425E+04	5.674E+01	1.629E+05	6.364E+04	1.560E+03	1.081E+04	1.440E+03	4.414E+01
S22032393	2.045E+04	2.736E+01	2.548E+01	1.445E+05	1.415E+04	1.410E+01	8.682E+00	1.137E+04	5.346E+04	4.353E+02	0.000E+00	1.270E+04	5.921E+01	1.594E+05	7.636E+04	1.660E+03	1.421E+04	1.290E+03	7.941E+01
S23032393	1.978E+04	3.323E+01	2.200E+01	1.470E+05	1.383E+04	1.374E+01	5.478E+00	1.136E+04	5.751E+04	4.278E+02	0.000E+00	1.302E+04	5.242E+01	1.625E+05	8.611E+04	1.690E+03	1.581E+04	1.330E+03	4.513E+01
S25032393	2.055E+04	3.209E+01	1.981E+01	1.497E+05	1.348E+04	1.107E+01	0.000E+00	1.160E+04	6.043E+04	4.307E+02	0.000E+00	1.326E+04	5.774E+01	1.676E+05	9.324E+04	1.730E+03	1.729E+04	1.340E+03	6.059E+01
S26032393	1.953E+04	2.707E+01	3.021E+01	1.503E+05	1.483E+04	1.343E+01	0.000E+00	1.093E+04	5.783E+04	4.194E+02	0.000E+00	1.238E+04	3.938E+01	1.628E+05	9.413E+04	1.710E+03	1.777E+04	1.240E+03	6.672E+01

APPENDIX C

PIXE (particle induced x-ray emission) limits of detection for aeolian dust samples from Owens (dry) Lake, California

11 March 1993 (μg g^{-1})								
Sample ID	**Location**	**Height**	**Barium**	**Cadmium**	**Chromium**	**Cobalt**	**Lead**	**Molybdenum**
H11031193	H1	10	1.305E+02	4.012E+01	4.918E+00	1.117E+01	8.833E+00	7.621E+00
H12031193	H1	20	1.303E+02	3.120E+01	4.973E+00	1.092E+01	7.966E+00	6.025E+00
H13031193	H1	30	1.231E+02	2.706E+01	4.749E+00	1.049E+01	8.072E+00	7.984E+00
H16031193	H1	60	1.129E+02	3.959E+01	5.019E+00	9.590E+00	7.392E+00	7.200E+00
H110031193	H1	100	1.102E+02	3.655E+01	4.574E+00	9.274E+00	8.025E+00	9.183E+00
H21031193	H2	10	1.325E+02	4.121E+01	5.122E+00	1.126E+01	8.730E+00	6.892E+00
H22031193	H2	20	1.211E+02	1.834E+01	4.794E+00	1.027E+01	8.246E+00	6.390E+00
H23031193	H2	30	1.208E+02	2.807E+01	4.759E+00	1.008E+01	7.777E+00	9.365E+00
H25031193	H2	50	1.097E+02	3.404E+01	4.444E+00	9.313E+00	8.311E+00	8.900E+00
H26031193	H2	60	1.074E+02	2.818E+01	4.657E+00	9.080E+00	7.936E+00	7.044E+00
H210031193	H2	100	1.172E+02	2.915E+01	4.747E+00	9.377E+00	7.317E+00	9.290E+00
H31031193	H3	10	1.304E+02	2.771E+01	5.093E+00	1.093E+01	8.131E+00	7.619E+00
H32031193	H3	20	1.281E+02	3.793E+01	5.452E+00	1.125E+01	8.211E+00	9.318E+00
H33031193	H3	30	1.226E+02	3.378E+01	5.059E+00	1.028E+01	8.877E+00	7.670E+00
H35031193	H3	50	1.010E+02	2.889E+01	4.637E+00	8.666E+00	8.990E+00	6.780E+00
H36031193	H3	60	9.709E+01	3.765E+01	4.181E+00	8.628E+00	7.526E+00	7.289E+00
H310031193	H3	100	9.528E+01	3.765E+01	4.518E+00	8.374E+00	8.820E+00	1.211E+01
H41031193	H4	10	1.382E+02	2.701E+01	5.240E+00	1.195E+01	8.361E+00	7.413E+00
H42031193	H4	20	1.225E+02	3.000E+01	4.838E+00	1.091E+01	7.844E+00	7.334E+00
H43031193	H4	30	1.102E+02	2.316E+01	4.351E+00	9.755E+00	7.955E+00	6.511E+00
H45031193	H4	50	9.764E+01	2.414E+01	4.201E+00	8.370E+00	7.556E+00	6.995E+00
H46031193	H4	60	9.746E+01	2.618E+01	4.217E+00	8.676E+00	7.066E+00	8.243E+00
H410031193	H4	100	9.590E+01	2.364E+01	4.217E+00	8.154E+00	7.214E+00	5.424E+00
S11031193	S1	10	1.232E+02	3.185E+01	4.890E+00	1.076E+01	8.405E+00	5.632E+00
S12031193	S1	20	1.244E+02	3.316E+01	5.006E+00	1.111E+01	8.241E+00	7.036E+00
S13031193	S1	30	1.205E+02	3.003E+01	4.985E+00	1.062E+01	7.391E+00	6.824E+00
S15031193	S1	50	1.226E+02	3.228E+01	4.853E+00	1.039E+01	8.297E+00	8.961E+00
S16031193	S1	60	1.205E+02	3.601E+01	4.823E+00	1.039E+01	8.531E+00	8.484E+00
S110031193	S1	100	1.182E+02	2.473E+01	4.761E+00	1.014E+01	7.422E+00	7.841E+00
S21031193	S2	10	1.216E+02	3.187E+01	5.065E+00	1.056E+01	8.363E+00	9.850E+00
S22031193	S2	20	1.202E+02	2.870E+01	5.107E+00	1.030E+01	8.188E+00	8.987E+00
S23031193	S2	30	1.211E+02	2.744E+01	4.895E+00	1.027E+01	8.211E+00	8.015E+00
S25031193	S2	50	1.198E+02	2.735E+01	5.070E+00	1.022E+01	8.468E+00	7.031E+00
S26031193	S2	60	1.169E+02	3.224E+01	4.897E+00	1.002E+01	8.021E+00	8.560E+00
S210031193	S2	100	1.199E+02	3.351E+01	5.030E+00	1.013E+01	8.734E+00	9.180E+00
S31031193	S3	10	1.228E+02	2.617E+01	5.207E+00	1.040E+01	8.058E+00	8.332E+00
S32031193	S3	20	1.289E+02	3.796E+01	5.113E+00	1.092E+01	8.435E+00	6.328E+00
S33031193	S3	30	1.183E+02	2.164E+01	4.983E+00	9.887E+00	8.381E+00	6.694E+00
S35031193	S3	50	1.207E+02	3.467E+01	5.207E+00	1.026E+01	8.515E+00	8.202E+00
S36031193	S3	60	1.236E+02	3.249E+01	4.950E+00	1.017E+01	8.591E+00	8.694E+00
S310031193	S3	100	1.257E+02	2.460E+01	5.098E+00	1.028E+01	8.449E+00	7.936E+00

17 March 1993 (μg g^{-1})								
Sample ID	**Location**	**Height**	**Barium**	**Cadmium**	**Chromium**	**Cobalt**	**Lead**	**Molybdenum**
H11031793	H1	10	1.549E+02	2.040E+01	5.932E+00	1.028E+01	9.692E+00	7.235E+00
H12031793	H1	20	1.465E+02	3.100E+01	5.931E+00	8.666E+00	9.424E+00	7.886E+00
H13031793	H1	30	1.678E+02	4.177E+01	6.688E+00	8.628E+00	1.089E+01	9.962E+00
H15031793	H1	50	1.579E+02	3.672E+01	6.320E+00	8.374E+00	1.148E+01	1.048E+01
H16031793	H1	60	1.636E+02	3.701E+01	6.493E+00	1.195E+01	1.059E+01	9.111E+00
H110031793	H1	100	2.115E+02	5.982E+01	9.325E+00	1.091E+01	1.667E+01	1.915E+01
H21031793	H2	10	1.762E+02	4.207E+01	6.819E+00	9.755E+00	1.062E+01	7.045E+00
H22031793	H2	20	1.820E+02	4.483E+01	6.800E+00	8.370E+00	1.034E+01	7.676E+00
H23031793	H2	30	1.707E+02	3.604E+01	6.829E+00	8.676E+00	1.008E+01	1.075E+01
H25031793	H2	50	1.557E+02	3.596E+01	6.507E+00	8.154E+00	9.848E+00	1.020E+01
H26031793	H2	60	1.571E+02	3.748E+01	6.533E+00	1.076E+01	1.026E+01	1.137E+01
H210031793	H2	100	2.254E+02	1.051E+02	1.030E+01	1.111E+01	1.822E+01	2.424E+01
H31031793	H3	10	1.571E+02	3.651E+01	5.959E+00	1.062E+01	9.185E+00	7.799E+00
H32031793	H3	20	1.641E+02	2.750E+01	6.380E+00	1.039E+01	1.001E+01	9.460E+00
H33031793	H3	30	1.392E+02	2.985E+01	5.539E+00	1.039E+01	9.344E+00	8.100E+00
H35031793	H3	50	1.349E+02	3.389E+01	5.319E+00	1.014E+01	8.566E+00	9.766E+00
H36031793	H3	60	1.440E+02	3.263E+01	5.549E+00	1.056E+01	9.428E+00	8.877E+00
H310031793	H3	100	2.178E+02	5.740E+01	1.039E+01	1.030E+01	1.590E+01	2.672E+01
H41031793	H4	10	2.093E+02	4.677E+01	8.075E+00	1.027E+01	1.182E+01	9.388E+00
H42031793	H4	20	2.021E+02	3.722E+01	8.269E+00	1.022E+01	1.126E+01	6.340E+00
H43031793	H4	30	1.790E+02	4.705E+01	7.366E+00	1.002E+01	1.026E+01	8.498E+00
H45031793	H4	50	1.737E+02	3.771E+01	7.191E+00	1.013E+01	1.164E+01	1.094E+01
H46031793	H4	60	1.784E+02	3.363E+01	7.173E+00	1.040E+01	1.150E+01	9.904E+00
H410031793	H4	100	1.790E+02	3.379E+01	7.147E+00	1.092E+01	1.258E+01	8.133E+00
S11031793	S1	10	2.109E+02	3.622E+01	7.918E+00	9.887E+00	1.287E+01	1.244E+01
S12031793	S1	20	1.993E+02	4.778E+01	7.952E+00	1.026E+01	1.292E+01	1.476E+01
S13031793	S1	30	1.874E+02	5.376E+01	7.726E+00	1.017E+01	1.194E+01	1.268E+01
S15031793	S1	50	1.762E+02	3.747E+01	7.301E+00	1.028E+01	1.077E+01	9.718E+00
S16031793	S1	60	1.836E+02	4.201E+01	7.291E+00	1.384E+01	1.168E+01	1.253E+01
S110031793	S1	100	1.723E+02	3.594E+01	7.111E+00	1.287E+01	1.229E+01	1.291E+01
S21031793	S2	10	2.121E+02	5.319E+01	8.015E+00	1.492E+01	1.211E+01	1.404E+01
S22031793	S2	20	1.888E+02	5.823E+01	7.744E+00	1.414E+01	1.289E+01	9.279E+00
S23031793	S2	30	1.293E+02	2.810E+01	5.322E+00	1.390E+01	8.464E+00	8.341E+00
S25031793	S2	50	1.282E+02	3.848E+01	4.935E+00	2.022E+01	9.156E+00	5.813E+00
S26031793	S2	60	1.236E+02	2.784E+01	5.289E+00	1.570E+01	9.074E+00	6.759E+00
S210031793	S2	100	1.280E+02	4.161E+01	5.261E+00	1.557E+01	9.119E+00	8.692E+00
S31031793	S3	10	1.664E+02	3.191E+01	7.025E+00	1.458E+01	1.188E+01	8.387E+00
S32031793	S3	20	1.494E+02	2.689E+01	5.972E+00	1.372E+01	9.262E+00	9.766E+00
S33031793	S3	30	1.324E+02	2.520E+01	5.544E+00	1.332E+01	9.565E+00	1.049E+01
S35031793	S3	50	1.303E+02	2.321E+01	5.398E+00	2.185E+01	9.367E+00	1.015E+01
S36031793	S3	60	1.360E+02	2.916E+01	5.415E+00	1.369E+01	9.123E+00	6.990E+00
S310031793	S3	100	1.416E+02	3.607E+01	5.881E+00	1.443E+01	1.101E+01	1.043E+01

23 March 1993 (μg g^{-1})								
Sample ID	**Location**	**Height**	**Barium**	**Cadmium**	**Chromium**	**Cobalt**	**Lead**	**Molybdenum**
H11032393	H1	10	1.607E+02	2.801E+01	5.733E+00	1.253E+01	9.289E+00	6.384E+00
H12032393	H1	20	1.659E+02	3.126E+01	7.663E+00	1.178E+01	1.052E+01	7.504E+00
H13032393	H1	30	1.575E+02	4.354E+01	6.344E+00	1.221E+01	1.130E+01	7.513E+00
H15032393	H1	50	1.600E+02	3.453E+01	6.366E+00	2.213E+01	1.168E+01	1.007E+01
H16032393	H1	60	1.460E+02	3.303E+01	5.692E+00	1.945E+01	1.039E+01	8.901E+00
H110032393	H1	100	1.506E+02	3.220E+01	5.930E+00	1.808E+01	1.078E+01	8.215E+00
H21032393	H2	10	1.590E+02	4.274E+01	5.865E+00	1.651E+01	1.017E+01	5.745E+00
H22032393	H2	20	1.613E+02	3.720E+01	5.941E+00	1.596E+01	1.057E+01	8.903E+00
H23032393	H2	30	1.418E+02	2.167E+01	5.562E+00	1.572E+01	9.878E+00	7.975E+00
H25032393	H2	50	1.563E+02	3.624E+01	6.194E+00	1.611E+01	1.111E+01	1.006E+01
H26032393	H2	60	1.534E+02	3.759E+01	5.851E+00	1.855E+01	1.071E+01	5.677E+00
H210032393	H2	100	1.630E+02	2.842E+01	6.571E+00	1.751E+01	1.127E+01	6.593E+00
H31032393	H3	10	1.680E+02	2.613E+01	6.045E+00	1.650E+01	1.030E+01	4.956E+00
H32032393	H3	20	1.556E+02	3.186E+01	5.889E+00	1.521E+01	9.732E+00	7.542E+00
H33032393	H3	30	1.574E+02	2.518E+01	6.204E+00	1.555E+01	1.063E+01	9.318E+00
H35032393	H3	50	1.520E+02	4.068E+01	5.982E+00	1.509E+01	1.083E+01	8.711E+00
H36032393	H3	60	1.608E+02	3.014E+01	6.380E+00	1.719E+01	1.124E+01	1.125E+01
H310032393	H3	100	1.475E+02	2.681E+01	6.054E+00	1.620E+01	1.047E+01	8.740E+00
H41032393	H4	10	1.895E+02	2.947E+01	6.885E+00	1.122E+01	1.177E+01	8.108E+00
H42032393	H4	20	1.864E+02	3.779E+01	7.128E+00	1.081E+01	1.186E+01	5.158E+00
H43032393	H4	30	1.609E+02	3.166E+01	6.317E+00	1.076E+01	1.032E+01	9.400E+00
H45032393	H4	50	1.657E+02	4.993E+01	6.847E+00	1.126E+01	1.206E+01	1.130E+01
H46032393	H4	60	1.732E+02	5.080E+01	7.052E+00	1.448E+01	1.271E+01	1.411E+01
H410032393	H4	100	1.712E+02	4.013E+01	6.994E+00	1.272E+01	1.290E+01	9.943E+00
S11032393	S1	10	1.640E+02	3.298E+01	6.040E+00	1.176E+01	1.012E+01	5.822E+00
S12032393	S1	20	1.555E+02	2.879E+01	5.873E+00	1.146E+01	9.687E+00	7.716E+00
S13032393	S1	30	1.416E+02	3.194E+01	5.757E+00	1.153E+01	1.064E+01	6.298E+00
S15032393	S1	50	1.447E+02	3.793E+01	5.730E+00	1.247E+01	1.081E+01	8.017E+00
S16032393	S1	60	1.424E+02	3.401E+01	5.551E+00	1.366E+01	1.072E+01	7.082E+00
S110032393	S1	100	1.419E+02	3.362E+01	5.710E+00	1.629E+01	1.026E+01	7.443E+00
S21032393	S2	10	1.438E+02	2.935E+01	5.360E+00	1.430E+01	9.617E+00	5.026E+00
S22032393	S2	20	1.377E+02	2.990E+01	5.344E+00	1.427E+01	9.958E+00	8.595E+00
S23032393	S2	30	1.379E+02	3.164E+01	5.196E+00	1.292E+01	1.039E+01	8.984E+00
S25032393	S2	50	1.407E+02	3.115E+01	5.631E+00	1.307E+01	1.019E+01	8.075E+00
S26032393	S2	60	1.340E+02	3.106E+01	5.365E+00	1.362E+01	1.025E+01	8.135E+00

APPENDIX D

ICP-AES (inductively coupled plasma atomic emission spectroscopy) elemental concentration for aeolian dust samples from Owens (dry) Lake, California

11 March 1993 (μg g^{-1})																
Sample ID	**Al**	**As**	**Ba**	**Cd**	**Co**	**Cr**	**Cu**	**Fe**	**K**	**Mn**	**Mo**	**Ni**	**Pb**	**Sr**	**Ti**	**Zn**
H11031193	7.82E+03	1.79E+01	2.14E+01	2.66E-01	3.36E+00	3.91E+00	9.93E+00	8.16E+03	6.96E+03	1.99E+02	5.29E-01	4.62E+00	8.28E+00	1.02E+03	5.46E+02	1.19E+02
H12031193	6.63E+03	1.85E+01	3.78E+01	2.39E-01	3.05E+00	3.75E+00	1.07E+01	6.76E+03	6.15E+03	1.89E+02	7.49E-01	3.88E+00	9.77E+00	1.14E+03	4.89E+02	7.51E+01
H13031193	6.90E+03	1.57E+01	1.89E+01	2.13E-01	3.01E+00	3.50E+00	8.38E+00	7.19E+03	6.75E+03	1.77E+02	5.34E-01	4.13E+00	7.54E+00	9.33E+02	4.93E+02	7.83E+01
H16031193	6.27E+03	1.33E+01	2.44E+01	1.47E-01	2.29E+00	3.54E+00	1.06E+01	6.38E+03	6.60E+03	1.46E+02	5.29E-01	7.03E+00	9.47E+00	9.26E+02	4.43E+02	7.60E+01
H110031193	3.55E+03	1.44E+01	3.16E+01	1.66E-01	2.31E+00	3.00E+00	9.58E+00	3.47E+03	3.53E+03	1.50E+02	5.58E-01	3.11E+00	7.49E+00	9.29E+02	3.83E+02	1.42E+02
H21031193	6.71E+03	1.69E+01	3.61E+01	2.33E-01	3.18E+00	3.94E+00	9.22E+00	7.62E+03	6.67E+03	1.90E+02	6.67E-01	4.71E+00	9.17E+00	1.05E+03	5.03E+02	3.74E+01
H22031193	6.62E+03	1.66E+01	2.77E+01	2.13E-01	2.90E+00	3.88E+00	1.19E+01	6.81E+03	6.27E+03	1.87E+02	6.67E-01	4.66E+00	9.77E+00	1.05E+03	4.82E+02	4.04E+01
H23031193	6.05E+03	1.53E+01	2.30E+01	2.18E-01	2.69E+00	3.54E+00	8.83E+00	6.33E+03	6.06E+03	1.63E+02	6.60E-01	5.04E+00	8.20E+00	9.30E+02	4.97E+02	5.89E+01
H25031193	5.10E+03	1.47E+01	2.17E+01	1.64E-01	2.37E+00	3.38E+00	1.04E+01	5.08E+03	5.24E+03	1.57E+02	5.75E-01	5.27E+00	9.31E+00	9.62E+02	4.40E+02	1.06E+02
H26031193	5.36E+03	1.69E+01	4.68E+01	1.91E-01	2.89E+00	3.76E+00	9.32E+00	5.68E+03	5.58E+03	1.78E+02	7.23E-01	3.70E+00	9.54E+00	9.16E+02	4.67E+02	1.96E+02
H31031193	6.51E+03	1.79E+01	2.46E+01	2.38E-01	3.11E+00	3.99E+00	9.69E+00	6.99E+03	6.18E+03	1.95E+02	7.12E-01	6.33E+00	1.04E+01	1.16E+03	5.20E+02	4.25E+01
H32031193	5.53E+03	1.72E+01	2.60E+01	2.03E-01	2.79E+00	3.56E+00	8.54E+00	6.14E+03	6.20E+03	1.85E+02	7.87E-01	4.62E+00	9.41E+00	1.14E+03	4.54E+02	3.08E+01
H33031193	4.79E+03	1.67E+01	2.27E+01	2.45E-01	2.82E+00	4.19E+00	9.44E+00	5.10E+03	4.96E+03	1.74E+02	9.12E-01	6.36E+00	1.06E+01	9.30E+02	4.72E+02	6.99E+01
H41031193	7.96E+03	1.90E+01	1.80E+01	2.84E-01	3.75E+00	4.63E+00	1.12E+01	8.33E+03	7.09E+03	2.23E+02	4.90E-01	5.87E+00	1.07E+01	1.21E+03	6.10E+02	4.66E+01
H42031193	5.73E+03	1.81E+01	4.49E+01	2.47E-01	3.32E+00	4.23E+00	1.03E+01	6.32E+03	5.63E+03	2.12E+02	5.64E-01	5.09E+00	1.04E+01	1.16E+03	5.27E+02	2.86E+01
H43031193	6.73E+03	1.72E+01	2.84E+01	2.55E-01	3.24E+00	4.45E+00	1.06E+01	6.91E+03	6.26E+03	1.90E+02	6.01E-01	6.36E+00	1.07E+01	1.05E+03	5.11E+02	5.61E+01
H45031193	5.46E+03	1.58E+01	1.39E+01	1.91E-01	2.53E+00	3.44E+00	9.15E+00	5.85E+03	6.05E+03	1.62E+02	8.09E-01	6.00E+00	8.11E+00	8.61E+02	4.27E+02	9.50E+01
H46031193	4.77E+04	1.52E+01	2.78E+01	1.96E-01	2.80E+00	3.99E+00	9.98E+00	4.43E+04	4.38E+04	1.73E+02	6.48E-01	6.61E+00	1.08E+01	1.19E+02	5.61E+01	1.07E+02
S11031193	7.74E+03	1.78E+01	1.27E+02	2.34E-01	3.25E+00	3.77E+00	8.37E+00	7.15E+03	7.49E+03	1.98E+02	3.95E-01	4.69E+00	9.63E+00	1.40E+03	5.29E+02	4.51E+01
S12031193	7.81E+03	1.85E+01	6.49E+01	2.12E-01	3.51E+00	4.10E+00	9.03E+00	7.24E+03	7.26E+03	2.09E+02	3.58E-01	5.30E+00	1.03E+01	1.41E+03	5.57E+02	5.69E+01
S13031193	7.86E+03	1.93E+01	5.56E+01	2.92E-01	3.62E+00	4.20E+00	1.03E+01	7.91E+03	7.81E+03	2.12E+02	4.51E-01	4.87E+00	1.07E+01	1.43E+03	5.48E+02	8.60E+01
S15031193	7.18E+03	1.67E+01	5.54E+01	2.31E-01	3.04E+00	3.70E+00	8.79E+00	6.67E+03	7.20E+03	1.87E+02	4.01E-01	5.27E+00	8.68E+00	1.38E+03	4.95E+02	2.81E+01
S16031193	6.97E+03	1.68E+01	2.81E+01	2.01E-01	3.03E+00	3.58E+00	9.00E+00	6.63E+03	6.62E+03	1.85E+02	3.93E-01	4.58E+00	8.36E+00	1.38E+03	4.99E+02	1.42E+02
S110031193	6.05E+03	1.56E+01	3.41E+01	1.56E-01	2.87E+00	3.50E+00	8.18E+00	6.11E+03	5.68E+03	1.77E+02	3.16E-01	4.23E+00	7.98E+00	1.25E+03	4.59E+02	3.54E+02
S21031193	6.86E+03	1.67E+01	1.32E+02	2.12E-01	2.90E+00	3.33E+00	7.07E+00	6.50E+03	6.30E+03	1.88E+02	3.70E-01	4.56E+00	9.27E+00	1.50E+03	4.43E+02	2.63E+01
S22031193	5.12E+03	1.91E+01	8.44E+01	2.46E-01	3.22E+00	3.92E+00	1.21E+01	5.05E+03	5.01E+03	2.05E+02	4.36E-01	4.90E+00	1.18E+01	1.54E+03	4.89E+02	1.06E+02
S23031193	7.26E+03	1.82E+01	3.30E+01	2.23E-01	3.01E+00	3.56E+00	8.21E+00	6.47E+03	7.33E+03	1.89E+02	4.75E-01	4.92E+00	1.44E+01	1.53E+03	4.70E+02	3.01E+01
S25031193	7.52E+03	1.77E+01	5.25E+01	2.37E-01	2.95E+00	3.66E+00	8.16E+00	6.56E+03	7.08E+03	1.87E+02	4.54E-01	4.77E+00	9.36E+00	1.50E+03	4.83E+02	3.13E+01
S26031193	7.18E+03	1.71E+01	6.00E+01	2.35E-01	2.97E+00	3.48E+00	8.22E+00	6.39E+03	7.07E+03	1.88E+02	4.84E-01	5.09E+00	9.33E+00	1.51E+03	4.55E+02	3.19E+01
S210031193	6.89E+03	1.72E+01	5.76E+01	2.43E-01	2.99E+00	3.67E+00	9.17E+00	6.61E+03	7.16E+03	1.85E+02	6.51E-01	4.53E+00	1.04E+01	1.34E+03	4.26E+02	3.49E+01
S31031193	5.85E+03	1.76E+01	2.34E+02	1.94E-01	2.73E+00	3.62E+00	8.27E+00	5.77E+03	6.10E+03	1.96E+02	5.10E-01	3.94E+00	1.11E+01	1.56E+03	4.09E+02	5.00E+01
S32031193	6.05E+03	1.84E+01	2.34E+02	2.03E-01	2.84E+00	3.57E+00	7.88E+00	5.93E+03	6.14E+03	1.98E+02	5.57E-01	4.17E+00	1.15E+01	1.51E+03	4.12E+02	2.05E+01
S33031193	5.04E+03	1.87E+01	5.16E+01	1.94E-01	2.99E+00	3.66E+00	1.02E+01	4.64E+03	5.06E+03	1.93E+02	5.59E-01	4.28E+00	1.13E+01	1.57E+03	4.39E+02	1.12E+02
S35031193	6.89E+03	1.75E+01	5.76E+01	2.05E-01	2.85E+00	3.71E+00	8.19E+00	6.70E+03	6.66E+03	1.91E+02	5.71E-01	4.62E+00	1.16E+01	1.49E+03	4.07E+02	2.92E+01
S36031193	5.78E+03	1.79E+01	7.87E+01	2.11E-01	2.91E+00	3.72E+00	8.68E+00	5.50E+03	5.94E+03	1.98E+02	5.27E-01	4.26E+00	1.13E+01	1.61E+03	4.41E+02	6.59E+01
S310031193	7.25E+03	1.79E+01	3.28E+01	2.19E-01	2.98E+00	3.87E+00	1.07E+01	6.66E+03	7.28E+03	1.90E+02	5.75E-01	7.19E+00	1.10E+01	1.53E+03	4.52E+02	3.52E+01

23 March 1993 (μg g^{-1})																
Sample ID	**Al**	**As**	**Ba**	**Cd**	**Co**	**Cr**	**Cu**	**Fe**	**K**	**Mn**	**Mo**	**Ni**	**Pb**	**Sr**	**Ti**	**Zn**
H11032393	1.07E+04	2.35E+01	1.33E+02	3.98E-01	5.24E+00	6.44E+00	1.62E+01	1.13E+04	8.63E+03	2.89E+02	8.81E-01	7.30E+00	1.32E+01	1.10E+03	7.92E+02	6.58E+01
H12032393	8.89E+03	2.44E+01	5.26E+01	3.09E-01	5.00E+00	5.84E+00	1.45E+01	9.63E+03	7.83E+03	2.75E+02	9.68E-01	6.66E+00	1.19E+01	1.18E+03	7.46E+02	4.42E+01
H13032393	9.37E+03	2.33E+01	8.32E+01	3.15E-01	4.65E+00	5.38E+00	1.32E+01	1.05E+04	8.68E+03	2.57E+02	9.56E-01	6.54E+00	1.24E+01	1.17E+03	6.49E+02	4.05E+01
H15032393	9.25E+03	2.32E+01	8.41E+01	2.80E-01	4.20E+00	5.04E+00	1.21E+01	9.15E+03	8.55E+03	2.43E+02	1.09E+00	5.84E+00	1.19E+01	1.32E+03	6.05E+02	3.57E+01
H16032393	9.66E+03	2.31E+01	7.00E+01	3.04E-01	4.30E+00	5.15E+00	1.22E+01	9.21E+03	8.78E+03	2.43E+02	1.08E+00	5.71E+00	1.25E+01	1.36E+03	6.76E+02	7.34E+01
H110032393	6.31E+03	2.30E+01	4.40E+01	2.76E-01	3.83E+00	4.74E+00	1.15E+01	6.86E+03	6.08E+03	2.28E+02	1.08E+00	5.58E+00	1.17E+01	1.29E+03	5.58E+02	2.82E+01
H21032393	8.34E+03	2.46E+01	1.21E+02	4.02E-01	5.33E+00	6.63E+00	1.54E+01	1.05E+04	7.14E+03	2.94E+02	8.65E-01	7.11E+00	1.35E+01	1.02E+03	7.87E+02	3.66E+01
H22032393	9.47E+03	2.76E+01	3.37E+01	4.59E-01	5.73E+00	7.18E+00	1.64E+01	1.01E+04	7.71E+03	3.26E+02	1.19E+00	8.13E+00	1.59E+01	1.15E+03	9.02E+02	4.05E+01
H23032393	8.30E+03	2.48E+01	7.42E+01	3.92E-01	4.57E+00	5.57E+00	1.27E+01	8.51E+03	7.45E+03	2.68E+02	1.06E+00	6.46E+00	1.34E+01	1.34E+03	7.01E+02	3.15E+01
H25032393	7.46E+03	2.34E+01	9.87E+01	3.33E-01	4.07E+00	5.01E+00	1.09E+01	8.51E+03	7.15E+03	2.49E+02	1.04E+00	5.88E+00	1.22E+01	1.33E+03	6.08E+02	3.13E+01
H26032393	8.89E+03	2.30E+01	4.28E+01	3.49E-01	4.07E+00	4.98E+00	1.11E+01	9.10E+03	8.20E+03	2.46E+02	1.02E+00	5.91E+00	1.18E+01	1.37E+03	6.29E+02	3.10E+01
H210032393	8.83E+03	2.43E+01	2.47E+01	3.16E-01	4.01E+00	5.04E+00	1.16E+01	8.51E+03	8.24E+03	2.45E+02	1.08E+00	6.30E+00	1.23E+01	1.33E+03	5.95E+02	3.06E+01
H31032393	1.09E+04	2.45E+01	1.02E+02	4.13E-01	4.97E+00	6.19E+00	1.40E+01	1.19E+04	8.49E+03	2.84E+02	8.64E-01	6.86E+00	1.35E+01	1.20E+03	7.74E+02	3.38E+01
H32032393	9.58E+03	2.47E+01	1.06E+02	4.15E-01	4.99E+00	6.29E+00	1.39E+01	1.08E+04	8.02E+03	2.94E+02	9.50E-01	6.82E+00	1.36E+01	1.23E+03	7.70E+02	3.50E+01
H33032393	8.69E+03	2.39E+01	5.01E+01	3.62E-01	4.46E+00	5.45E+00	1.23E+01	9.29E+03	7.55E+03	2.61E+02	9.85E-01	6.24E+00	1.36E+01	1.34E+03	6.84E+02	3.27E+01
H35032393	9.19E+03	2.42E+01	4.56E+01	3.50E-01	4.20E+00	5.12E+00	1.17E+01	9.40E+03	8.06E+03	2.54E+02	9.91E-01	5.92E+00	1.31E+01	1.32E+03	6.22E+02	3.46E+01
H36032393	9.44E+03	2.41E+01	2.78E+01	3.52E-01	4.32E+00	5.33E+00	1.10E+01	9.72E+03	9.03E+03	2.57E+02	9.79E-01	6.09E+00	1.34E+01	1.31E+03	6.45E+02	3.04E+01
H310032393	9.40E+03	2.38E+01	4.35E+01	3.30E-01	4.01E+00	5.04E+00	1.09E+01	9.27E+03	8.15E+03	2.45E+02	1.07E+00	5.86E+00	1.28E+01	1.33E+03	6.34E+02	3.65E+01
H41032393	8.57E+03	2.43E+01	1.07E+02	4.02E-01	5.06E+00	6.36E+00	1.41E+01	9.73E+03	6.47E+03	2.82E+02	9.95E-01	7.25E+00	1.39E+01	1.19E+03	8.01E+02	3.53E+01
H42032393	1.08E+04	2.46E+01	1.16E+02	4.21E-01	5.02E+00	6.36E+00	1.46E+01	1.17E+04	8.41E+03	2.82E+02	9.82E-01	6.75E+00	1.44E+01	1.11E+03	7.24E+02	3.62E+01
H43032393	8.50E+03	2.31E+01	4.30E+01	3.48E-01	4.28E+00	5.29E+00	1.16E+01	8.50E+03	7.86E+03	2.51E+02	9.22E-01	6.32E+00	1.28E+01	1.26E+03	5.89E+02	3.11E+01
H45032393	9.23E+03	2.46E+01	3.45E+01	3.15E-01	3.96E+00	4.88E+00	1.12E+01	9.32E+03	8.77E+03	2.32E+02	9.30E-01	5.65E+00	1.19E+01	1.33E+03	6.00E+02	3.28E+01
H46032393	7.73E+03	2.34E+01	6.02E+01	3.27E-01	4.00E+00	4.93E+00	1.17E+01	7.98E+03	6.62E+03	2.41E+02	1.00E+00	5.88E+00	1.35E+01	1.29E+03	5.83E+02	3.08E+01
H410032393	8.66E+03	2.35E+01	3.98E+01	3.27E-01	4.06E+00	5.03E+00	1.18E+01	7.89E+03	8.25E+03	2.41E+02	1.03E+00	6.00E+00	1.31E+01	1.36E+03	5.58E+02	3.22E+01
S11032393	7.99E+03	2.29E+01	2.17E+02	2.99E-01	4.08E+00	5.15E+00	1.12E+01	8.99E+03	7.59E+03	2.55E+02	8.89E-01	5.48E+00	1.33E+01	1.38E+03	5.80E+02	4.07E+01
S12032393	7.19E+03	2.18E+01	2.31E+02	2.57E-01	3.63E+00	4.51E+00	9.40E+00	7.88E+03	7.13E+03	2.32E+02	8.69E-01	5.20E+00	1.28E+01	1.46E+03	5.29E+02	4.90E+01
S13032393	7.41E+03	2.37E+01	1.47E+02	2.86E-01	3.74E+00	4.66E+00	1.02E+01	7.77E+03	7.75E+03	2.39E+02	1.07E+00	5.37E+00	1.34E+01	1.43E+03	5.17E+02	6.36E+01
S15032393	8.57E+03	2.48E+01	9.42E+01	2.70E-01	3.88E+00	4.83E+00	1.11E+01	8.78E+03	8.44E+03	2.40E+02	1.19E+00	6.49E+00	1.32E+01	1.47E+03	5.49E+02	3.54E+01
S16032393	7.73E+03	2.63E+01	8.58E+01	2.55E-01	3.84E+00	4.84E+00	1.10E+01	8.13E+03	8.56E+03	2.41E+02	1.18E+00	5.80E+00	1.33E+01	1.45E+03	5.54E+02	5.21E+01
S110032393	8.09E+03	2.49E+01	1.39E+02	2.31E-01	3.64E+00	4.61E+00	9.90E+00	8.36E+03	8.32E+03	2.29E+02	1.23E+00	5.29E+00	1.30E+01	1.46E+03	5.26E+02	1.07E+02
S21032393	6.84E+03	2.22E+01	2.17E+02	2.25E-01	3.54E+00	4.32E+00	9.45E+00	7.20E+03	6.47E+03	2.31E+02	9.82E-01	4.98E+00	1.32E+01	1.40E+03	5.00E+02	2.84E+01
S22032393	6.50E+03	2.39E+01	2.28E+02	2.25E-01	3.44E+00	4.50E+00	9.13E+00	7.08E+03	7.28E+03	2.33E+02	1.23E+00	5.06E+00	1.32E+01	1.50E+03	5.51E+02	5.09E+01
S23032393	7.41E+03	2.42E+01	2.38E+02	2.34E-01	3.41E+00	4.37E+00	9.56E+00	7.69E+03	8.05E+03	2.26E+02	1.48E+00	6.36E+00	1.33E+01	1.43E+03	4.66E+02	3.40E+01
S25032393	6.82E+03	2.70E+01	1.57E+02	2.54E-01	3.55E+00	4.36E+00	1.03E+01	7.05E+03	7.26E+03	2.25E+02	1.83E+00	6.44E+00	1.33E+01	1.51E+03	4.77E+02	3.96E+01
S26032393		2.69E+01	8.41E+01	2.37E-01	3.53E+00	4.39E+00	1.15E+01			2.18E+02	1.70E+00	8.26E+00	1.28E+01			4.17E+01

VITA

Analila Rojo was born in Ruidoso, New Mexico where she attended school up to second grade and later attended school in Mexico for three years to learn Spanish. She completed her middle and high school years in El Paso, Texas. Analila later moved to San Antonio and Dallas, Texas to pursue a career as a District Manager in the Air Freight industry. She returned to El Paso to resume her studies at the University of Texas at El Paso. She received a Bachelor's degree in Industrial Engineering and a Master's in Biomechanics. She worked in the manufacturing industry as a Quality and Safety Engineer for eight years before returning to the University of Texas at El Paso to pursue a Doctoral degree in Environmental Science and Engineering under the guidance of Dr. Thomas E. Gill. Her research interests included dust storms and their effects on public health and the environment and particle size and chemical composition of aeolian dust. During her years in the Ph.D. program, Analila worked as a research assistant, and taught and tutored 9^{th} and 10^{th} grade students in math, science and engineering at some of the local high schools. Analila was a "Pathways to the Geosciences" fellow from 2005-2009. Her main objectives are to serve as a mentor for middle and high school students and persuade them to stay in school and learn more about math, science, and engineering.

Permanent address: 525 Via de Los Arboles
El Paso, Texas 79932